AD-A175 884 RESEARCH ON CHARACTERIZATION OF DAMAGE STATES IN CONTINUOUS FIBER COMPOSI (U) TEXAS A AND M UNIV COLLEGE STATION MECHANICS AND MATERIALS CE V K KINRA

1/2

UNCLASSIFIED MAY 86 MM-5024-86-12 AFOSR-TR-86-2182 F/G 11/4 NL

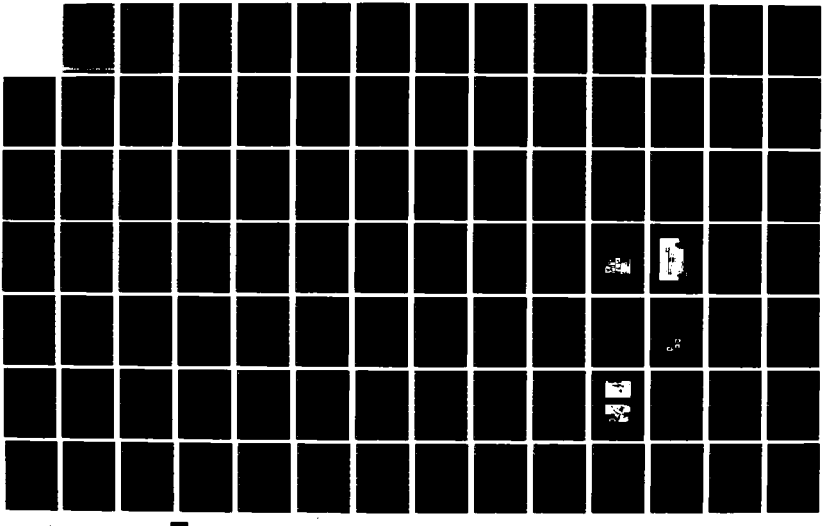

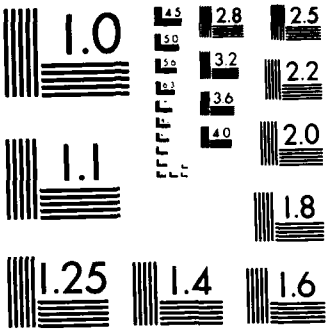

Mechanics and Materials Center
TEXAS A&M UNIVERSITY
College Station, Texas

AFOSR-TR- 86-2182

Research on Characterization of Damage States in Continuous Fiber Composites Using Ultrasonic Nondestructive Evaluation

Annual Technical Report

by

Vikram K. Kinra
Department of Aerospace Engineering

and

Mechanics and Materials Center

to the

Air Force Office of Scientific Research
Office of Aerospace Research
United States Air Force

MM 5024-86-12

Grant No. AFOSR-84-0066
May 1986

SECURITY CLASSIFICATION OF THIS PAGE

REPORT DOCUMENTATION PAGE

1a. REPORT SECURITY CLASSIFICATION: Unclassified	1b. RESTRICTIVE MARKINGS
2a. SECURITY CLASSIFICATION AUTHORITY	3. DISTRIBUTION/AVAILABILITY OF REPORT: Unlimited
2b. DECLASSIFICATION/DOWNGRADING SCHEDULE	
4. PERFORMING ORGANIZATION REPORT NUMBER(S)	5. MONITORING ORGANIZATION REPORT NUMBER(S): AFOSR-TR- 86-2182
6a. NAME OF PERFORMING ORGANIZATION: Dept. of Aerospace Engr. / 6b. OFFICE SYMBOL (If applicable)	7a. NAME OF MONITORING ORGANIZATION: Air Force Office of Scientific Research
6c. ADDRESS (City, State and ZIP Code): Texas A&M University, College Station, Texas 77843	7b. ADDRESS (City, State and ZIP Code): Bolling Air Force Base, Washington, D.C. 20332
8a. NAME OF FUNDING/SPONSORING ORGANIZATION: AFOSR / 8b. OFFICE SYMBOL (If applicable): NA	9. PROCUREMENT INSTRUMENT IDENTIFICATION NUMBER: Grant No. AFOSR - 84 - 0066
8c. ADDRESS (City, State and ZIP Code): B10 410, BAFB D.C. 20332	10. SOURCE OF FUNDING NOS.

PROGRAM ELEMENT NO.	PROJECT NO.	TASK NO.	WORK UNIT NO.
61102F	2302	B2	

11. TITLE (Include Security Classification): Research on Characterization of DamageStates in Continuous Fiber Composites Using Ultrason Nondestruction Evaluation

12. PERSONAL AUTHOR(S): V.K. Kinra

13a. TYPE OF REPORT	13b. TIME COVERED	14. DATE OF REPORT (Yr., Mo., Day)	15. PAGE COUNT
Annual	FROM 02/01/85 TO 01/31/86	May 86	+3Appendices 23

16. SUPPLEMENTARY NOTATION

17. COSATI CODES			18. SUBJECT TERMS (Continue on reverse if necessary and identify by block number)
FIELD	GROUP	SUB. GR.	Composites, Ultrasonic Nondestructive Testing, Damage, Lamb Waves

19. ABSTRACT (Continue on reverse if necessary and identify by block number)

It is well known that composite materials suffer complex damage when they are subjected to either monotonic or fatigue loading. This damage affects both the velocity and attenuation of ultrasonic waves. The primary objective of this research is to correlate the damage states with the changes in the velocity and attenuation. Once this has been accomplished the pair of ultrasonic parameters becomes a measure of the damage.

A particular damage mode, namely, transverse cracking has been examined in detail. The Through-the-thickness attenuation was found to be a very sensitive measure of transverse cracking. In order to study the influence of damage on axial stiffness, we have studied the propagation of Leaky-Lamb waves. As expected the transverse cracking significantly reduces the axial stifness.

Finally, a new experimental technique for measuring speed and attenuation of ultrasonic waves in laminates of very small thickness has been developed.

20. DISTRIBUTION/AVAILABILITY OF ABSTRACT	21. ABSTRACT SECURITY CLASSIFICATION
UNCLASSIFIED/UNLIMITED ☐ SAME AS RPT. ☐ DTIC USERS ☐	UUU

22a. NAME OF RESPONSIBLE INDIVIDUAL	22b. TELEPHONE NUMBER (Include Area Code)	22c. OFFICE SYMBOL
George K. Haritos,	202- 767- 4987	NA

DD FORM 1473, 83 APR — EDITION OF 1 JAN 73 IS OBSOLETE.

SECURITY CLASSIFICATION OF THIS PAGE

Research on Characterization of Damage States in Continuous Fiber Composites Using Ultrasonic Nondestructive Evaluation

Annual Technical Report

by

Vikram K. Kinra

Department of Aerospace Engineering

and

Mechanics and Materials Center

to the

Air Force Office of Scientific Research
Office of Aerospace Research
United States Air Force

MM 5024-86-12

Grant No. AFOSR-84-0066
May 1986.

TABLE OF CONTENTS

1. INTRODUCTION

1.1 Summary

It is well-known that components made of composite materials suffer complex damage when they are subjected to either monotonic or fatigue loading. We submitted a three year proposal to develop ultrasonic nondestructive techniques to measure the damage states in fiber-reinforced composite materials (Texas A&M Research Foundation Proposal No. RF-84-34). The objective of this Annual Technical Report is to summarize the progress made during the second year of the grant period.

When the damage occurs it has two effects upon the propagation of a mechanical wave through the composite: (1) It decreases the stiffness, and therefore, the speed of wave propagation; (2) It increases the attenuation of the wave. Thus by measuring the speed and attenuation as functions of frequency at various known levels of damage, we propose to establish the necessary calibration curves for damage.

The central objective of this research is to develop experimental techniques for ultrasonic nondestructive evaluation of damage in fiber-reinforced composite materials.

1.2 Work Proposed in the Original Proposal.

We include below an excerpt from the original three-year proposal in which we defined the work to be performed during this grant:

" Let C^{o}_{ijkl} and C^{*}_{ijkl} be the stiffness of an undamaged (virgin) and a damaged composite, respectively. Corresponding to each of these there is a wave-type and an associated wavespeed and attenuation. We will measure the speed and attenuation as function of frequency over a very broad range of frequencies. The speed measurement will yield information concerning stiffness and stiffness degradation; the attenuation measurements will provide information concerning defect type, size, and population. <u>This is precisely the type of information needed for the development of the damage models.</u>

Instead of obtaining voluminous results, our research philosophy will be to gather accurate, reliable, and reproducible results for a few carefully selected cases."

2. RESEARCH COMPLETED TO DATE

2.1 Summary of completed research

The following research has been completed during the second year of the grant period:

1. Several cross-ply laminates were subjected to tensile loading so as to produce transverse cracks. Wavespeed and attenuation in the thickness direction were measured as functions of frequency and "extent of damage". As expected, the wavespeed (or stiffness) was insensitive to transverse cracking. On the other hand, the attenuation was found to be a rather sensitive function of transverse cracking (Appendix I and II).

2. The technique used in item (1) above works only for relatively "thick" laminates (at least 16 ply or about 2 mm thick). However, we foresee a substantial use of "thin" laminates. With this in mind we have developed a new technique which works for thick as well as thin laminates. Using this thin-laminate technique we have interrogated the growth of transverse cracks in 10-ply laminates. As in [1] the attenuation was found to be a sensitive function of transverse cracking (Appendix III).

3. The technique described above measures through-the-thickness parameters. In order to measure the in-plane stiffness components, we have examined the application of Lamb waves. The wavespeed in the axial direction was measured both before and after damage. A significant reduction in the wavespeed (or axial stiffness) was observed.

2.2 Propagation of Longitudinal Plane Waves in the Thickness Direction

The theory supporting this experimental technique was developed during the first year of the grant period and the details may be found in our 1985 annual report . For continuity of reading we reproduce here the final results of our calculations.

Consider a composite coupon immersed in water. Let a plane longitudinal wave be incident upon the coupon. Let f(t) and s(t) be the front-surface and the back-surface reflections, respectively. Let $F^*(\omega)$ and $S^*(\omega)$ be their Fourier Transforms, respectively. It is shown in Appendix I that

$$\alpha R_{21}^2 \exp(-i2kh) = S^*(\omega)/F^*(\omega) \qquad (1)$$

where

$\alpha = T_{12}T_{21}/R_{21}R_{12}$
R_{12}=Reflection coefficient in water from composite
R_{21}=Reflection coefficient in composite from water
T_{12}=Transmission coefficient from water into composite
T_{21}=Transmission coefficient from composite into water

h=coupon thickness
ω=circular frequency, radians/second.

Thus, the only unknown in Eq.(1) is the complex-valued wave-number $k=k_1+ik_2$. From k_1 one can calculate the wavespeed: $c=\omega/k_1$; k_2 is the attenuation of the wave. Furthermore, it is well-known that

$$c^2=E/\rho$$

where E is some appropriate stiffness and ρ is the density of the specimen. Thus, measurement of k_1 is equivalent to a measurement of some element of the stiffness matrix. Further, let λ be the wavelength ($c=\omega\lambda/2\pi$), then we define a dimensionless attenuation $k_2\lambda$. Physically, $k_2\lambda$ is attenuation over one wavelength. The motivation for this particular choice of dimensionless parameter is that for a liner viscoelastic material $k_2\lambda$ is independent of frequency. (For more details see THEORY OF OPERATION, p.12, Appendix I). It is noted that this technique assumes that the front-surface and back-surface reflections can be separated in time domain. Therefore, it is good for relatively "thick" specimens. Several cross-ply layups were tested and the results have been documented in Appendix I. Here we include only one set of data which typifies the results reported in Appendix I.

The particular damage mode chosen is transverse cracking. This mode was chosen because it is the most common damage mode in most practical layups. The layup for which we report the results here is $[0_6 90_4 0_2]_s$. The laminate was subjected to simple tensile loading in small discrete steps. At the end of each load-step the coupon was removed from the Instron machine, subjected to an ultrasonic examination and returned to the Instron for the next load-step. Edge replications were taken at each load-step to record the transverse cracks. In Figure 1 we have plotted attenuation as a function of applied load (and hence of damage) at three discrete frequencies. Line drawings of the edge replications showing the damage state are also included. It is noted that the edge replication shown is that portion of the total replica which is insonified by ultrasonic beam (10 mm). The total number of cracks "seen" by the beam is also shown. We make the following observations:

1. Attenuation increases monotonically and significantly with transverse cracking.
2. Attenuation decreases with frequency.
3. Appearance of a single additional crack in the path of the sound beam increases the attenuation by a measurable amount.

Since for the particular layup all cracks are of equal length (in the direction of wave propagation or in the thickness direction) their contribution to the total attenuation is identical. This allows us to define a cumulative crack length as the total number of transverse cracks encountered by the sound beam multiplied by the crack length which, for the present case is 0.5 mm (four 90°-plies). This allows us to consolidate the

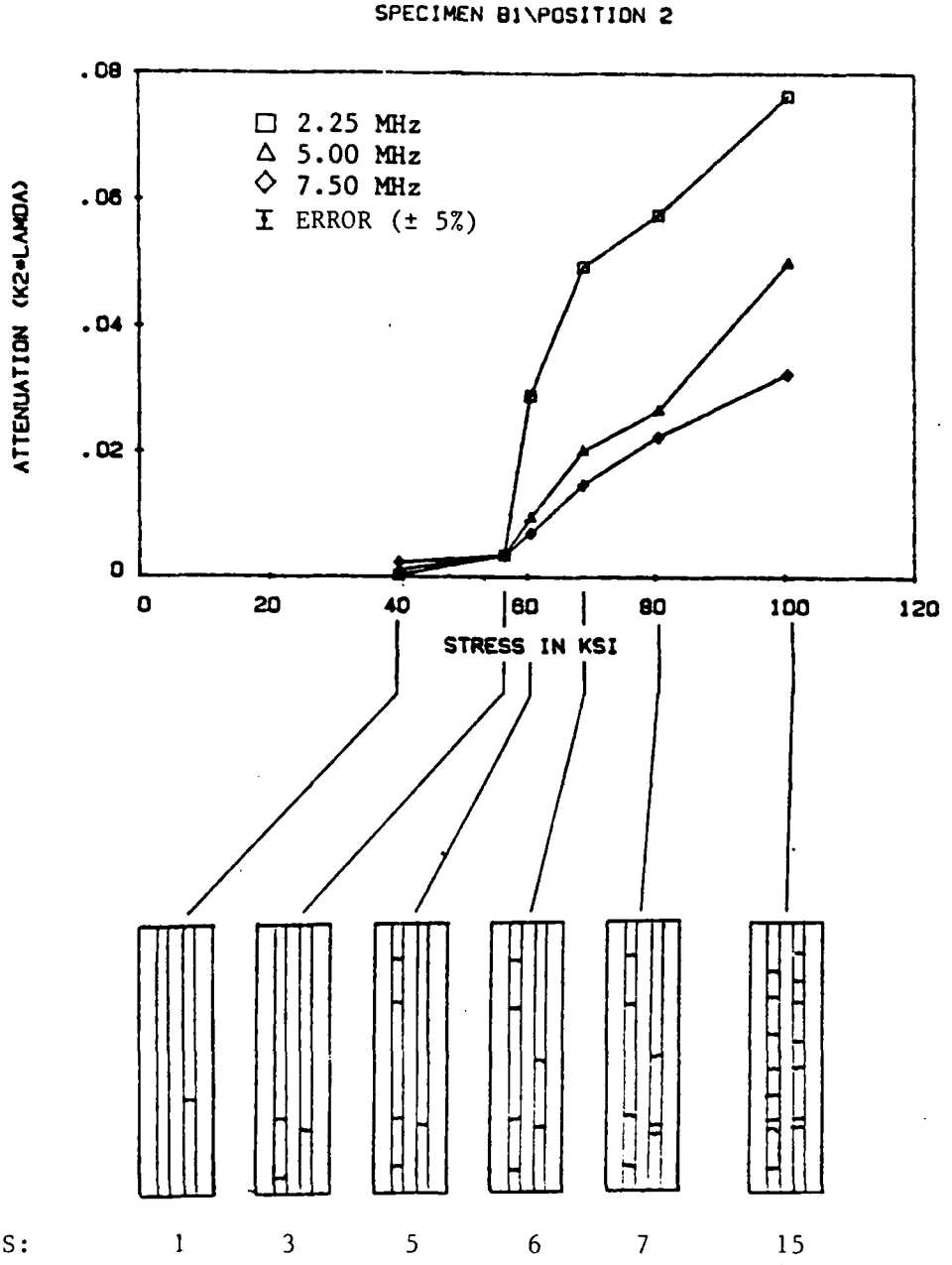

Fig. 1. Attenuation increases dramatically with transverse cracking in a $[0_6 90_4 0_2]_s$ Laminate at all three frequencies tested. The extent of damage is shown in the edge replication sketches.

data on each edge replication into a single cumulative crack length. In Fig. 2 attenuation is plotted versus cumulative crack length at three different positions along the length of a coupon. In an "ideal" experiment with an ideal material all three curves would have reduced to a single "master" curve; as it is they are within the error of measurement (about ±5%).

These results are quite encouraging. With some more refinement in the experimental technique, we hope that these curves will fall even closer together to form a master curve. In the next phase of our research we hope to produce such master curves for a wide variety of layups. These will then constitute a damage metric for transverse cracking i.e. a measurement of $k_2\lambda$ will yield the cumulative crack length, provided, of course, that is the only damage mode present.

We have also tried to seek an experimental answer to the following question. As a coupon is gradually loaded to failure, is it possible to predict the LOCATION of the final failure fairly early in the loading history? The technological implications of this question are obvious. We took the following approach. A coupon was loaded in discrete steps. After each load step, it was subjected to an ultrasonic examination at several locations along the length. The results are shown in Fig.3 where we have plotted attenuation versus applied stress at various locations. The line drawings of edge replications are also included. Now, this set of experiments was based on the following conjecture. If there is a position where damage will localize, then the attenuation there should be highest. Thus the curve for that particular location will form an upper bound on the remaining curves. The experiments did not corroborate this conjecture. We conclude, therefore, that from an ultrasonic examination one cannot predict apriori the location of the final failure for this type of specimen. In fact, from the edge replication it is clear that the damage spreads in a fairly random manner and that it does not localize in any particular location. This is consistent with the prediction of the shear-lag model of the formation of transverse cracks[6].

The attention is now turned to k_1. Recall that $c=\omega/k_1$. The stiffness in the thickness direction is given by $C_{33}=\rho c^2$. The longitudinal wavespeed as a function of applied stress for specimen B_1 (same as in Fig.1) is shown in Fig.4. Within the error of measurement, ±0.5%, the wavespeed remains unchanged with damage; see Fig.1 for edge replications. This may be explained as follows. A crack has least amount of influence on stiffness in the direction parallel to the crack faces and this is confirmed by the results presented here.

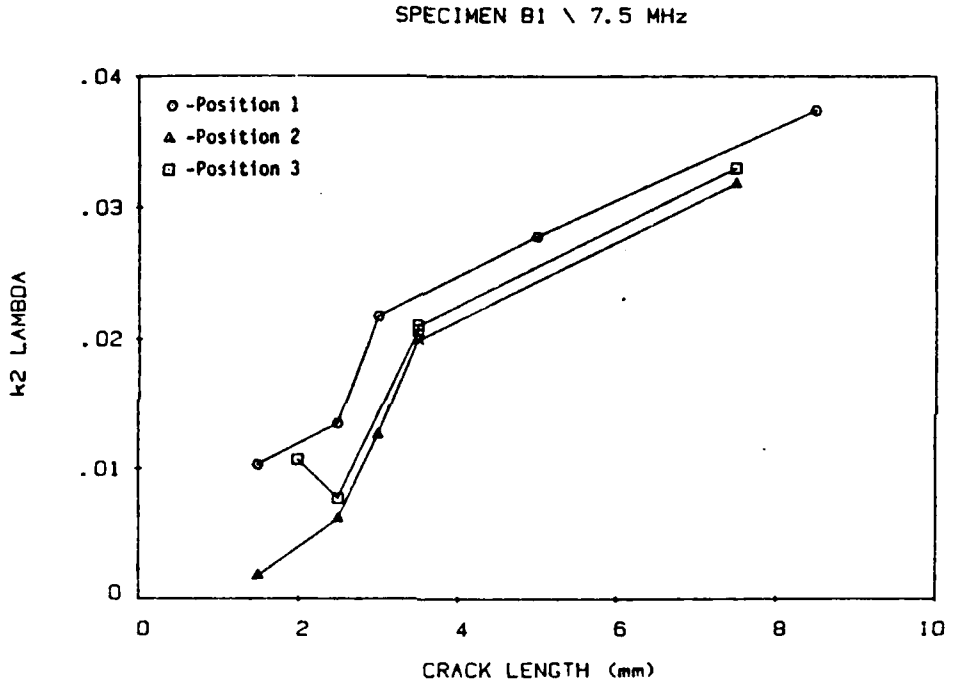

Fig. 2 Attenuation increases rapidly as the total crack length increases at all locations. Results are shown at 7.5 MHz only.

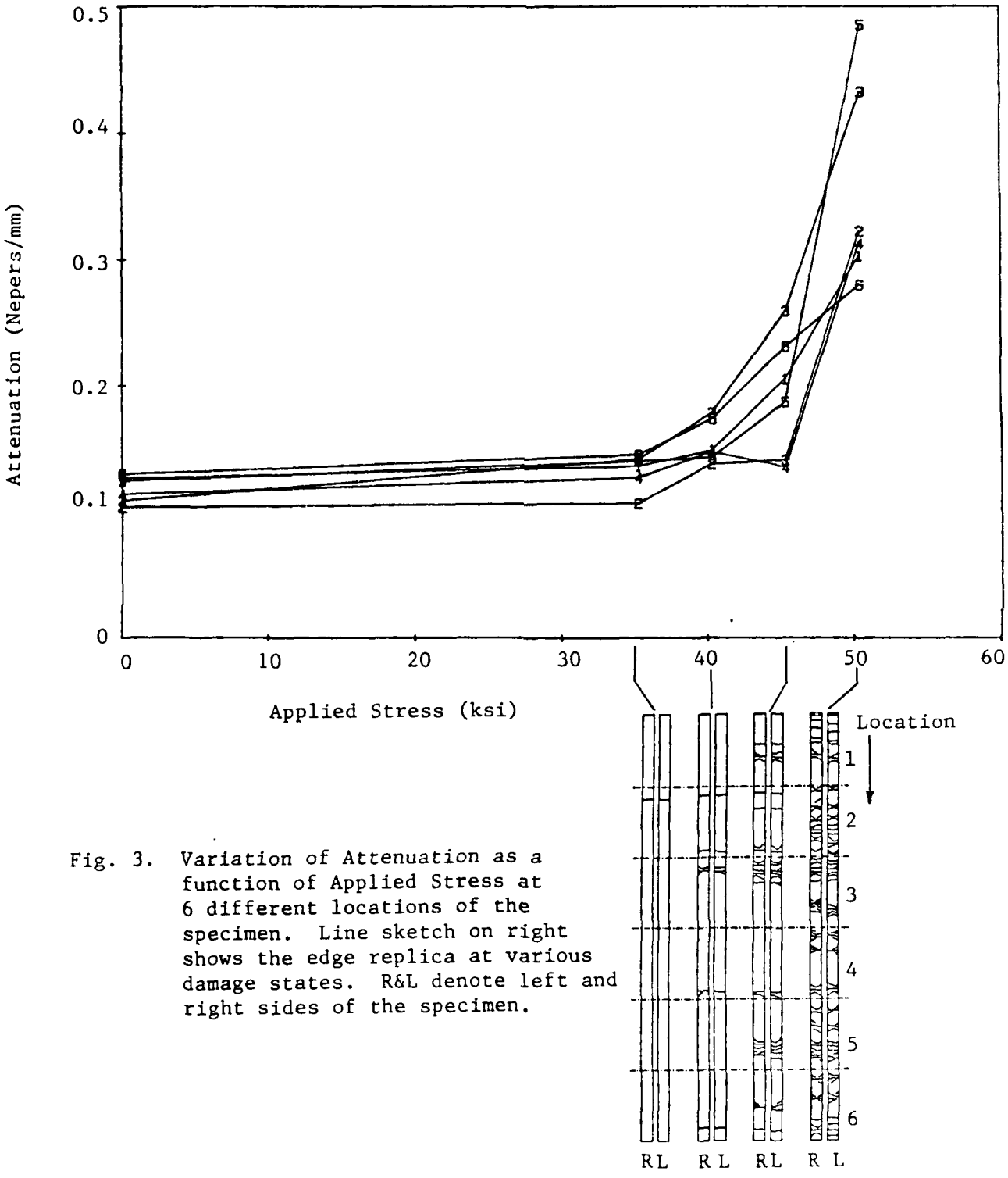

Fig. 3. Variation of Attenuation as a function of Applied Stress at 6 different locations of the specimen. Line sketch on right shows the edge replica at various damage states. R&L denote left and right sides of the specimen.

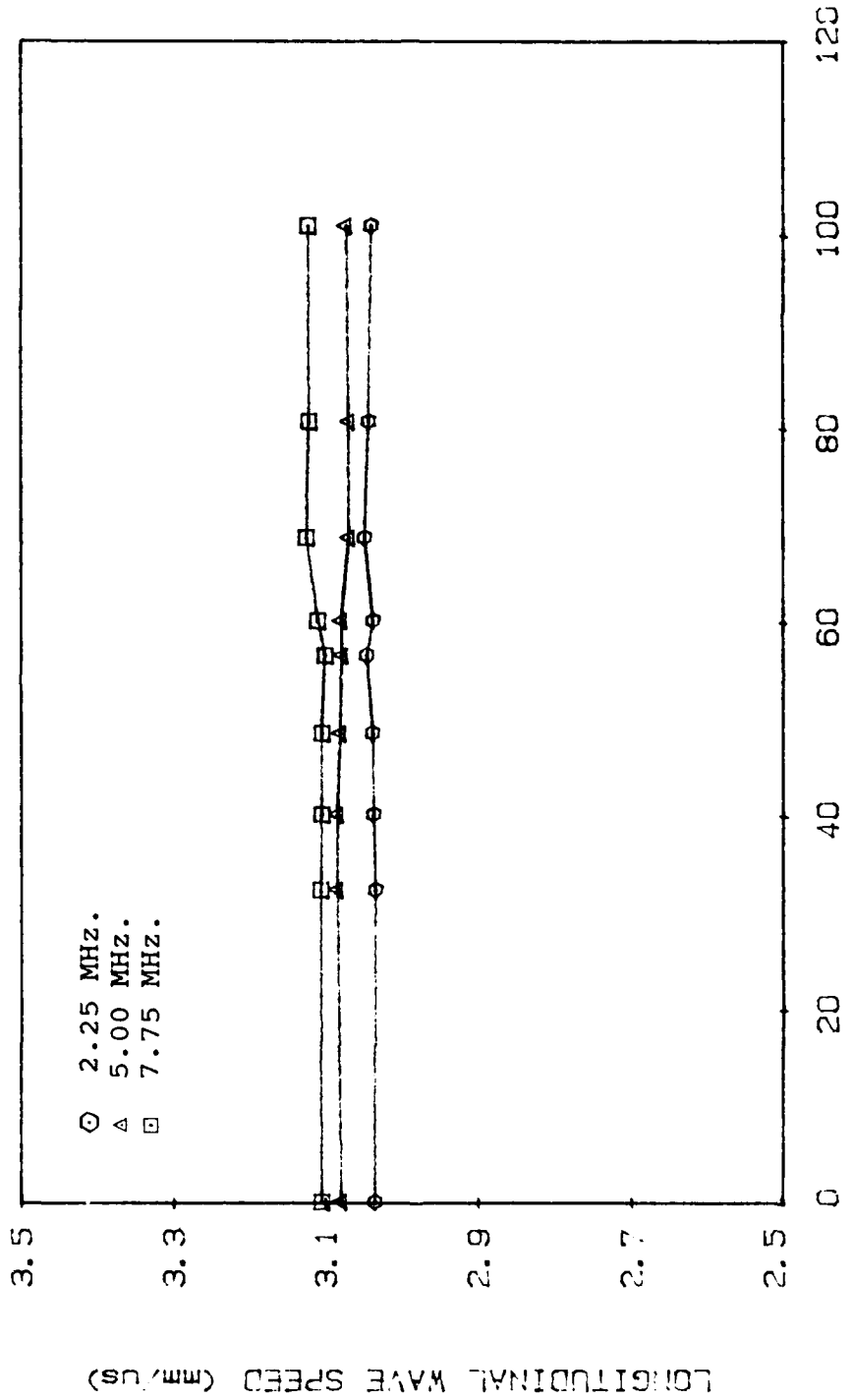

Fig. 4 Longitudinal Wavespeed variation as Damage is induced, for specimen B1, Position 1, at 2.25, 5.0, 7.5 MHz.

2.3 Propagation of Lamb Waves in the axial direction.

It was shown in the previous section that the speed of sound in the thickness direction is insensitive to transverse cracking. Now, if a longitudinal wave is propagated in the axial direction, the wave propagation will be normal to the crack faces and hence a strong crack-wave interaction will result. The scattering cross-section of the crack in this mode of wave-motion is much higher than when the wave propagation direction is in the plane of the crack faces. Therefore, one should observe larger changes in stiffness and attenuation for the case of axial wave propagation. These waves travelling in the plane of the plate are called Lamb Waves. They have been used quite successfully as NDT tools for isotropic materials. We have extended the use of Lamb waves to composites. Since Lamb waves can be generated just as easily in curved plates, this mode of measurement has a definite potential for field applications.

A preliminary study has been made to measure the changes in wavespeed and attenuation as the damage is induced in the specimens. It was found that the attenuation increases whereas the stiffness decreases with damage.

2.3.1 Theoretical Analysis

The governing equations for the Lamb wave propagation in isotropic plates both in air and in water were given and analyzed by Viktorov [2]. The dispersion relations for plates in water have been analyzed by Merkulov[3]. When the plate is immersed in a liquid the Lamb wave radiates acoustic energy into the liquid. These radiated waves have been named Leaky Lamb waves in the literature. In his analysis Merkulov assumes that the density of the plate material is large compared to the density of water. He obtains the dispersion curves and the attenuation by a first order approximation. The governing equations for the Lamb waves in composite plates in air have been given by Habegar et.al in [4]. These are complex transcendental equations and hence cannot be solved analytically. The equations yield multiple roots which correspond to the various Lamb wave modes. We have extended the analysis to composite plates immersed in liquid to obtain numerical solution in the form of dispersion equations. The detailed derivation of these equations is given in section 2.3.5. A computer program is being developed for the calculation of wavespeed and attenuation of Lamb waves in composite plates in water.

2.3.2 Experimental Procedure

The block diagram of the experimental setup is shown in Fig.5a. The pulse generator/function generator combination produces a tone-burst of about 10 cycles of sinusoidal signal. This signal is amplified by an amplifier to drive the transmitter. The waves received by the receiver are amplified by the signal amplifier and fed into the digital oscilloscope. The

oscilloscope digitizes, averages, stores and provides the necessary data to the computer for analysis.

The specimen is mounted in the grips attached to a turntable which is graduated to 0.2° angle. The transducers are mounted on precision travelling mechanisms graduated to 0.001 inch.

For the purpose of exciting and detecting Lamb waves the transducers and the specimen are positioned as shown in Fig.6b. The transmitter emits a toneburst signal shown as 1 in the figure. This signal strikes the specimen and generates Lamb waves in the plate. Since the plate is immersed in water, leaky waves ,3, are setup in water. The receiver is kept well away from the line of sight of the transmitter so that the directly transmitted waves ,2, do not interfere with the leaky Lamb waves. The amplitude of the signal received by the receiver is recorded as the angle of incidence θ_i is changed. Lamb angles are identified by the peaks in the recorded signals. The wavespeed of the Lamb waves is calculated from the Snell's Law

$$c_w/c_x = \mathrm{Sin}(\theta_i)/\mathrm{Sin}(\theta_t) \qquad (2)$$

where θ_i= Angle of incidence
θ_t= Angle of refraction, $\pi/2$
c_w= Longitudinal wavespeed in water, and
c_x= Lamb wave wavespeed

Thus,

$$c_x=c_w/\mathrm{Sin}(\theta_i) \qquad (3)$$

2.3.3 Results

An aluminum specimen was tested first, as a check for the experimental setup and data collection program. The received signal amplitude as a function of the angle of incidence is shown in Fig.6. The first peak occurs at 10.5°±0.2. This corresponds to the first antisymmetric or flexural mode of vibration (a_1); the theoretical value for this mode is 11.8° [2]. In view of the fact that the theoretical value is for the case of aluminum in air, while in the experiment the plate is immersed in water, the agreement between the theory and experiment is considered very good; this serves to calibrate our experimental procedures. Next the same procedure is applied to the testing of the composites.

The layup of the composite tested is $[0/90_4]_S$. This test was conducted at a frequency of 5 MHz. The received amplitude as a function of angle of incidence, θ_i is shown in Fig.7. From the theoretical calculations for composite in air it can be deduced that the dominant peak at about 28° is the lowest order antisymmetric mode (a_0). In going from the undamaged to damaged state, the peak shifts by 1.5 degrees from 28° to 29.5°. By Snells Law, Eq.(2), the Lamb wavespeed changes from 3.17 mm/μsec

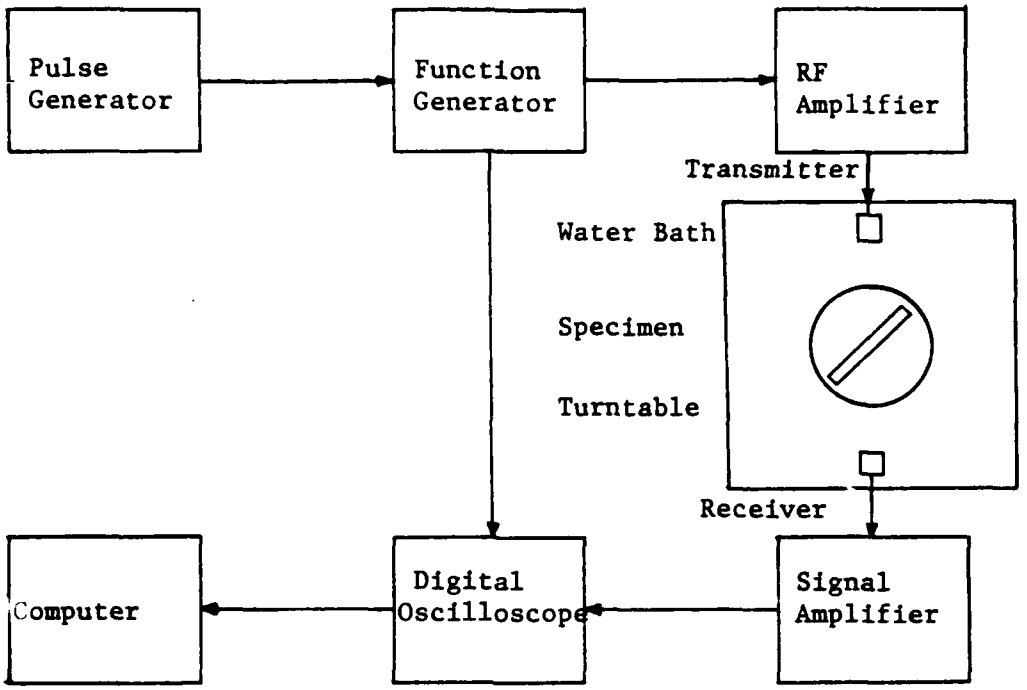

(a)

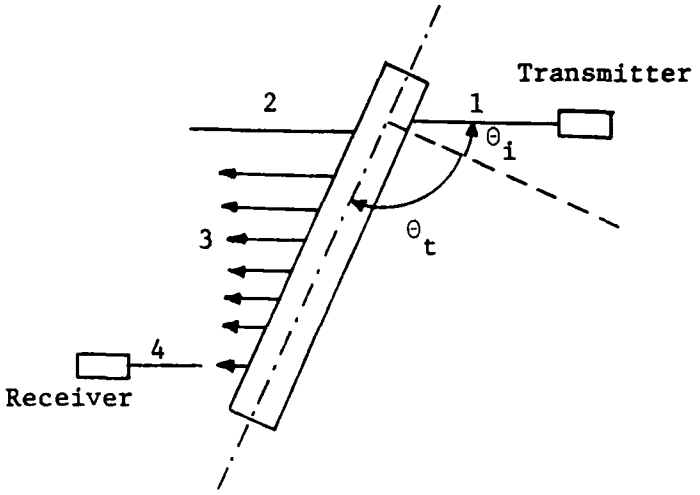

(b)

Fig. 5. a. Block diagram of the Experimental Setup.

b. Relative position of the transmitter, receiver and the specimen.

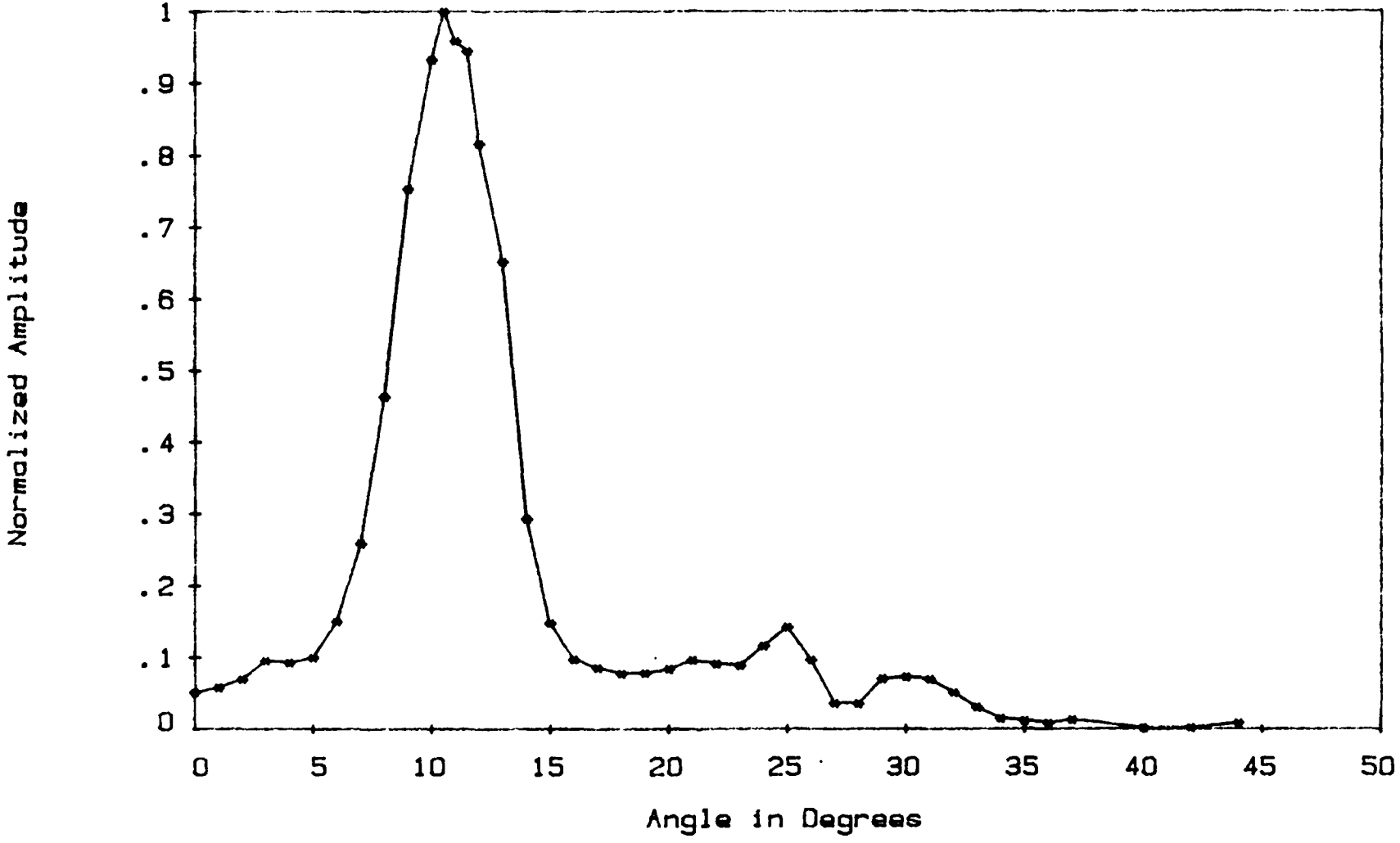

Fig. 6 Lamb Waves in an aluminum plate at 1 MHz

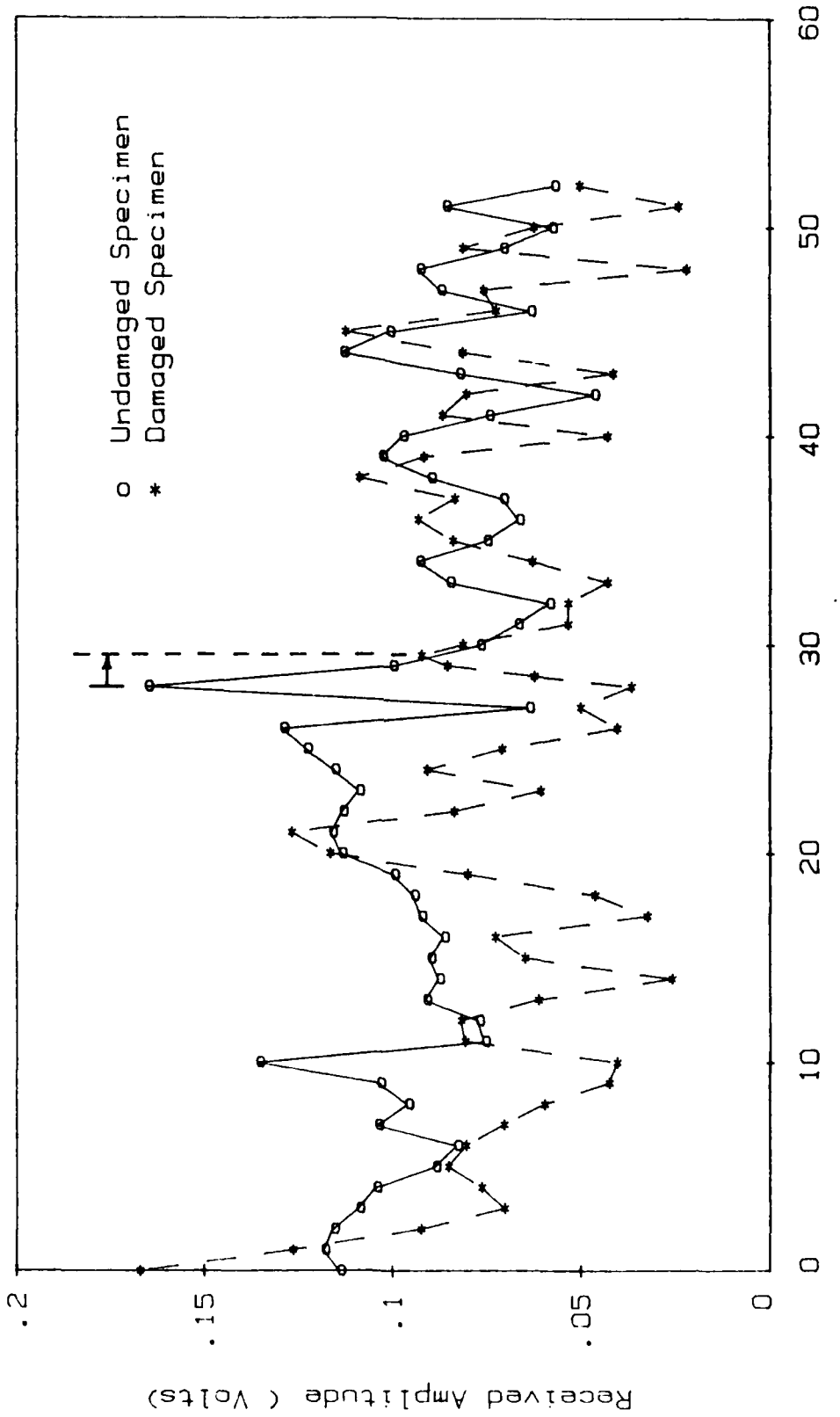

Fig. 7 Lamb Angle detection in $[0/90_4]_s$ Specimen at 5 MHz.

to 3.02 mm/μsec . Now, $\rho c^2 = C_{11}/(1-\nu_{12}\nu_{21})$, where C_{11} is the axial stiffness, ν_{12} is the Poisson's ratio with load in the axial direction and the strain in the transverse direction, and ν_{21} is the Poisson's ratio with the directions reversed. Furthermore $\nu_{12}\nu_{21} \simeq 0.006 << 1$, hence $\rho c^2 \simeq C_{11}$. The axial stiffness is 15.37 GN/m^2 for the undamaged specimen and 13.95 GN/m^2 for the damaged specimen; the reduction is about 10% which is consistent with similar data reported in the literature [5]. These preliminary results have demonstrated the efficacy of the Lamb wave method to monitor damage via the degradation of axial stiffness.

2.3.4 Future goals

A computer program is being developed which will enable us to calculate the various Lamb modes of the composite plates in water. Specimens of various layups will be made and the wavespeed and attenuation in the dominant modes will be measured as a function of the damage. The overall stiffness degradation of the specimen will be measured and related to the amount of damage in the specimen.

2.3.5 Detailed derivation of Lamb Wave Equations for Composites in Liquid.

Generally, all the layups for composites used in practical situations are symmetric and balanced where there is no coupling between the extensional and bending coefficients of the stiffness matrix. In the following, we restrict our analysis to such cases.

The stress strain relation for a composite material is given by

$$\tau_{ij} = C_{ijkl}\epsilon_{kl} \qquad \text{for } i,j,k,l=1,2,3 \tag{1}$$

where the strain displacement relation can be written as

$$\epsilon_{ij} = (U_{i,j}+U_{j,i})/2 \qquad \text{for } i,j=1,2,3 \tag{2}$$

The coordinate directions used here are the ones used commonly in the literature. Directions 1 and 2 are in the plane of the plate and 3 is normal to it.

The equation of motion in an elastic medium is

$$\sum_{j=1}^{3} \tau_{ij,j} = \rho\ddot{U}_i \quad i=1,2,3 \tag{3}$$

We assume a plane strain condition for the wave propagation. Under this condition the displacement U_2 and all derivatives with respect to 2 vanish. Substituting Eqns.(1)&(2) in Eq.(3) and changing to the contracted notation for the stiffness matrix, the following equations are obtained;

$$\rho\ddot{U}_1 = C_{11}U_{1,11}+C_{13}U_{3,31}+C_{55}(U_{1,33}+U_{3,13}) \tag{4}$$

$$\rho\ddot{U}_3=C_{33}U_{3,33}+C_{13}U_{1,13}+C_{55}(U_{1,13}+U_{3,11}) \quad (5)$$

We now seek plane wave solutions of the form

$$U_1=U_{10}\exp[i(k_x x+k_z z-\omega t)] \quad (6)$$

$$U_3=U_{30}\exp[i(k_x x+k_z z-\omega t)] \quad (7)$$

where U_{10} and U_{30} are the wave amplitudes

Substituting Eq.(4)&(5) in Eq.(6)&(7)

$$\rho U_{10}\omega^2=C_{11}U_{10}k_x^2+(C_{55}+C_{13})U_{30}k_x k_z+C_{55}U_{10}k_z^2 \quad (8)$$

$$\rho U_{30}\omega^2=C_{55}U_{30}k_x^2+(C_{55}+C_{13})U_{10}k_x k_z+C_{33}U_{30}k_z^2 \quad (9)$$

Let us define R as

$$R=U_{30}/U_{10}=(\rho\omega^2-C_{11}k_x^2-C_{55}k_z^2)/(C_{55}+C_{13})k_x k_z \quad (10)$$

Eliminating U_{10} and U_{30} from Eq.(8) & (9) we get a quadratic equation for k_z in terms of k_x and the elastic constants as

$$k_z^2=k_x^2[-B\pm SQR(B^2-4D)]/2 \quad (11)$$

where $B=[(C_{33}/\rho)(C_{11}/\rho-\omega^2/k_x^2)-(C_{13}/\rho)(2C_{55}+C_{13})/\rho$

$$-C_{55}\omega^2/\rho k_x^2]/\{(C_{33}C_{55})/\rho^2\}$$

$$D=(\omega^2/k_x^2-C_{55}/\rho)(\omega^2/k_x^2-C_{11}/\rho)/\{(C_{33}C_{55})/\rho^2\}$$

Let us define k_{zp} and k_{zm} as the two values of k_z obtained from Eq.(10) with + or - signs. Also Rp and Rm be the value of R when k_{zp} and k_{zm} ,respectively, are substituted in Eq.(10).

The equations derived above are for bulk waves travelling in an unbounded medium. Now we analyze these bulk waves travelling in a plate subject to the proper boundary conditions so that the plate wave solution is obtained.

The two possible plate wave solutions will have the following forms

$$U_1=\exp\{i(k_x x-\omega t)\}[M\exp(ik_{zp}z)+N\exp(-ik_{zp}z)+P\exp(ik_{zm}z)$$

$$+Q\exp(-ik_{zm}z)] \quad (12)$$

$$U_3=\exp\{i(k_x x-\omega t)\}[Rp\{M\exp(ik_{zp}z)-N\exp(-ik_{zp}z)\}$$

$$+Rm\{P\exp(ik_{zm}z)-Q\exp(-ik_{zm}z)\}] \quad (13)$$

where M,N,P,Q are arbitrary constants.

The boundary conditions to be satisfied for a plate of

thickness 2b, for the plate mode of wave-motion to exist are

$$\tau_{33}=C_{33}U_{3,3}+C_{13}U_{1,1}=-p \quad \text{at } z=\pm b \tag{14}$$

and

$$\tau_{31}=C_{55}U_{1,3}+C_{55}U_{3,1}=0 \quad \text{at } z=\pm b \tag{15}$$

i.e, the normal stresses in the plate are equal to the fluid pressure and the shear stresses on the plate surface can not exist as the fluid does not sustain shear. The displacement boundary condition is that the normal displacements in water, W_L, and the plates at $z=\pm b$, have to be equal ,or

$$U_3=W_L \quad \text{at } z=\pm b \tag{16}$$

Substituting Eq.(12) & (13) in Eq.(14) & (15)

$$M\ GpX + N\ Gp/X + P\ GmY + Q\ Gm/Y = ip \tag{17.1}$$

$$M\ Gp/X + N\ GpX + P\ Gm/Y + Q\ GmY = ip \tag{17.2}$$

$$M\ HpX - N\ Hp/X + P\ HmY - Q\ Hm/y = 0. \tag{17.3}$$

$$M\ Hp/X - N\ HpX + P\ Hm/Y - Q\ HmY = 0. \tag{17.4}$$

where $G_{p,m}=C_{33}k_{zp,m}+C_{13}k_x$; $H_{p,m}=k_{zp,m}+k_xR_{p,m}$

and $X=\exp(ik_{zp}b)$; $Y=\exp(ik_{zm}b)$

The wave motion in water satisfies the following wave equation

$$\frac{\partial^2\phi_L}{\partial x^2} + \frac{\partial^2\phi_L}{\partial z^2} + k_L^2\phi_L=0. \tag{18}$$

where $k_L=\omega/c_L$ is the wavenumber for the wave in water and c_L is the wavespeed in water.

The form of the potential ϕ_L in water to satisfy Eq.(18) is

$$\phi_L = \phi_0\exp[i(k_xx+k_zz-\omega t)] \tag{19}$$

substituting Eq.(18) in Eq.(17) we can easily see that

$$k_z^2=k_L^2-k_x^2$$

The potential ϕ_L corresponds to a wave in liquid which propagates along the plate in the x-direction and decays exponentially along the z-direction. This wave in liquid has to fit in with the Lamb wave in the plate. This means that this wave must pursue a path along the x-axis with a velocity equal to the phase velocity of the Lamb Waves. At the plane $z=\pm b$ the two waves must have equal normal displacements. The displacement in water

W_L can be calculated from the potential as

$$W_L = \frac{\partial \phi_L}{\partial z} = ik_z \phi_o \exp[i(k_x x + k_z z - \omega t)] \quad (20)$$

applying the boundary condition Eq.(16) we get

$$mM+nN+rP+sQ=ik_z\phi_o\exp(ik_z b) \quad (21)$$

$$-nM-mN-sP-rQ=-ik_z\phi_o\exp(-ik_z b) \quad (22)$$

where $m=Rp\ \exp(ik_{zp}b)$; $n=-Rp\ \exp(-ik_{zp}b)$

$r=Rm\ \exp(ik_{zm}b)$; $s=-Rm\ \exp(-ik_{zm}b)$

and from Eqns.(17.3) & (17.4) we can write

$$aM-bN+cP-dQ=0. \quad (23)$$

and $$bM-aN+dP-cQ=0. \quad (24)$$

From Eqns.(23)&(24) we get

$$N=[(ad-bc)P+(bd-ac)Q]/(a^2+b^2)=N1*P+N2*Q \quad (25)$$

and,

$$M=[(bd-ac)P+(ad-bc)Q]/(a^2+b^2)=N2*P+N1*Q \quad (26)$$

where $N1=(ad-bc)/(a^2+b^2)$ and $N2=(bd-ac)/(a^2+b^2)$

Substituting the values of M and N into Eqns.(21)&(22) we can write

$$(g+h)(P+Q)=ik_z\phi_o[\exp(ik_z b)+\exp(-ik_z b)] \quad (27)$$

where $g=mN2+nN1+r$ and $h=mN1+nN2+s$

Similarly substituting the values of M and N into Eq.(17.1) and Eq.(17.2)

$$P+Q=i\{p(z=b)-p(z=-b)\}/(F1+F2) \quad (28)$$

where $F1=N2*Gp*X+N1*Gp/X+Gm*Y$; $F2=N1*Gp*X+N2*Gp/X+Gm/Y$

comparing Eqns.(27) and (28)

$$\frac{p(z=b)+p(z=-b)}{F1+F2} = \frac{k_z\phi_o[\exp(ik_z b)+Exp(-ik_z b)]}{(g+h)} \quad (29)$$

The pressure in the fluid can be calculated from the potential ϕ_L from the relation

$$p=\lambda\{\frac{\partial^2\phi_L}{\partial x^2} + \frac{\partial^2\phi_L}{\partial z^2}\}$$

which gives

$$p(z=b)+p(z=-b)=-\lambda_L(k_x^2+k_z^2)\phi_0[\exp(ik_zb)-\exp(-ik_zb)] \tag{30}$$

substituting Eq.(30) in Eq.(29)

$$\frac{SQR(k_L^2-k_x^2)}{g+h}+\frac{\rho_L\omega^2}{F1+F2}=0. \tag{31}$$

Simplification of F1+F2 and g+h and substitution into Eq. (31) and rearranging the equations gives for the symmetric modes

$$\frac{Tan(k_{zp}b)}{Tan(k_{zm}b)}-\frac{Gp*Hm}{Gm*Hp}+\frac{i\rho_L\omega^2Tan(k_{zm}b)}{\rho(Gm/\rho)SQR(k_x^2-k_L^2)}[-\frac{Hm}{Hp}Rp+Rm]=0.$$

Symmetric Modes (32)

Similarly, we can show that for the antisymmetric modes the governing equation is

$$\frac{Tan(k_{zm}b)}{Tan(k_{zp}b)}-\frac{Gp*Hm}{Gm*Hp}+\frac{i\rho_L\omega^2Cot(k_{zp}b)}{\rho(Gm/\rho)SQR(k_x^2-k_L^2)}[\frac{Hm}{Hp}Rp-Rm]=0.$$

Asymmetric Modes (33)

It is quite laborious but not difficult to reduce these equations to the equations derived by Viktrov if the stiffness matrix of an isotropic material is used.

The solution of these equations is not possible in a closed form. Also, these equations change their form depending on the value cf k_x in Eq.(11), where B^2-4D can become negative and thus make k_{zp} and k_{zm} complex. Hence, these equations have to be written for different ranges of the values of k_x. The solution method is basically a search method where for a particular frequency, the wavespeed is slowly incremented and at the solution points the value of the equation changes sign.

2.3.6 References

1. Ringermacher,H.I., "Ultrasonic velocity characterization of Fatuge damage in Gr/Ep composites", 1980 Ultrasonic Symposium Proc.,pp 957-960.
2. Viktorov,I.A., "Rayleigh and Lamb waves", Plenum Press, New York 1967.
3. Merkulov,L.G., "Damping of Normal Modes in a plate

immersed in a liquid.", Soviet Physics-Acoustics, Vol 10, No.2, Oct-Dec 64, pp 169-173.
4. Habegar,C.C.,Mann,R.W.,Baum,G.A., "Ultrasonic plate waves in Paper", Ultrasonics, March 79,pp 57-62.
5. Jamison, R.D., "Advanced Fatigue damage development in Graphite/Epoxy Laminates",Ph.D. Thesis, VPI&SU, 1982.
6. Refsnider, K.L. "Some fundamental Aspects of the Fatigue and Fracture response of Composite Materials", Proc. of the Fourteenth Annual Meeting of the Society of Engineering Science, Leigh Univ., Nov. 1977.

4. PROFESSIONAL PERSONNEL

1. Dr. Vikram K. Kinra, Principal Investigator
2. Mr. Vinay Dayal, Ph.D. Student
3. Mr. Vasu Iyer, Ph.D. Student
4. Mr. J. Grillo, Laboratory Technician
5. Mrs. Mary Klements, Secretary

5. INTERACTIONS

1. Organized and Chaired a session,"Ultrasonic Nondestructive Evaluation of Composites" at Spring Conference of the Society for Experimental Mechanics, Las Vegas, June 1985.

2. V.K. Kinra and C.Q. Rousseau, "Acoustical and Optical Branches of Wave Propagation", to appear in the Proceedings of the Symposium on Multiple Scattering of waves in random Media and by Random Rough Surfaces (Eds. V.K.Vardan and V.V. Vardan) Pennsylvania State University July 1985.

3. "Stress Pulses Emitted During Fracture", Presented an invited review paper at the Flow, Fracture and Fragmentation Conference in Neve Ilan, Israel, Jan. 1986.

4. V.Dayal,V.K.Kinra and J.G. Eden, "Ultrasonic Nondestructive Testing of Fiber Reinforced Composite Materials" Proc. of the International Symposium on Composite Materials, Beijing, China 1986.

5. V. Dayal and V.K. Kinra, " Ultrasonic Nondestructive Testing of composite Materials" Proc. of the Third Japan U.S. Conference on Composite Materials, 1986, Tokyo, Japan.

APPENDIX I

THE APPLICATION OF ULTRASONICS TO ASSESS DAMAGE IN COMPOSITE MATERIALS

A Thesis

by

JOHN GREGORY EDEN

Submitted to the Graduate College of
Texas A&M University
in partial fulfillment of the requirements
for the degree of

MASTER OF SCIENCE

December 1985

Major Subject: Aerospace Engineering

ABSTRACT

The Application of Ultrasonics to Assess
Damage in Composite Materials (December 1985)
John Gregory Eden, B.S., Aerospace Engineering
Texas A&M University
Chairman of Advisory Committee: Dr. Vikram K. Kinra

A recently developed method involving the use of Fast Fourier Transform (FFT) signal processing to calculate wave speed and attenuation was applied to the analysis of damage in continuous fiber composite materials. Several extraneous factors that affected the precision of the measurement technique were eliminated. Wave speed and attenuation can be measured with a precision of ±0.1% and ±1.0%, respectively.

Graphite/epoxy laminates were monotonically loaded and at each step the wave speed and attenuation were measured at 2.25, 5.0, and 7.5 MHz. The wave speed showed no apparent decrease as the damage (transverse matrix cracks) increased. However, the attenuation did increase with increasing damage. It was found that attenuation values are not reliable until there is an even distribution of damage within the area being examined. Although at 2.25 MHz greater changes in attenuation were recorded it is believed that the 7.5 MHz attenuation results give a better representation of the damage within the composite.

ACKNOWLEDGEMENTS

The financial Support of the Air Force Office of Scientific Research under Grant No. AFOSR - 84-0066 is gratefully acknowledged.

TABLE OF CONTENTS

LIST OF TABLES

LIST OF FIGURES

INTRODUCTION

Since the application of composite materials has become widespread, accurate qualitative as well as quantitative techniques have been developed to evaluate their performance. One focus of the applied research has been to correlate the life of the composite component to the amount of damage accumulation due to fatigue or monotonic loading. The development of damage in composite materials is a cumulative process. Damage growth can be described as a coalescence of damage modes which develop and interact in a manner subject to the orientation of the plies in the laminate, the loading history, and the current state of damage in the laminate. Reifsnider [1] describes damage in terms of 'critical elements' and 'subcritical elements'. Critical elements are defined as damage which results in the final failure of a laminate (i.e., 0 degree ply failure in tensile loading, unstable plies that have not buckled under compressive loading, etc.). Subcritical elements include porosity, microvoid growth, matrix cracking, matrix/fiber debonding, and matrix splitting along fiber directions. It is likely that the degree of subcritical damage in a composite component will influence the final failure modes of damage. Thus, it becomes apparent that monitoring subcritical damage growth and its behavior

This thesis follows the format of the Journal of Composite Materials.

may lead to better predictions of the expected life of composite parts.

Recently there has been considerable work done in the use of ultrasonics. Reasons for this are quite easily explained. The connection between speed of sound in a material and its elastic stiffness is well known [2,3]. In the case of composite materials, as the subcritical damage accumulates the stiffness of the laminate will decrease. Another basis for ultrasonic evaluation is the scattering of energy when a wave passing through the the composite interacts with the newly created damage surfaces. This scattering will cause a relative decrease in the amplitude of the wave. Therefore, one may be able to detect damage growth by monitoring changes in wave velocity and attenuation.

A technique to accomplish this is being developed in the Wave Propagation Laboratory in the Department of Aerospace Engineering at Texas A&M University. The method involves the use of Fast Fourier Transform (FFT) signal processing to calculate the wave speed and attenuation through a given specimen. It is the purpose of this thesis to implement the technique in the area of fiber reinforced composite materials. Since the method is relatively new it took some time before actual experimental results could be obtained. Many of the test results did help to produce a reliable measurement system.

SURVEY OF LITERATURE

The methods for detecting damage may be separated into two categories: 1) Destructive testing, and 2) Nondestructive Testing and Evaluation (NDTE). An example of destructive testing is the deply technique [4]. Composite test specimens are pyrolized after being impregnated with gold chloride diethylether solution. Upon unstacking, the laminate damage due to loading may be viewed with the use of a stereo microscope and fluorescent lamp. Destructive testing has one obvious drawback - the specimens are destroyed. Therefore, NDTE techniques are much more desirable from the veiwpoint of field applications.

Reifsnider, et al. [5] define NDTE as `...that activity associated with experimental schemes used to interrogate the state of stress and state of the material without influencing either of those states or altering the strength, stiffness, and life of the laminates being evaluated'. A complete description and comparison of NDTE techniques is given by Sendeckyj [6]. Nondestructive techniques such as surface replication, X-ray radiography, vibrothermography, holography, and liquid crystal coatings have been applied to composite materials by Stalnaker [7], Dance [8], Jones [9], Maddux [10], and Charles [11], respectively.

The main focus of the present research concerns the application of ultrasonics to assess damage in composite

materials due to fatigue or monotonic loading. Much work has been done in the area of Acoustic Emissions (AE). Whenever a micro-failure takes place (i.e., fiber breakage, matrix cracking, etc.) stress waves are emitted from the source. By monitoring a test specimen under loading with a triangular array of transducers one may locate the failure site by using the arrival times of the stress pulses received at the transducers. Bailey, Freeman, and Hamilton [12] used the above technique in conjunction with X-ray radiography to correlate AE signal amplitudes with different types of damage progression in fatigue loaded composite plates. R. Williams [13] has combined AE and thermography to monitor damage growth in boron/epoxy and boron/aluminum specimens subjected to fatigue loading. Arora and Tangri [14] used AE techniques to detect and continuously monitor subcritical crack growth in Zr-2.5% Nb. Block [15] tested a number of composite specimens and determined that AE events generated by fiber fracture have substantially higher peak amplitudes than those generated by resin-controlled mechanisms. Ulman [16] observed that an increase in AE count rate coincided with the onset of matrix plasticity and also damage development at high loads in metal matrix composites.

As reported by Williams and Egan [17] AE results contained in much of the literature are largely qualitative even though quantitative measures are often presented. Comparison of AE research is almost impossible due to the

insufficient reporting of the technique used. Also, due to the complexity of the problem, even within a single specimen a small change in stress may result in a number of AE events, some of which may initiate from different sources. Therefore, comparison of single AE events to one another will most likely not lead to source mechanism discrimination. However, by combining individual AE spectral densities to derive 'mean' normalized densities which in turn could be statistically analyzed, Williams and Egan were able to provide quantitative discrimination between AE from 10, 90, [±45,±45] degree specimens during tensile loading.

Another type of ultrasonic evaluation is the C-scan. Blake [18-21] has reported the application of C-scan digital systems to NDTE of composite materials. The technique involves coupling a transducer to the specimen and propagating longitudinal waves through the thickness direction. The same transducer is used to receive the reflected sound waves. The received signal may now be processed by analog or digital methods. Analyzing the signature formed by digitally monitoring the amplitude of a particular segment of a received ultrasonic waveform can lead to information regarding material discontinuities. Time domain representations of the wave form can be used to correlate discontinuities which appear similar in the amplitude signature. If an analog system is being used, the gated portion of the total waveform is peak-height

analyzed. In other words, the peak output is discretized to ten levels in 0.1 volt increments. Each increasing level corresponds to a darker shade of gray when transmitted to a pen amplifier. The pen burns the surface layers of an ink-impregnated, electrically conductive paper to produce a picture of the material integrity of the specimen. Alternatively, as in Blake's research, one could digitize the received signal. The digitized signal can then be processed by a computer. Peak data (voltages) are sent through a microprocessor which performs gray scale conversions and in turn sends the data to either a dot matrix prirter, an analog conductive paper system, or a color graphics system. Chang, et al. [22,23] have developed an in-service inspection system (ISIS) which can produce hard-copy real time plots and post-inspection C-scans to be used in production hand scanning. Post-inspection flaw magnification, flaw-amplitude listing, and RF (radio frequency) waveform digitization are the major advantages of the ISIS. Kiraly and Meyn [24] have developed a computer controlled scanning system to monitor the initiation and progression of local damage patterns in composite specimens under tensile loading. While scanning a specimen, a 16-level gray scale image is displayed on a CRT and stored on a floppy disk. The images may be stored in sequence of load step which can be played back to create a movie showing damage growth as a function of loading. Daniel [25] has conducted C-scan evaluations of fatigue loaded specimens

with temperature and moisture variations to monitor flaw growth in graphite/epoxy laminates containing initial flaws. Liber [26] has used C-scan to determine damage behavior in flat and cylindrical composite specimens with pre-existing flaws. The limitation of the C-scan technique is that it only works with relatively large delamination flaws; it yields little information about other flaw types. However, the technique is useful in that it provides a pictorial view of specimen quality.

In the work done by Dreumal and Speijer [27,28] a technique called Polar Scan was developed which can generate an image that is a unique fingerprint of a specific laminate. The technique involves rotating the particular specimen of interest between two transducers and monitoring the amplitude of the through transmitted ultrasonic wave. In this way layer orientation and stacking sequence may be determined. In the same manner as C-scan, the signal is transformed into brightness modulation to be viewed on a video screen.

In a series of papers Vary and his co-workers [29-37] have studied the ultrasonic stress wave factor (SWF) and its relation to material characteristics. This technique works on the principle of energy dissipation in a material. During the failure of composites stress waves are generated which interact with the different plies to promote microcracking and crack extension. The effect of the stress waves is restricted by the amount of scattering,

dispersion, and reflections due to microstructure and boundary conditions of the specimen. Broad-band ultrasonic pulses are propagated at normal incidence to the specimen by a transducer. A stress wave is excited by the pulses and travels in the lengthwise direction where it is received by another ultrasonic transducer. The received signal consists of a great number of oscillations due to multiple reverberations in the specimen. In order to analyze the signal Vary defines the SWF as E=(R)*(T)*(C). SWF is a measure of the efficiency of stress wave energy transmission, R is the pulse repetition rate, T is an interval of time predetermined for the reset timer of the receiver circuit, and C is the number of ringdown oscillations exceeding a preset threshold voltage. Vary has shown that microvoid content, ultimate tensile strength, cure pressure, and interlaminar shear strength all effect the value of SWF. Also, the SWF was determined at various positions along specimens and the location of minimum values of SWF correlated with the actual failure sites when the specimens were loaded to failure.

Following Vary, Williams, et al. [38-42] have studied the effect of fatigue and impact loading on SWF and attenuation. In earlier works with metals, Truell and Hikata [43] established a relation between the attenuation and number of recorded fatigue cycles in aluminum. Joshi and Green [44] have successfully used attenuation to monitor fatigue damage in polycrystalline aluminum and

steel specimens. Williams and Doll [38] have monitored attenuation and wave velocity in the frequency range of 0.5 to 2 MHz in compression-compression fatigue loaded unidirectional composites. Within ±5% accuracy, no change in wave velocity as a function of fatigue was detected. However, initial attenuation above 1.5 MHz was found to be a good indicator of relative fatigue life. Williams and Lampert [42] determined that impact damage in graphite fiber composites can be assessed quantitatively using either the through the thickness attenuation or the SWF. Williams, Hashemi, and Lee [41] conducted a complete study of ultrasonic attenuation and velocity in AS/3501-6 composites. In the range of 0.25 to 14 MHz they found the wave velocity to be frequency independent although attenuation was frequency dependent. Williams, Yuce, and Lee [39] measured the attenuation at 4 MHz through composite specimens which varied in cure temperature and pressures and found good correlation with the number of fatigue cycles to failure and an increase in attenuation. Hayford, et al. [45] determined correlations between initial attenuation and shear strength in graphite polyamide composites. Henneke, et al. [46] have also studied the relation between SWF and fatigue life in composite materials. Talreja [47] has applied spectral frequency analysis and obtained close agreement between spectral density and stiffness changes. Nimmer [48] has used attenuation and wave velocity to monitor damage

accumulation in composite flywheel disks. Hemann [49] has conducted a study of the effect of stress on ultrasonic pulses in fibrous composites. The velocities were found to be frequency dependent, but weakly dependent on the stress in the specimen.

The anisotropy of composite materials can greatly complicate the interpretation of the received ultrasonic signal. Kriz, et al. [50-52] and Kinra and Eden [53] have applied the solutions of the Christoffel equations [54] to graphically depict stiffness, longitudinal wave velocity, and shear wave velocity variations in specified planes for graphite/epoxy laminates. Deviations between wave propagation direction and energy propagation were found to be as large as 60 degrees. This has some rather interesting implications concerning the interpretation of received ultrasonic pulses. Kriz [51], Tauchert and Guzelsu [55,56] have experimentally determined elastic moduli by relating wave velocity measurements in various propagation directions to stiffness.

The previous velocity measurements in composites have relied on monitoring the time-of-flight of a through transmitted pulse. This technique works well if the specimen is thick. If it is too thin, then multiple reflections within the composite from the front and back surfaces may interfere with the received wave packet. In order to alleviate this problem a new technique, ultrasonic spectroscopy, has been investigated. Chang, et al., have

utilized the connection of resonance and frequency to determine wave velocities in thin composite specimens within ±2% [57].

THEORY OF OPERATION

A complete derivation of the governing equations is given in Reference 58, but for continuity in the discussion of the measurement technique a brief summary is presented here.

First, consider a compressional wave travelling through medium 1 (for our case medium 1 is water) striking the specimen, medium 2, as shown in Figure 1. A portion of the wave, f(t), is reflected at the front surface, and the rest enters the specimen and is reflected at the back surface, s(t). Of course, multiple reflections propagate back and forth between the two surfaces, but for now consider only s(t). From Ref. 58 if we let $S^*(\omega)$ and $F^*(\omega)$ be the inverse Fourier Transforms of s(t) and f(t), respectively, then it can be shown that

$$\frac{S^*(\omega)}{F^*(\omega)} = \alpha R_{21}^2 \, e^{-i2kh} \tag{1}$$

where

$$\alpha = \frac{T_{21} T_{12}}{R_{21} R_{12}} \tag{2}$$

$$R_{12} = \frac{\rho_1 C_1 - \rho_2 C_2}{\rho_1 C_1 + \rho_2 C_2} \quad , \quad R_{21} = -R_{12} \tag{3}$$

$$T_{12} = \frac{2\rho_1 C_1}{\rho_1 C_1 + \rho_2 C_2} \quad , \quad T_{21} = 2 - T_{12} \, . \tag{4}$$

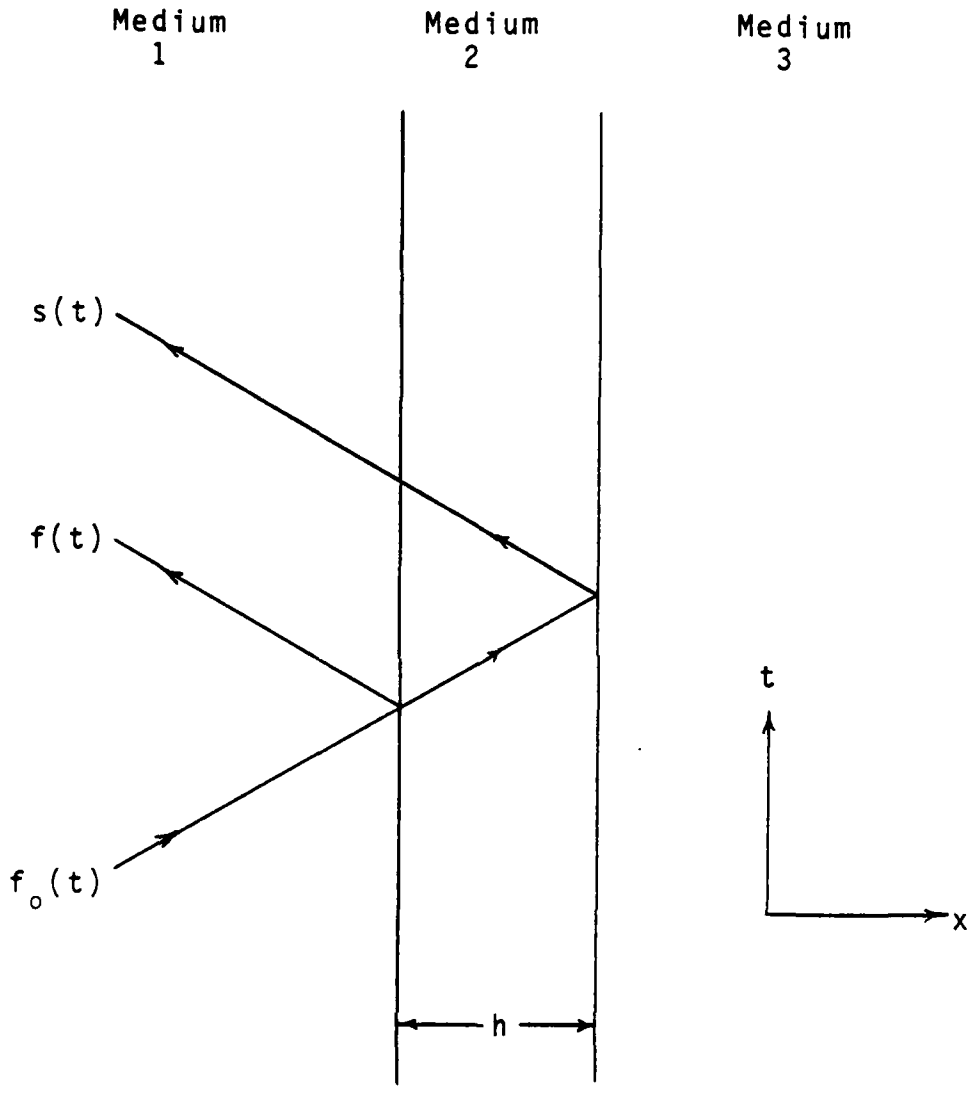

Figure 1. Problem description.

k is the complex wave number ($k=k_1+ik_2$), h is the specimen thickness, R_{12} is the reflection coefficient in medium 1 at its interface with medium 2, and T_{12} is the transmission coefficient from medium 1 into 2; R_{21} and T_{21} have similar interpretations. C is the wave speed, and ρ is the density.

Substituting for α into equation 1, and recognizing the real and imaginary parts of $S^*(\omega)$ and $F^*(\omega)$ we have,

$$Me^{i\phi} = T_{21}T_{12}e^{-i2kh} \tag{5}$$

where

$$M = \frac{|S^*(\omega)|}{|F^*(\omega)|} \quad , \text{ and} \tag{6}$$

ϕ is the phase difference between the second reflection and the first reflection.

Substituting $k=k_1+ik_2$ into equation 5, where $k_1=2\pi f/C$, k_2 is the attenuation, and f is the frequency, we have,

$$Me^{i\phi} = T_{21}T_{12}e^{2k_2h}e^{-i2k_1h}. \tag{7}$$

Next, equating the amplitudes and then taking the natural log of each side gives

$$k_1 = \phi/2h = 2\pi f/C \quad , \tag{8}$$

or

$$\text{wave speed} = C = 4\pi h/(\phi/f) \quad , \text{ and} \qquad (9)$$

$$\text{attenuation} = k_2 = [\ln M - \ln(T_{21}T_{12})]/2h. \qquad (10)$$

In this study attenuation is expressed in terms of the normalized quantity $k_2\lambda$, where λ, the wavelength, equals C/f.

Therefore, to calculate the wave speed one must take the Fourier transforms of the first and second reflections, extract the phase information from each, calculate the phase difference between the two, and then plot this phase difference versus frequency. From this plot the slope ϕ/f is obtained and used in equation 9, to calculate the wave speed.

The attenuation is calculated using the amplitude information given by the Fourier transforms. These data are substituted into equation 10 for M.

EXPERIMENTAL PROCEDURE

Equipment Setup

Figure 2 is an overview of the equipment used. The experiment is initiated at the pulser/receiver (Panametrics Ultrasonic Analyzer Model 5052UA). The analyzer is a broadband ultrasonic device which includes a pulser, a receiver, a stepless gate, and an assortment of damping and energy controls. The analyzer sends a broadband pulse of approximately 300 volts peak-to-peak to the transducer at a repetition rate selected by the operator. At the same instant (taken as time t=0) a triggering pulse is sent to the digitizing oscilloscope (Data Precision Model Data 6000). The transducer launches a compressional wave in water towards the specimen. The same transducer is used to receive the reflected signals from the specimen. The signals are then sent back through the analyzer where the stepless gate is used to isolate the desired portion of the waveform from the spurious signals. From the analyzer the gated waveform is sent to the Data 6000 for signal processing. All Fast Fourier Transform (FFT) computations are performed at the Data 6000 and the results are sent to the Minc PDP 11/23 through an IEEE 488 bus line at which time the data are used to calculate the wave speed and attenuation.

Figure 3 is a picture of the water tank. Although not shown, the tank was insulated with 3/4 inch styrofoam for

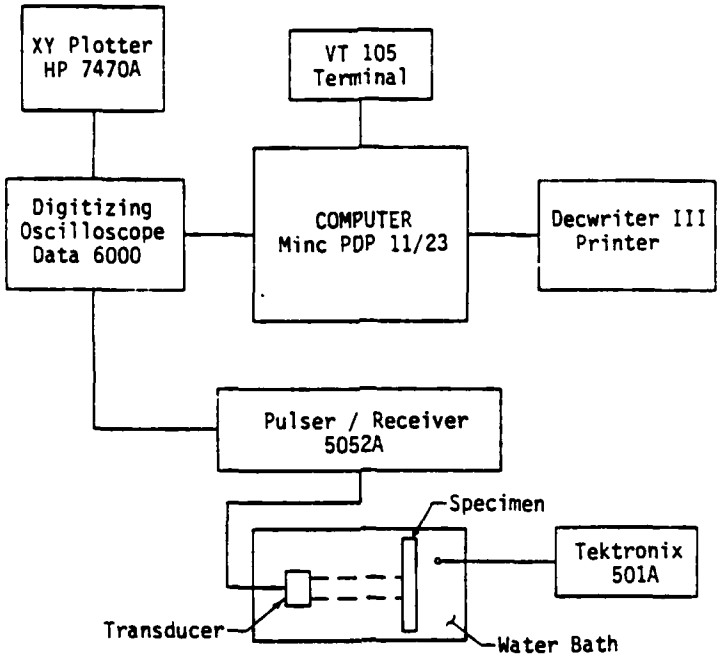

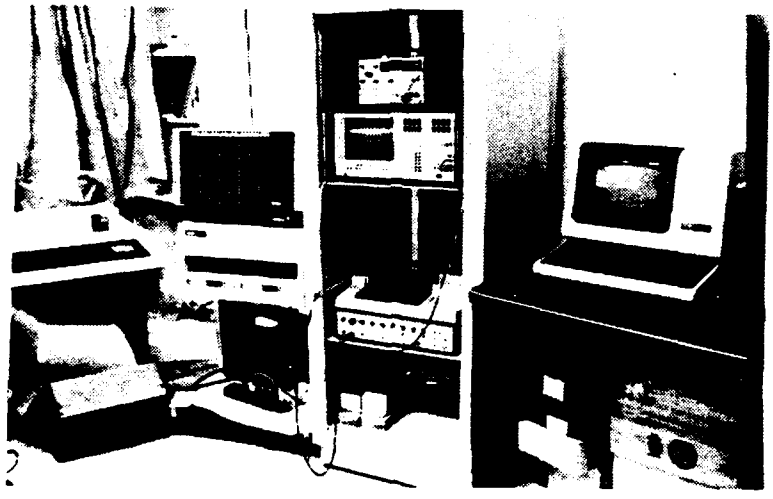

Figure 2. Equipment schematic.

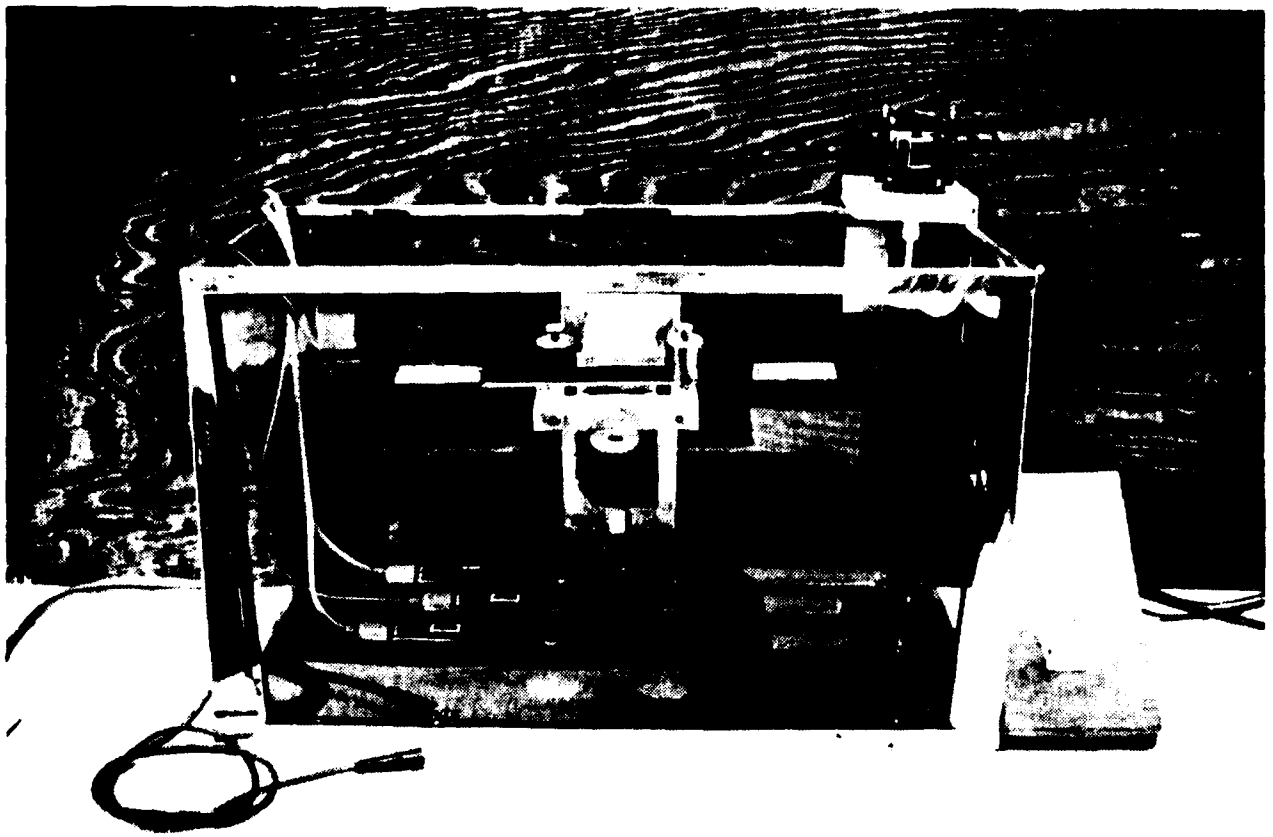

Figure 3. Water tank.

better temperature control. Located at the bottom of the tank are three thermostatically-controlled submersible heaters. The heaters were used to maintain the tank's water temperature within ±0.5°C during the tests. The tank was also equipped with a small electric fan which was used to stir the water and eliminate temperature gradients. The fan was always turned off prior to a measurement and ample time was given for the water to become quiescent. Temperature was monitored using a Tektronix 501A Digital Multimeter and its associated platinum tipped probe.

Specimen Preparation

All composite specimens were fabricated using Magnamite AS4/3502 graphite prepreg tape supplied by Hercules Incorporated. The prepreg tape came in the form of 12 inch wide rolls and was stored at 0°C until use. Magnamite AS4/3502 is an amine-cured epoxy resin reinforced with unidirectional graphite fibers. The fibers are Hercules continuous type AS4 (high-strength) graphite filaments that have been surface-treated to increase the composite shear and transverse tensile strength. Hercules 3502 resin was developed to produce improved mechanical properties in temperature environments of 350°F.

Specimen layup geometry was chosen on the basis of a somewhat controllable damage mode (i.e., transverse matrix cracking). Also, it was the purpose of this investigation to determine how damage affects the propagation of

longitudinal waves. Therefore, complicated layups would yield a more complicated damage mode making it difficult to correlate specific changes in wave speed and attenuation to certain damage states. It was for the above reasons that only [0n,90n]s specimens were manufactured because when loaded the primary source of damage is transverse matrix cracking in the 90° plies. Table 1 , page 21, gives a listing of the geometries chosen.

The laminates were layed up in accordance with the method used by the Vought Corporation. The press used for the curing process was designed at Texas A&M University from a similar press located at General Dynamics Ft. Worth Division. The press is controlled through a microprocessor which regulates temperature, pressure, and vacuum. The microprocessor was programmed to perform the manufacturer's curing profiles in Figure 4. After curing, the composite plates were cut into 1 inch wide by 11 inch long test specimens using a Precision slicing and dicing diamond saw made by Micromech MFG. Corporation. The edges of the specimens were then polished with 0.5μm and then 0.1μm alumina powder in order to produce better quality edge replications. The ends of the specimens were tabbed with cross-ply fiberglass so as not to damage them during loading.

Loading Procedure

All loading of the specimens was performed on an

Table 1. Specimen Geometries

Specimen Number	Layup
A2	$[0_2/90_8/0_2]_S$
A3	$[0_2/90_8/0_2]_S$
B1	$[0_6/90_4/0_2]_S$
B2	$[0_6/90_4/0_2]_S$

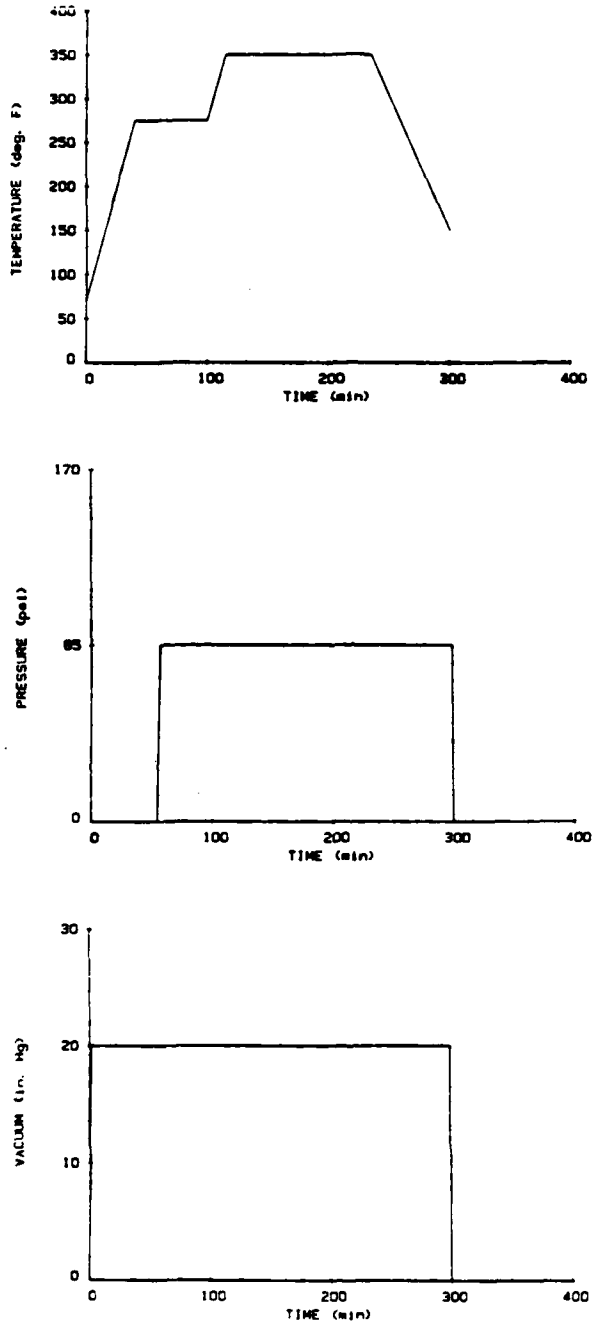

Figure 4. Cure cycles for AS4/3502 composite.

Instron Model 1125 equipped with a twenty thousand pound load cell. The tests were conducted at a crosshead speed of 0.05 in/min. The loading direction is given by Figure 5. Two inch wide wedge grips were used to hold the specimens in place. After loading, the specimens were reloaded to 1000 lb and edge replications were recorded. Replications were made by presoftening the replicating tape with acetone and then pressing this softened tape against the polished edge of the specimen. Upon hardening the tape was peeled off and could be viewed under a microfiche reader. Edge replications were taken from both edges at the end of each load step.

Transducer Selection

As stated earlier, the technique used for making wave speed and attenuation measurements involves the distinction between the front and back surface reflection from the specimen being analyzed. Since no previous work had been done, the choice of the transducer from which the best signal (i.e., clarity and pulse separation) would be obtained was done on a trial and error basis. The transducers which were examined for use in this investigation were 1.0, 2.25, 5.0, 7.5 and 10.0 MHz center-frequency. Figure 6a represents the signal from a $[0/90_3]s$ 8-ply laminate when analyzed by a 10.0 MHz transducer. It is obvious that the first reflection interferes with the second. Figure 6b is the signal from a $[0/90_4]s$ 10-ply

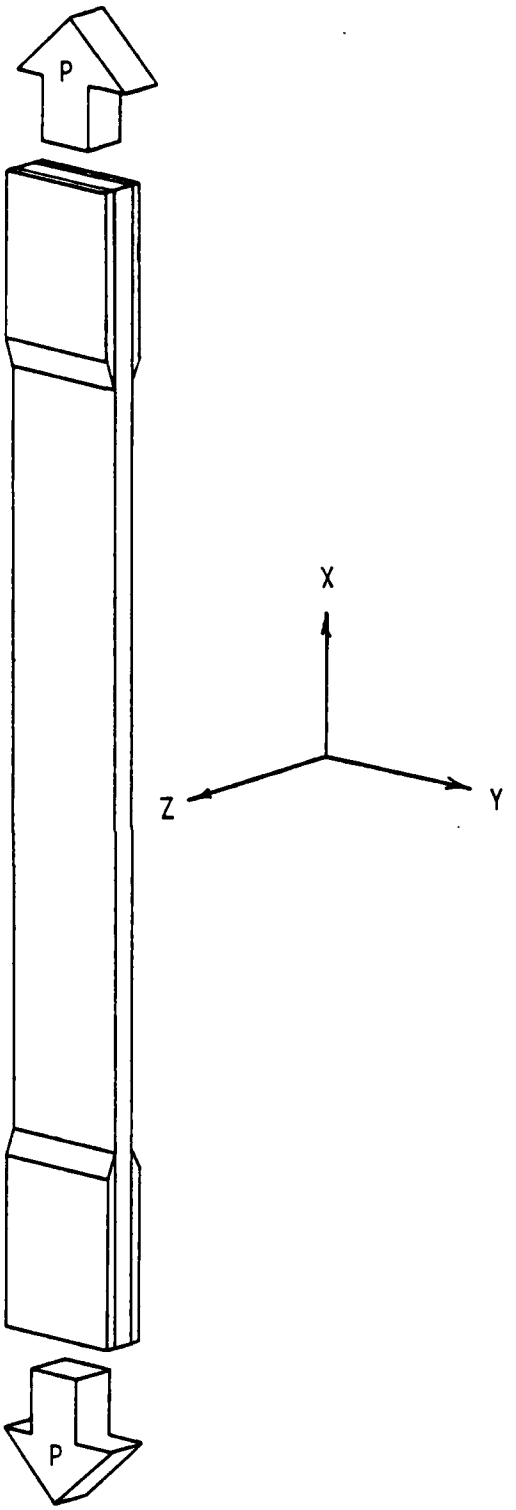

Figure 5. Loading direction and coordinate system.

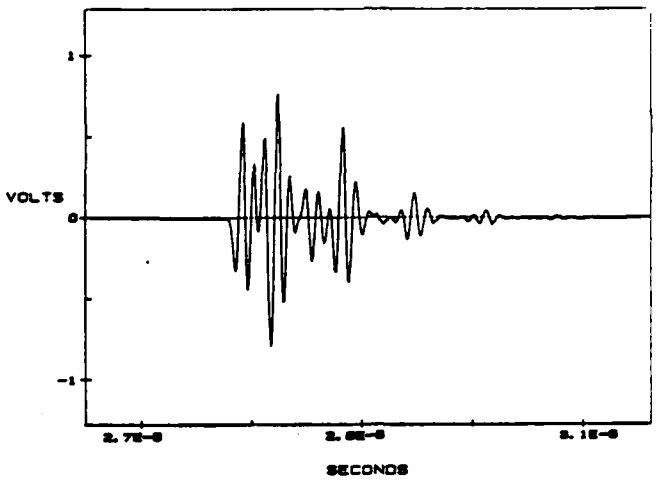

Figure 6a. Response for 8 ply at 10 MHz.

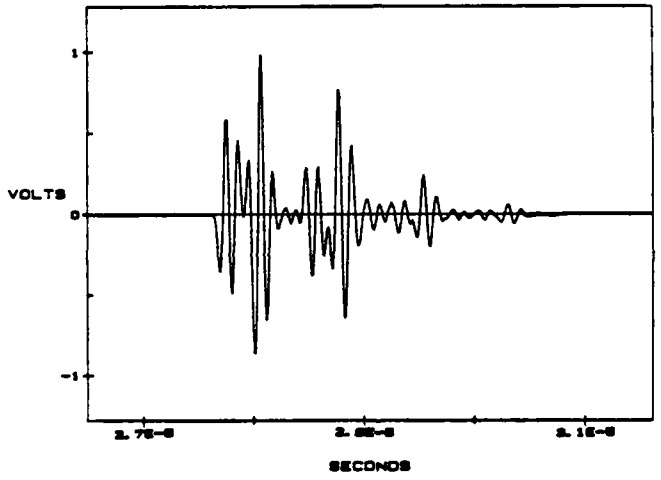

Figure 6b. Response for 10 ply at 10 MHz.

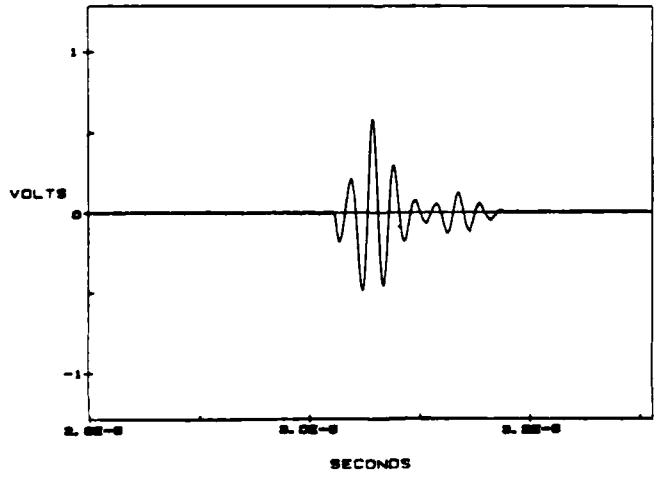

Figure 6c. Response for 10 ply at 5.0 MHz.

specimen. The beginning and ending points of the first two reflections are impossible to locate. Figure 6c is the same specimen as above, but now the transducer being used is 5.0 MHz. The signal is very clear, but it is still impossible to separate the two pulses. Figure 6c led us to believe that if a thicker specimen were used, then perhaps the front surface reflection would die out before the second reflection arrived. Accordingly, a 16-ply, $[0_2/90_2]_2s$ specimen was made to check the above conjecture. At 10.0 MHz, Figure 7a, separation was still very poor. However, when at 5.0 MHz transducer the signal received signal with the 16-ply specimen showed good clarity and fairly clear separation (Figure 7b). For continuity the 16-ply specimen was examined using a 2.25 and then a 1.0 MHz transducer (Figures 7c and 7d, respectively). The response for the 2.25 MHz indicated clarity was not a problem, but the separation was indistiguishable. At 1.0 MHz the signal became completely undefinable.

With the success of the 16-ply-5.0 MHz combination an 18-ply, $[0/90_2]_3s$ and a 24-ply, $[0_3/90_3]_3s$ were made in the hope of improving the signal at the other frequencies. Figures 8a and 8c show the response for the 18 and 24-ply specimens at 5.0 MHz. Clarity and separation are both acceptable. Figures 8b and 8d again show the responses for the 18 and 24-ply, but this time at 2.25 MHz. Both have acceptable clarity, but for the 18-ply separation of the two reflections is difficult. However, the 24-ply shows

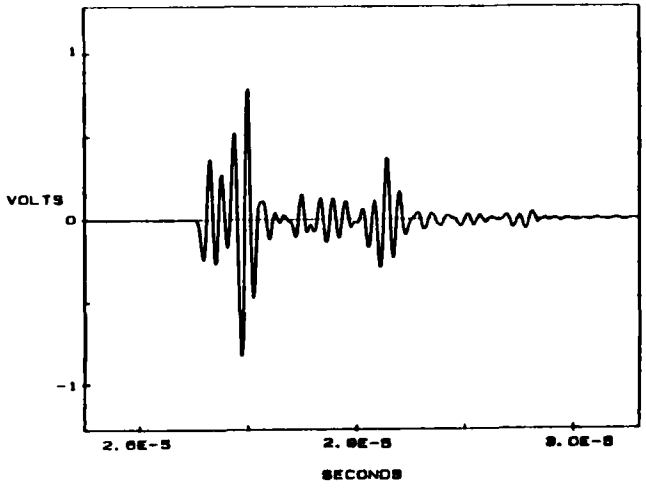

Figure 7a. Response for 16 ply at 10 MHz.

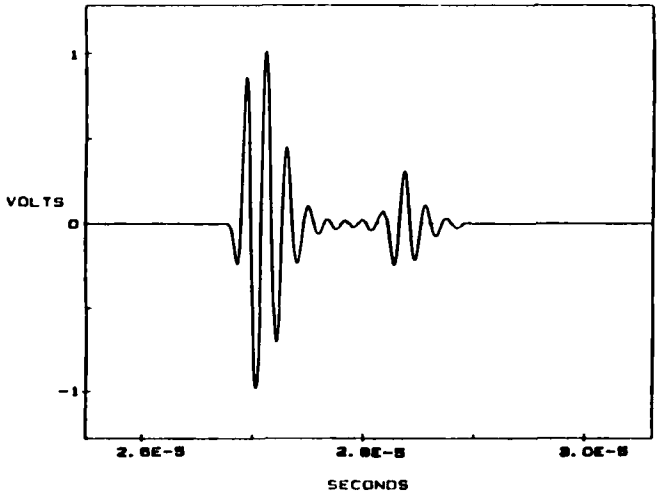

Figure 7b. Response for 16 ply at 5.0 MHz.

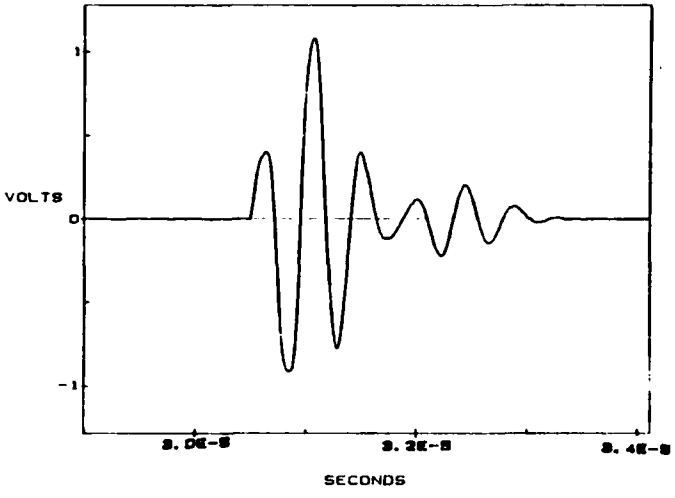

Figure 7c. Response for 16 ply at 2.25 MHz.

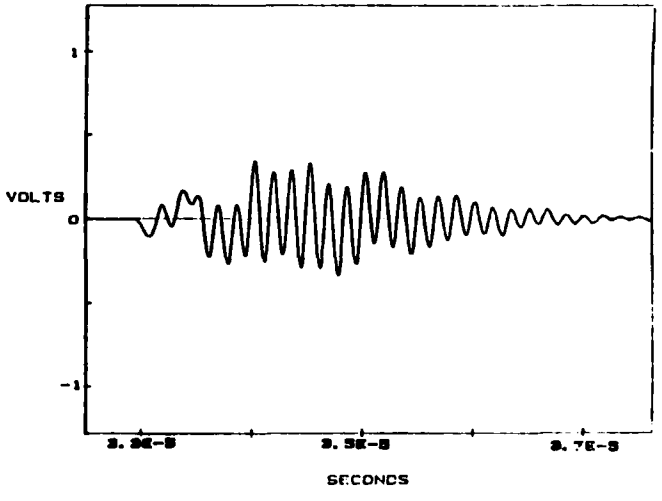

Figure 7d. Response for 16 ply at 7.5 MHz.

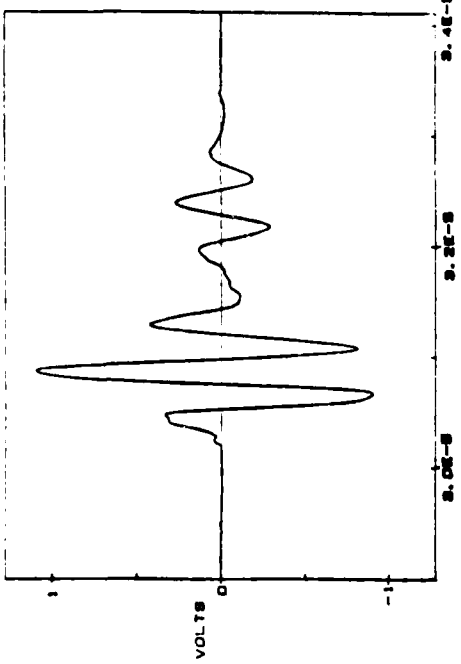

Figure 8a. Response for 18 ply at 5.0 MHz.

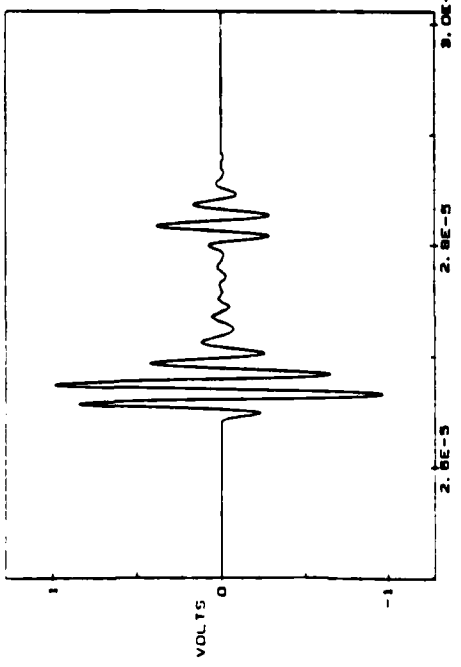

Figure 8b. Response for 18 ply at 2.25 MHz.

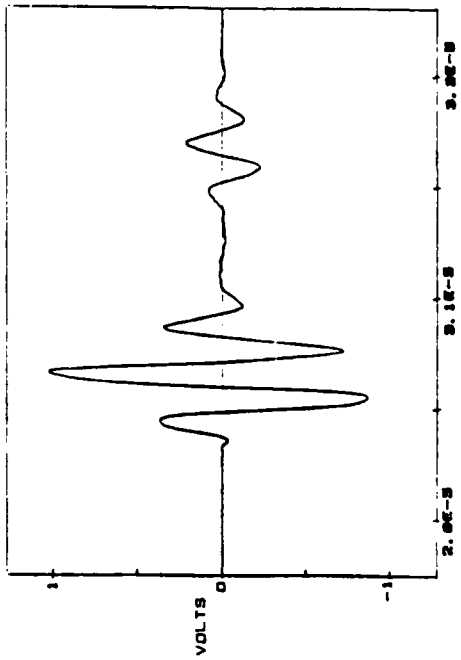

Figure 8c. Response for 24 ply at 5.0 MHz.

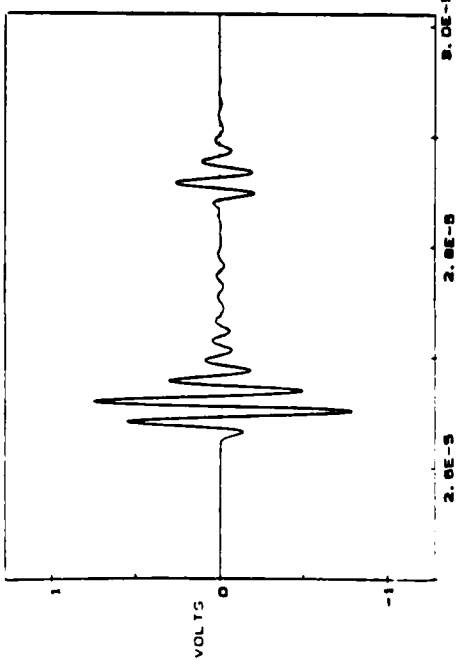

Figure 8d. Response for 24 ply at 2.25 MHz.

excellent separation. The 24-ply was then examined at 7.5 MHz (Figure 9). Clarity and separation were excellent. The responses for the 24-ply specimen at 10.0 and 1.0 MHz were still unacceptable. Therfore, in this study only 24-ply specimens were tested at 2.25, 5.0, and 7.5 MHz due to the consistent nature of both clarity and pulse separation. It should be mentioned that when we say the signal is unacceptable we mean that it is unacceptable for the pulse-echo technique under consideration. The signal still contains information about the specimen.

Transducer Modification

In order to insure that each transducer was interrogating the same area, a slight modification of the transducer's piezoelectric crystal was necessary. The transducers used had circular piezoelectric crystals of different diameters. Two problems arose from the circular crystals. The most obvious was that the larger diameter crystal would be examining a larger area on the specimen which could contain damage not seen by the smaller diameter transducers. This would make comparison of the results from each transducer impossible. Secondly, suppose a crack appeared at the edge of the transducer viewing area as opposed to the center (Figure 10). The crack at the edge would appear to be a smaller than its true length.

To alleviate the above problems a square window was attached to each transducer (Figure 11). The material used

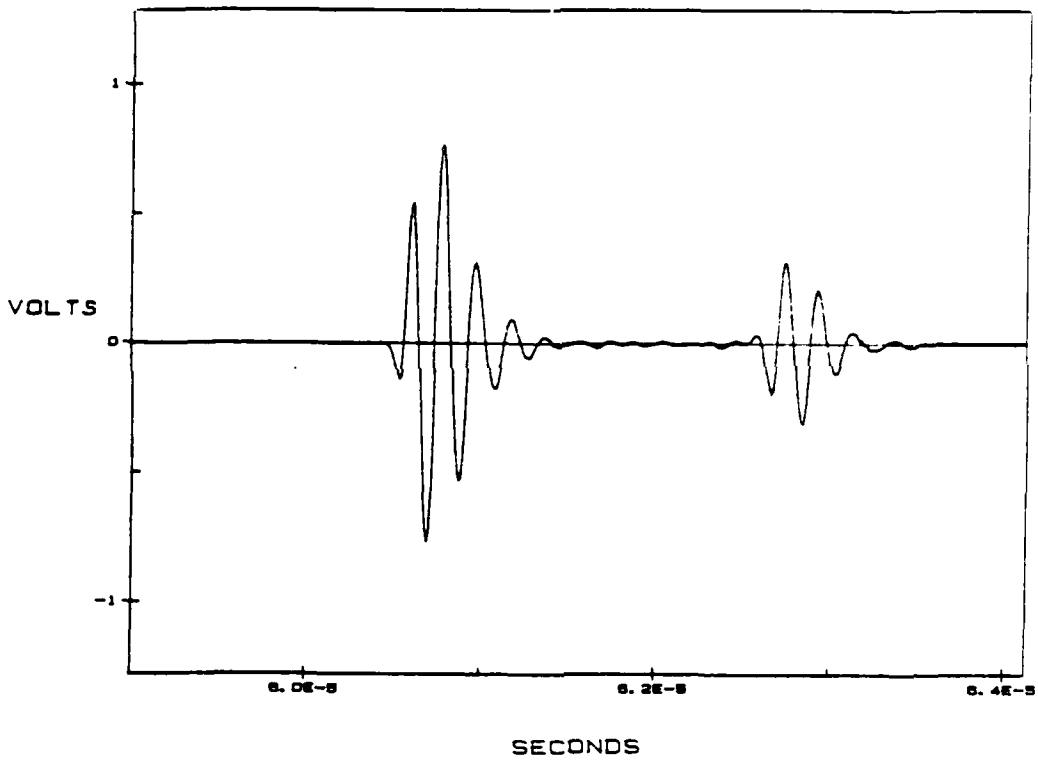

Figure 9. Response for 24 ply at 7.5 MHz.

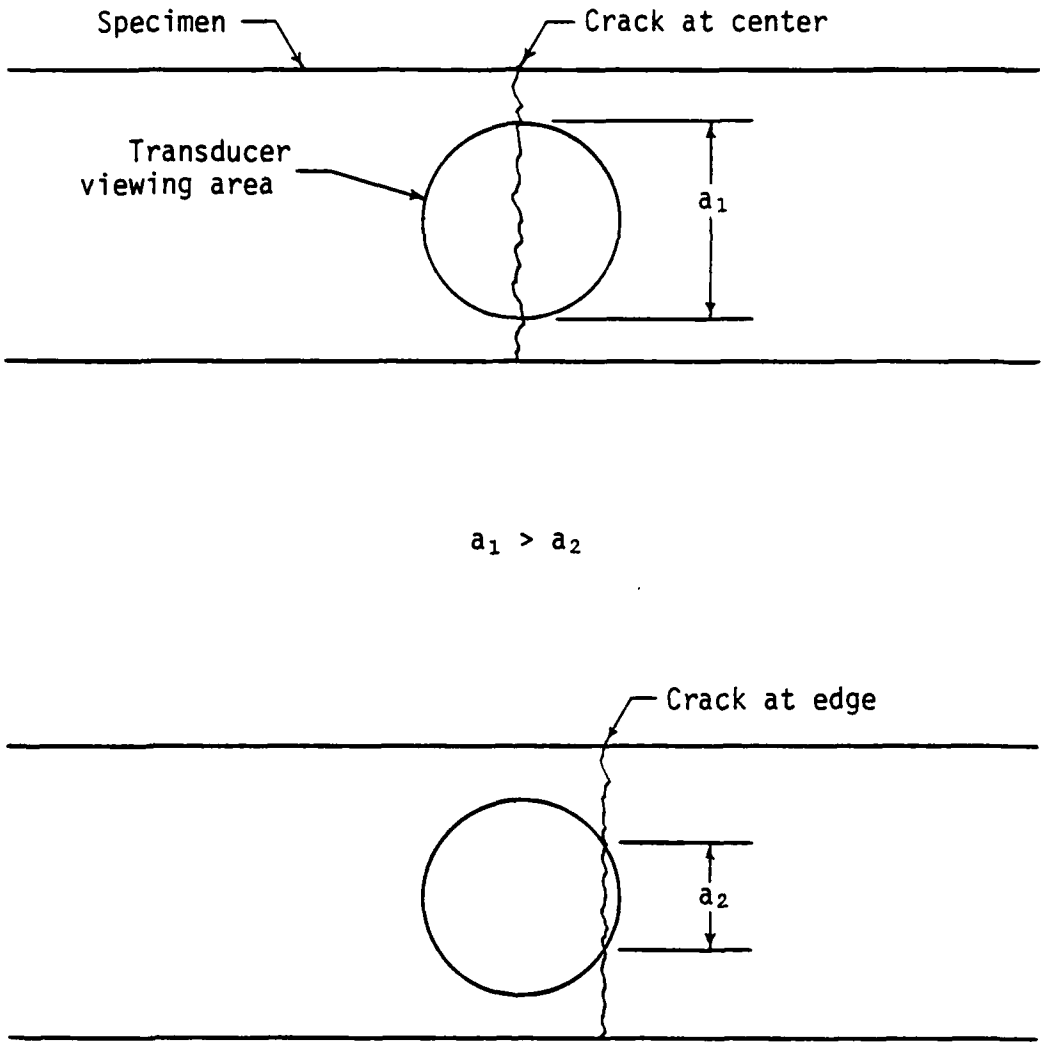

Figure 10. Effect of circular piezoelectric crystal on crack size.

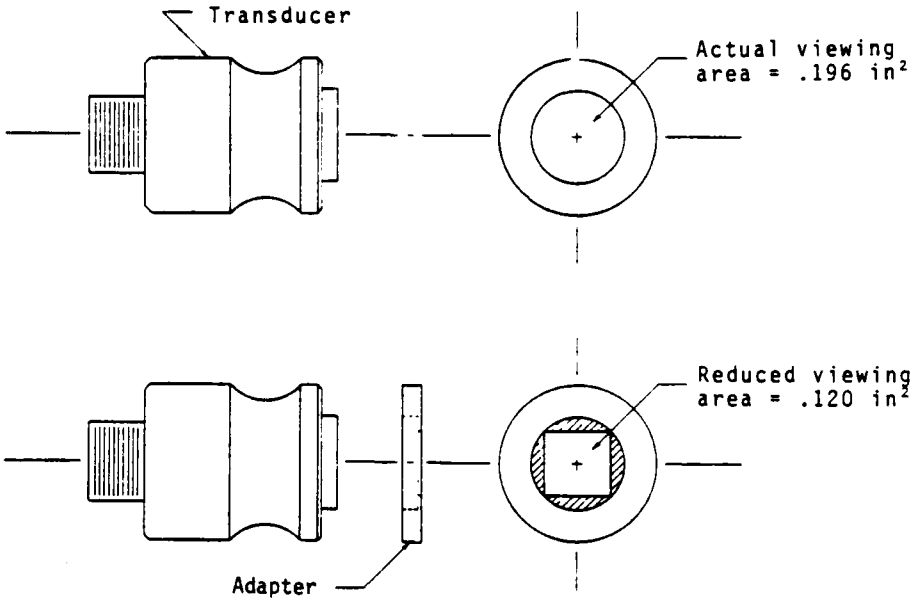

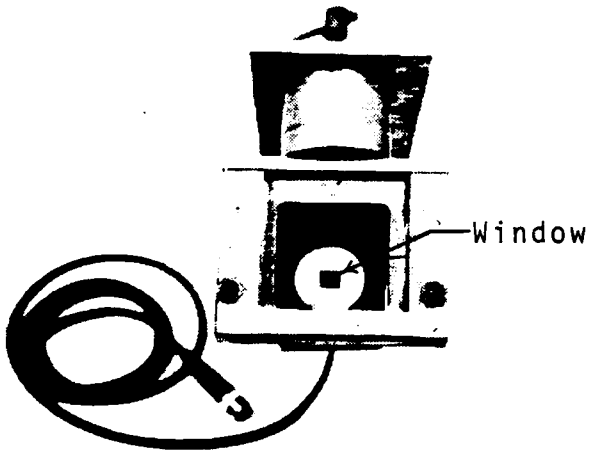

Figure 11. Square window modification.

to make the window had to be able to completely block all the signal not passing through the square window. It was found that by mixing PMMA polystyrene crystals with 382 Medical Grade Elastomer (room temperature curing silicon rubber) the signals at 2.25, 5.0, and 7.5 MHz would be totally blocked. This may be attributed to the comparable size of wavelength and PMMA particle size.

Wave Speed and Attenuation Measurements

Once the specimen had been loaded the last phase was to measure the wave speed and attenuation. First, the specimen was placed in the water bath and positioned at the desired location for measurement. Air bubbles that were attached to the specimen were swept off using a small paint brush. It was found that if one used one's finger to remove the bubbles this would leave a thin film of oil on the specimen. Figure 12a shows the multiple reflections from an aluminum specimen at 5.0 MHz. The stepless gate within the pulser/receiver is then used to isolate the front-surface reflection and the first back-surface reflection (Figure 12b). In order to process each signal individually a point of separation between the two reflections had to be chosen. From earlier tests with the 16 and 18-ply specimens at 5.0 MHz it was determined that picking a point closer to the end of the first reflection would prevent other problems from occurring as the loading progressed. For example, Figure 13a shows the response from an undamaged 18-ply

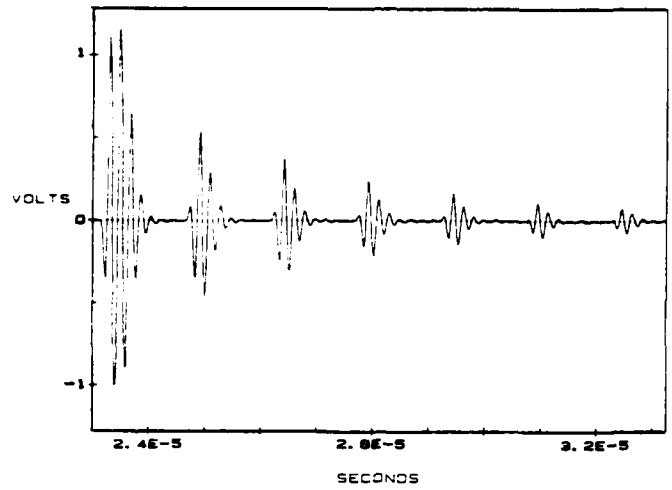

Figure 12a. Multiple reflections from aluminum at 5.0 MHz.

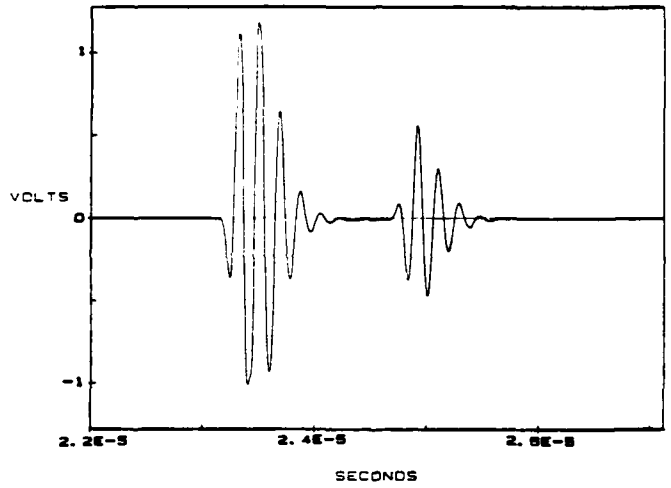

Figure 12b. Gated first and second reflections for aluminum.

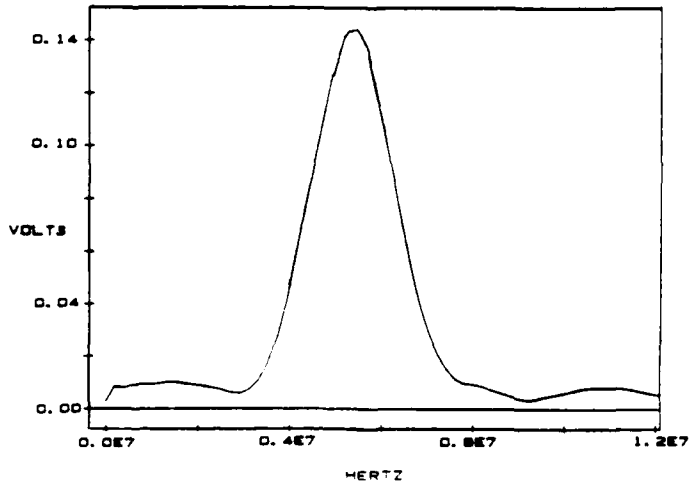

Figure 12c. FFT of first reflection off aluminum.

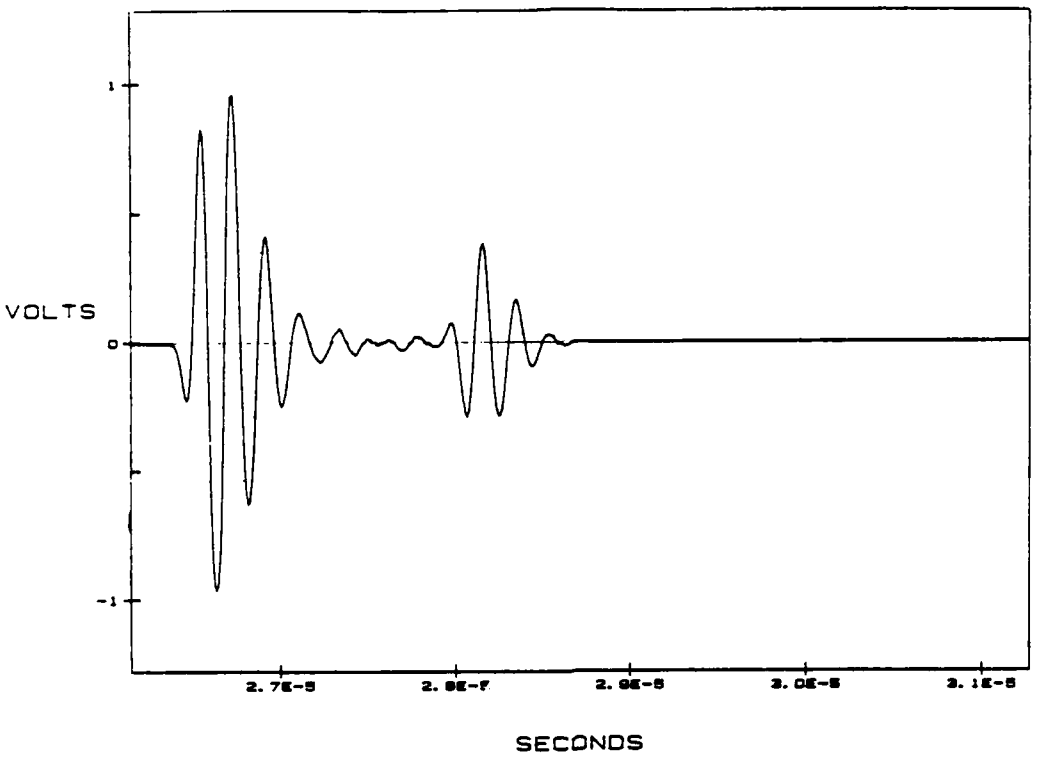

Figure 13a. Response for 18 ply at 5.0 MHz prior to loading.

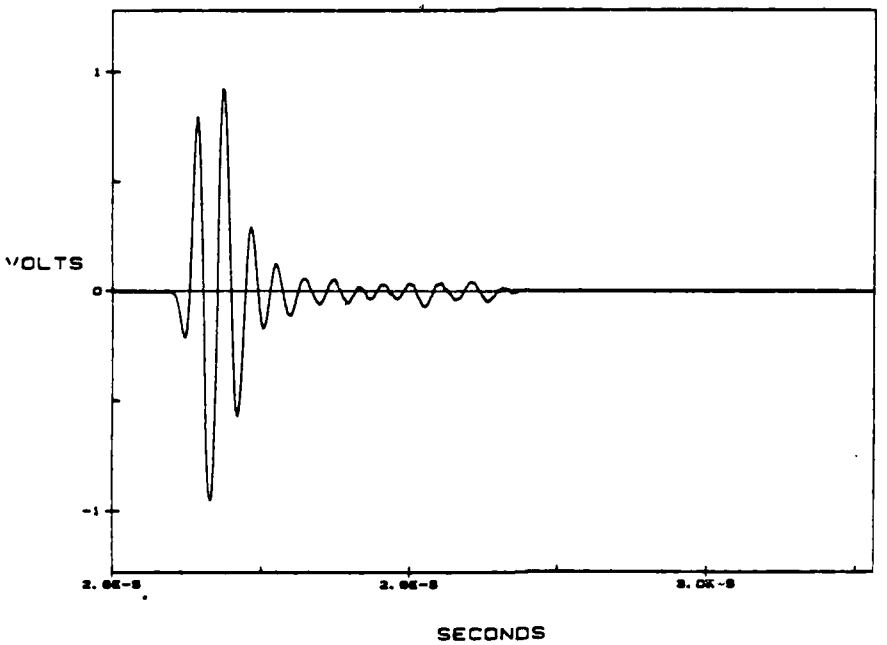

Figure 13b. Response for 18 ply at 5.0 MHz at 80% ultimate.

specimen at 5.0 MHz. The end of the front and the beginning of the back reflection are fairly distinguishable. Figure 13b shows the same specimen at 5.0 MHz, but here the specimen had been loaded to approximately 80% of its ultimate strength. Now there is no point of separation between the first and second reflections. What has happened is that the second pulse, which sees the inside of the specimen, has spread out due to its interaction and scattering with the large amount of damage in the interior. The above problem was another reason why only the 24-ply specimens were tested. The 24-ply specimens provided more room for the second reflection to spread out without interfering with the first reflection due to the increased pulse separation shown earlier.

The next step prior to running the program was to determine the range of frequency to be used when calculating the wave speed and attenuation. As stated earlier, the wave speed is computed using the slope of the phase vs. frequency plot. For demonstration, Figure 12c shows the FFT of the front surface reflection from the previous (Figure 12b) aluminum specimen at 5.0 MHz. The range chosen should be close to the center frequency to insure the response of the transducer outside its normal operating range will not be used. A generally good rule to follow is to pick a range where the magnitude is 25% of the center frequency on each side. Figure 14 shows the phase versus frequency plot for the aluminum specimen. The range

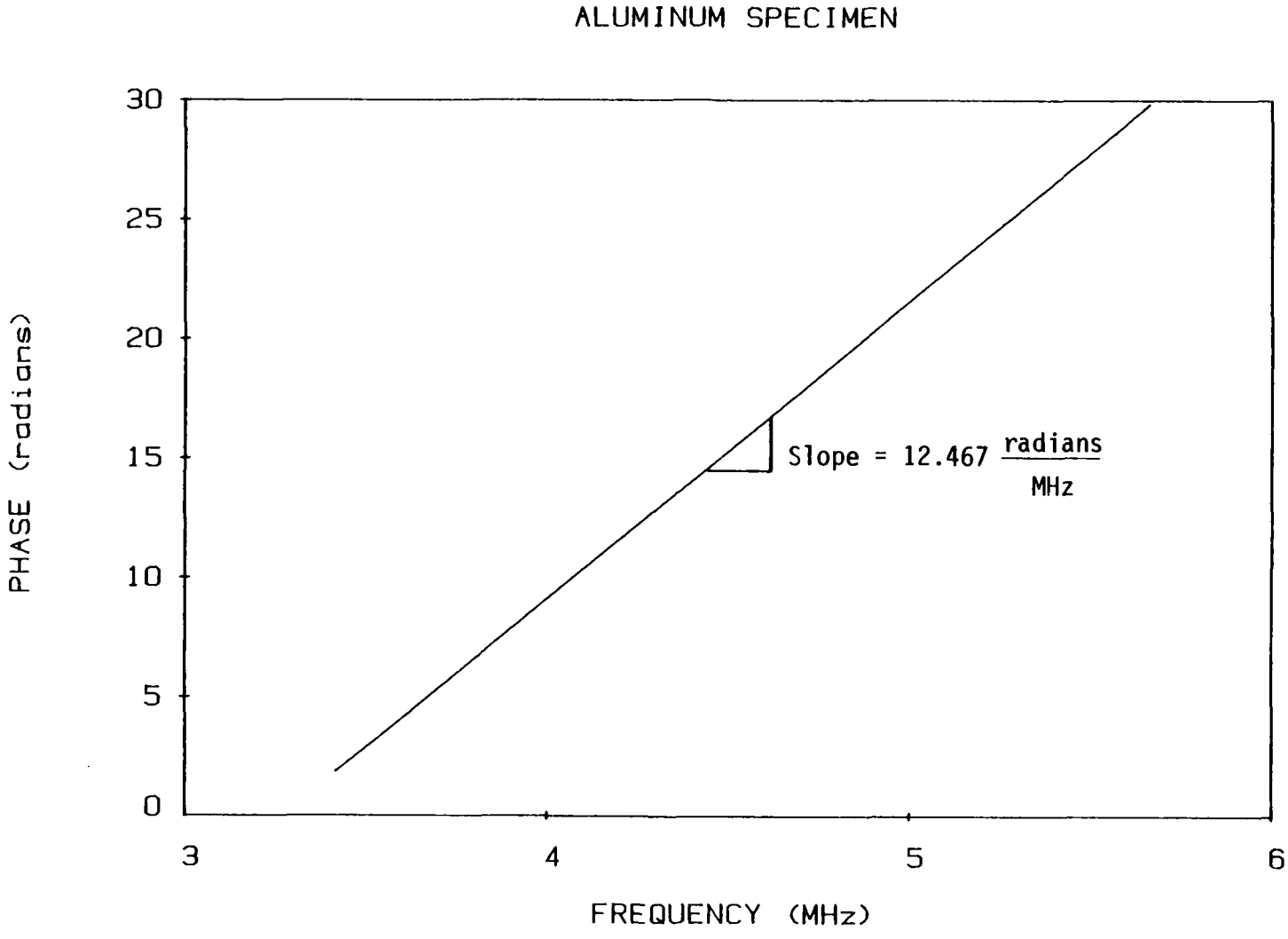

Figure 14. Phase versus frequency plot used in aluminum wave speed measurement.

of frequency used to evaluate the slope was from 3.4 to 5.75 MHz, as given by Figure 12c. At each position on the specimen the range for each transducer was chosen prior to loading and remained constant throughout the loading history.

All attenuation results are reported in terms of the quantity $k_2\lambda$ where k_2 is the complex part of the wave number k and λ=C/f (see theory of operation). At the start of the tests it was believed that the same range of frequency (for a particular transducer) used in computing wave speed could be carried over to the attenuation calculations. Figures 15a, 15b, and 15c show the plots of $k_2\lambda$ vs. frequency for a 24-ply specimen at 2.25, 5.0, and 7.5 MHz, respectively. The solid lines indicate the frequency range used in the determination of the wave speed. It is evident that over these ranges the attenuation varies greatly making it impossible to assign a specific value for $k_2\lambda$. For this reason the ranges were narrowed to eliminate some of the scatter. The new ranges are indicated by the dashed lines. The * indicates the averaged value of $k_2\lambda$ and is assigned to the mid-point of the frequency range. Figure 16 depicts the three values of $k_2\lambda$ determined from the previous figures.

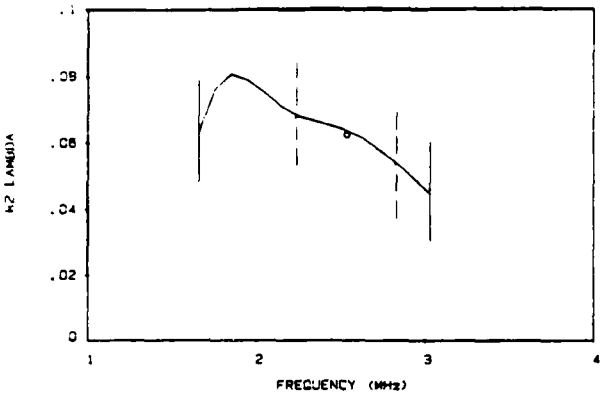

Figure 15a. Attenuation for 24 ply at 2.25 MHz.

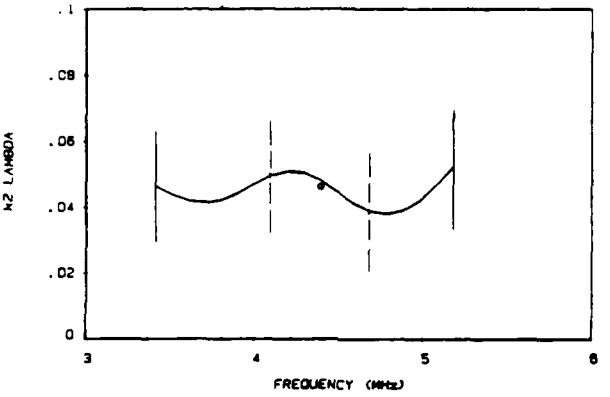

Figure 15b. Attenuation for 24 ply at 5.0 MHz.

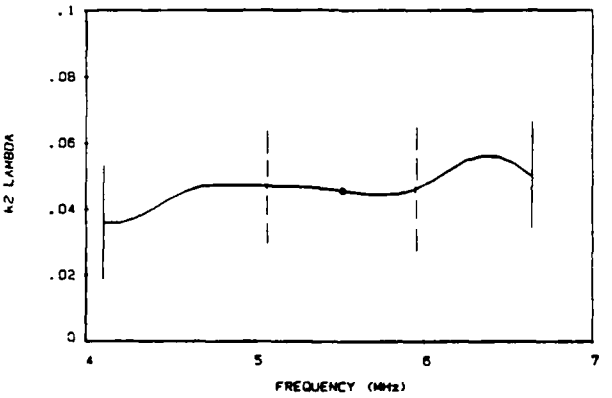

Figure 15c. Attenuation for 24 ply at 7.5 MHz.

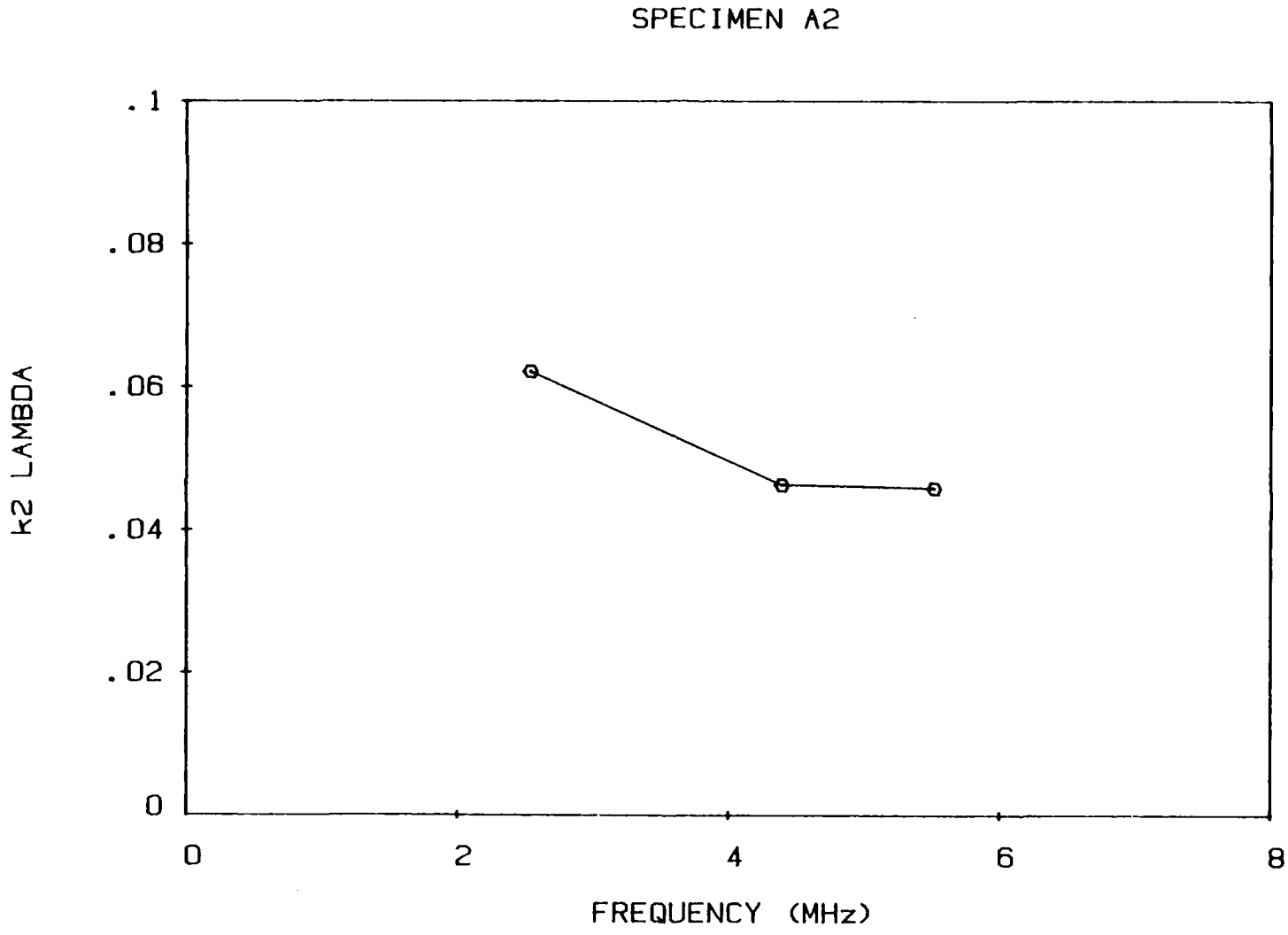

Figure 16. Averaged attenuation results obtained from Figure 15.

IMPROVEMENT OF MEASUREMENT TECHNIQUE

The main objective for using FFT signal processing was to achieve a very high level of precision in wave speed measurement (±0.1%) and attenuation measurement (±1.0%). The reason that FFT analysis is so powerful as opposed to time delay or amplitude measurements is that the FFT makes use of the fact that each point within the wave form contains information about the specimen. Time delay and amplitude measurements usually involve monitoring the position of only one point within a wave packet. In order to utlize the effectiveness of FFT signal processing all extraneous factors that affect the measurement technique had to be eliminated, if possible. To this date we have identified five major sources of error: 1) temperature, 2) water absorption, 3) positioning of the specimen, 4) repetition rate, and 5) FFT window choice.

Temperature

It is well known that in most materials the stiffness, and therefore the wave speed depends upon temperature. In order to carry out a well controlled experiment it was deemed essential to study the temperature dependence of the wave speed in composite materials. The temperature range investigated was from 6 to 30°C. Specimen 16-5, $[0_2/90_2]_2s$, was used for this investigation. From Figure 17 it was observed that over the temperature range of 6 to 30°C there

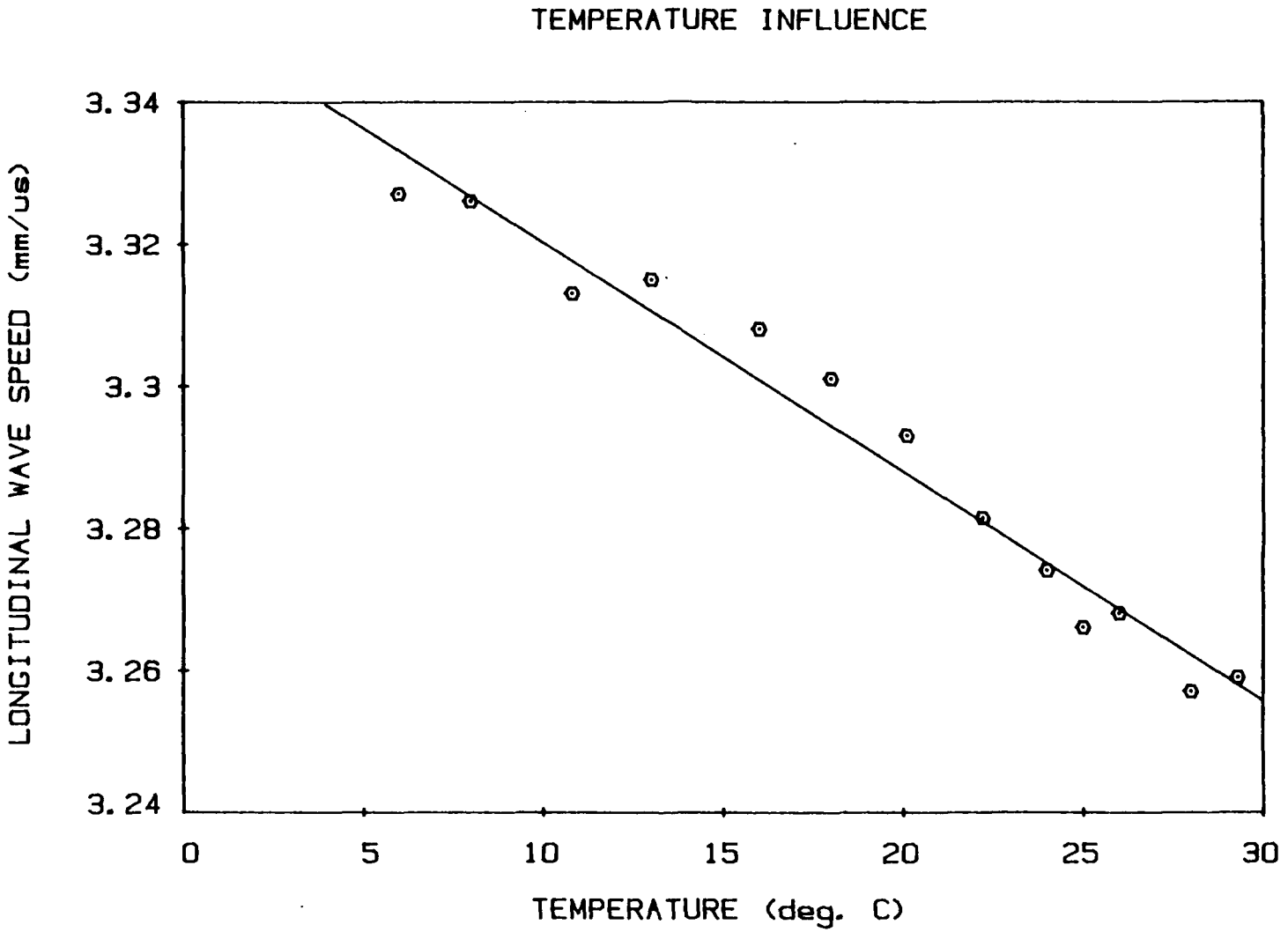

Figure 17. Effect of temperature on wave speed for composite specimen at 5.0 MHz.

was an approximately 2% decrease in the wave speed. The straight line is the result of a linear least squares fit. In the present set-up we have the capability to control the temperature to ±0.5°C. From Figure 17 it was found that a 0.5°C change in temperature corresponded to only a 0.05% change in wave velocity- the temperature contribution to the total error is about 0.05% which in view of the overall objective of ±0.1% is an acceptable figure.

Water Absorption

For [0n/90n] geometry laminates the major form of damage created by tensile loading is transverse matrix cracking. Since this technique involves water immersion it was of some concern that the damaged composite may be absorbing moisture via the newly created cracks. It was found that for highly damaged specimens water absorption during measurements could cause variations of ±3%. In order to eliminate this problem the specimen was dipped into a strippable rubber coating, made by Dupont, prior to submersion. The coating would dry in about 5 minutes and then could be peeled from the top and back surfaces leaving the edges sealed. This precaution measurably eliminated the problem.

Positioning

Due to the inconsistencies within a composite (i.e., matrix or fiber rich regions, thickness variations, surface

marks, etc.) a means for reproducing the same position of the transducer relative to the specimen was developed. Figure 18 represents the end result. First, the location tabs must be mounted on the specimen (Figure 19). These tabs allow for exact reproduction of three horizontal positions located on the specimen. The guides on the fixture keep the vertical position constant. The transducer location is permanantly fixed as well as the specimen holder. One-hundred gram weights were used to keep the specimen completely flat and also to insure the specimen did not move during the measurement. It was estimated that the position accuracy is within ±.001 inches.

Repetition Rate

As mentioned earlier a repetition rate is selected by the operator. In the early stages of this work, we selected a repetition rate of 5 kHz, for no particular reason. This means that the experiment was repeated every 0.2 milli-seconds (ms). Random errors as high as ±5% were observed. A careful examination of the experimental procedure revealed the following source of error. Suppose the transducer is energized at time t=0. It will take some time (say t_0) before the mechanical energy, propagating in the form of waves, will be completely dissipated. If the subsequent experiment is initiated at some time $t<t_0$, the results will be erroneous: the waves left over from the previous experiment will interfere with the waves of the present

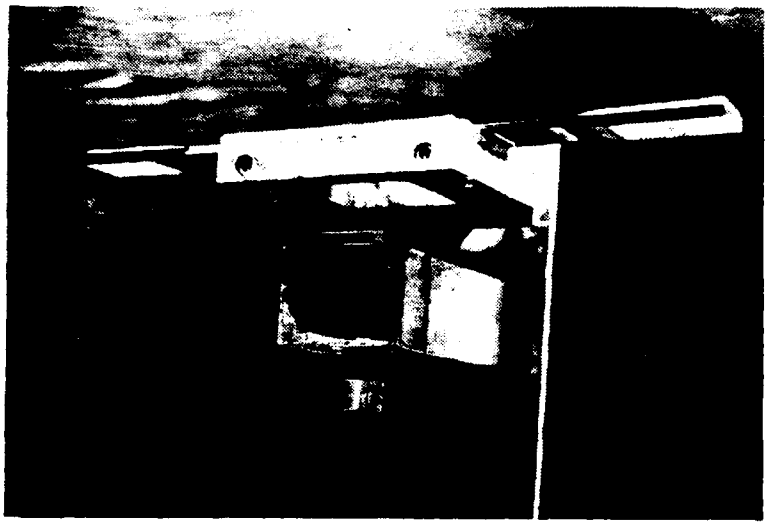

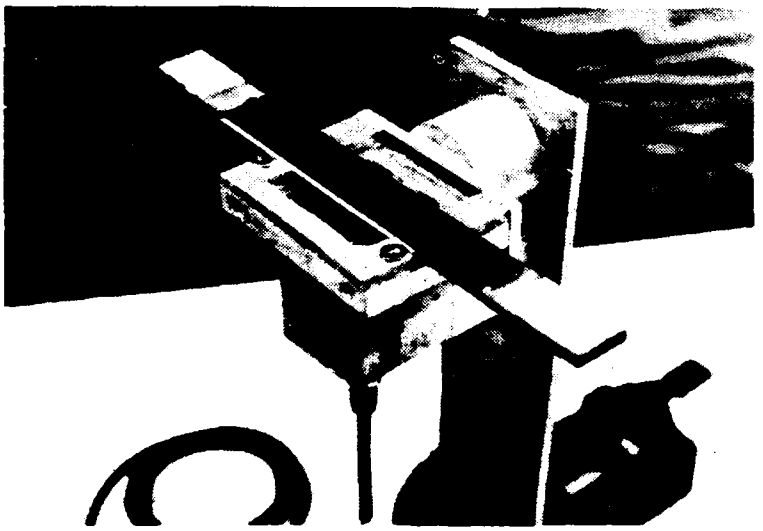

Figure 18. Specimen holder.

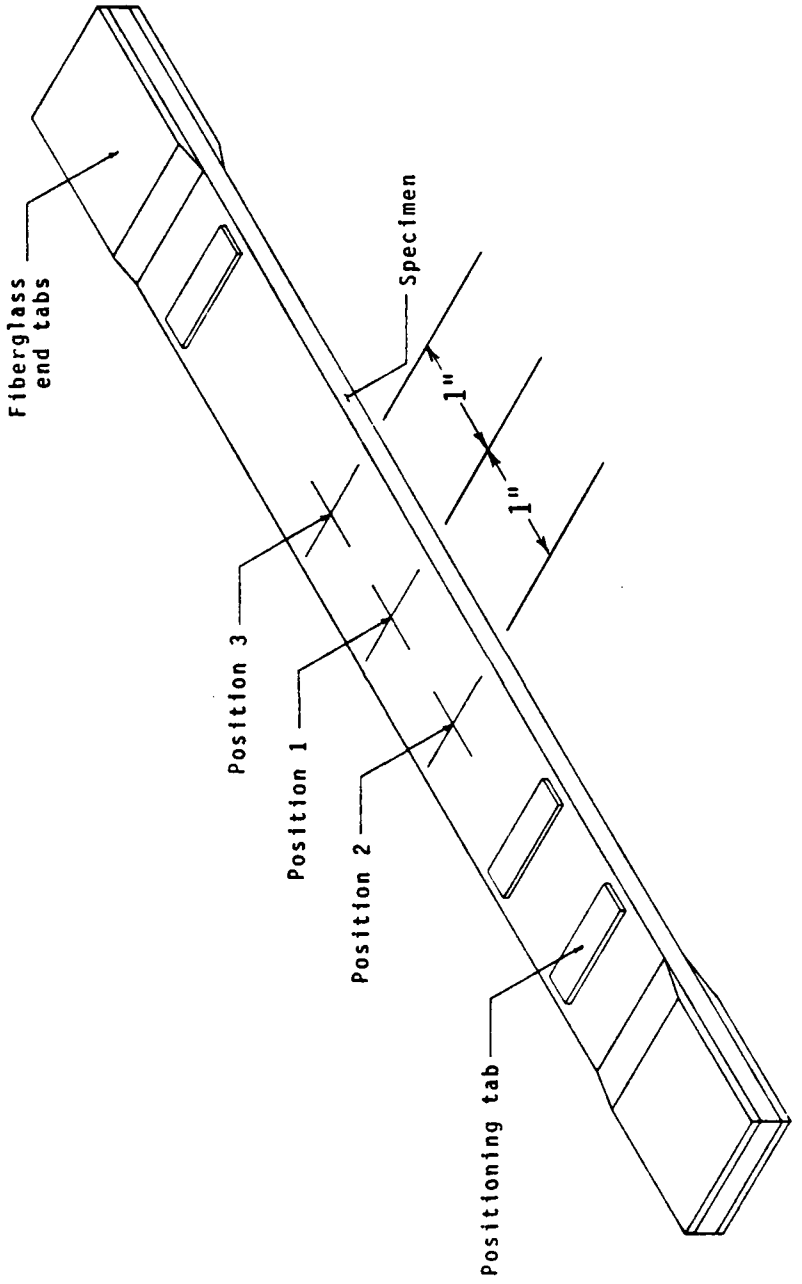

Figure 19. Specimen configuration.

experiment. This phenomenon sets an upper limit on the repetition rate (lower limit on the time between two experiments). By trial and error we found the upper limit on repetition rate to be 1 kHz. To eliminate the problem completely we chose a repetition rate of 500 Hz (i.e., time interval of 2.0 ms).

FFT Window Choice

The most common window used in FFT signal processing is the Hanning window. The Hanning window is a $\cos^2$ weighting function which smooths out the starting and stopping points of the signal to be processed. Through the course of technique preparation it was determined that the position of the pulse within the total signal length would greatly affect the output from the FFT. For example, suppose we have one pulse whose frequency contents we wish to examine. For brevity, Figure 20a shows only three positions along the signal length at which we have stopped to analyze the pulse. Figures 20b, 20c, and 20d are the corresponding FFTs for the three signal positions. It is apparent that the amplitudes of the frequency distributions reach a peak value at the center of the total signal. To determine how this affected wave speed measurements the above analysis was repeated using the front and back reflections from a piece of aluminum and then a composite. Wave speed was measured at constant intervals as the two pulses were moved along the signal length. Figures 21 and

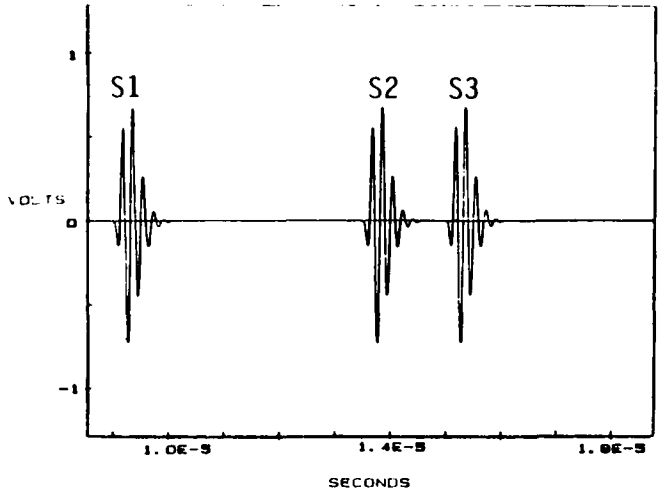

Figure 20a. First reflection at three positions along the total signal length (S1,S2,S3).

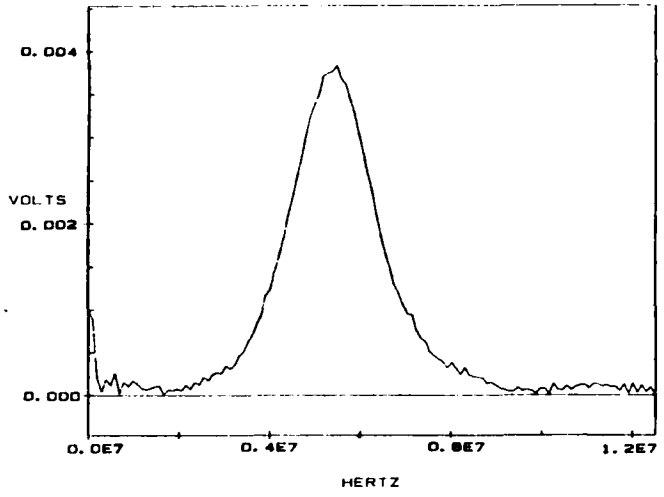

Figure 20b. FFT of first reflection at S1.

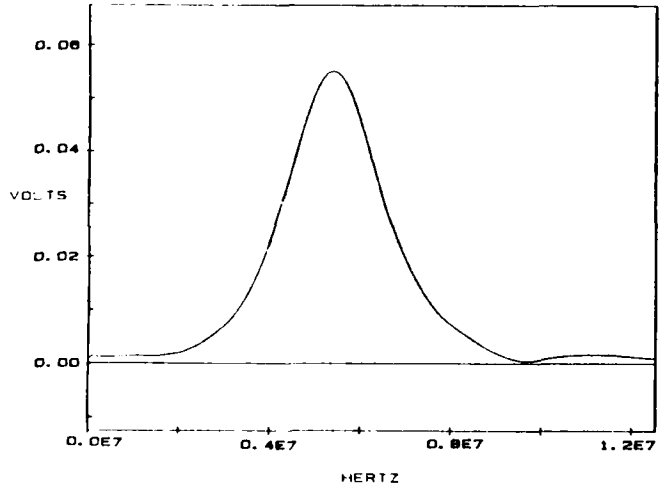

Figure 20c. FFT of first reflection at S2.

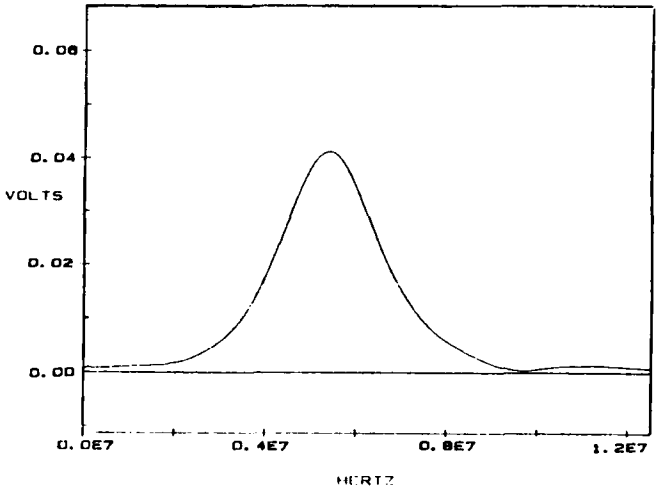

Figure 20d. FFT of first reflection at S3.

22 show the results for the aluminum and composite specimens, respectively. Both plots indicated a strong dependence of wave speed on position at the beginning and end of the total signal length. The relatively constant behavior of the wave speed towards the center led us to believe that the $\cos^2$ tapering effect of the Hanning window was the problem. Since the signals used in this investigation are well behaved (i.e., no jump discontinuities it was assumed that a rectangular window would yield better results because there would be no tapering. To verify this the above experiments were repeated using a rectangular window instead of a Hanning window. The rectangular window proved to eliminate position along the signal length as a source of error in wave speed measurements.

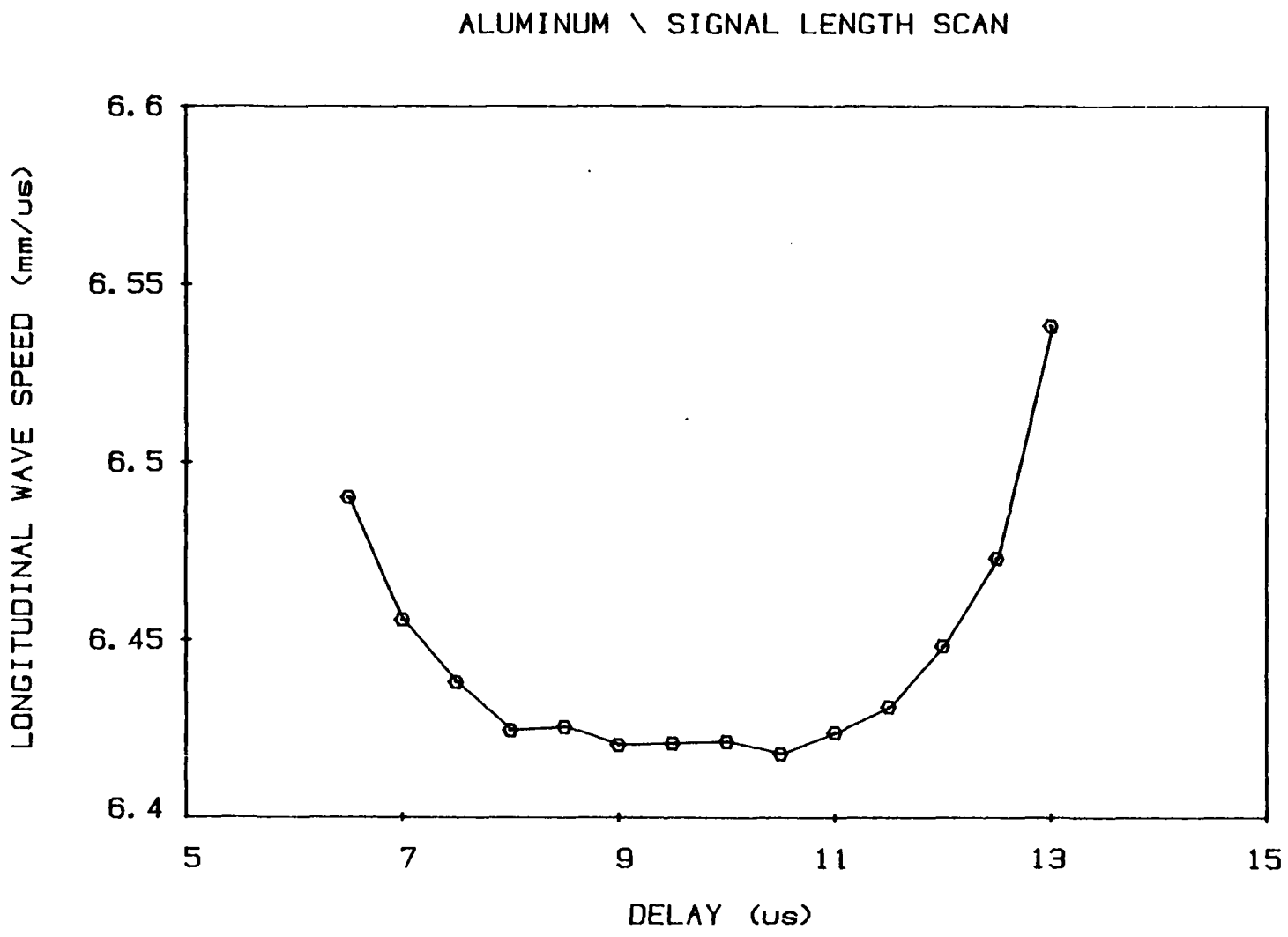

Figure 21. Effect of pulse position on wave speed for aluminum.

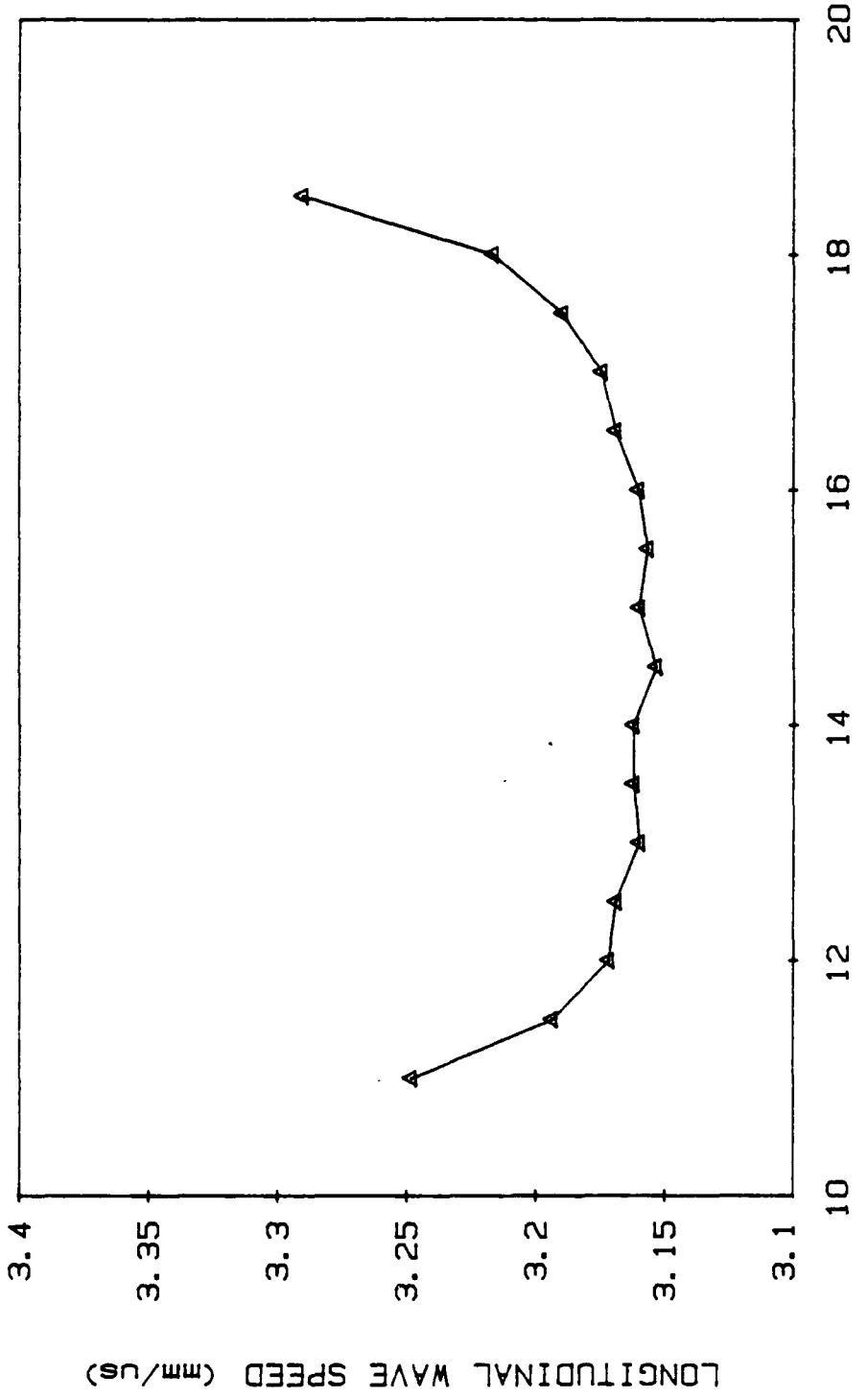

Figure 22. Effect of pulse position on wave speed for composite.

TECHNIQUE CALIBRATION

In order to calibrate the technique the longitudinal wave speed in aluminum was measured first. The surfaces of a block of aluminum (6.35 mm) were polished to a 0.1 μm finish. The water bath temperature was held fixed to ±0.1°C. A transducer with a 5.0 MHz center frequency was used. The specimen was held fixed at one place and the results of five measurements are shown in Figure 23. The reproducibility of the measurements is ±0.02% (i.e., two parts per ten thousand). Solid lines indicate the error bounds. Next, we studied the effect of removing, drying, and replacing the specimen (simulating the corresponding events for an actual composite specimen). The results are shown in Figure 24. The precision is reduced from ±0.02% to ±0.08%.

The attention is now turned to a graphite/epoxy specimen. This was a 24-ply specimen that had been loaded to 30% of its ultimate strength. As before, when left in place the precision in wave speed measurement was ±0.02%. When removed, dried, and replaced the precision was reduced to ±0.08% (Figure 25).

The attenuation was checked in the same manner as above and it was determined that after removing, drying, and replacing the specimen, the precision in measurement was ±1.0% (Figure 26).

In summary, the technique has been developed to a

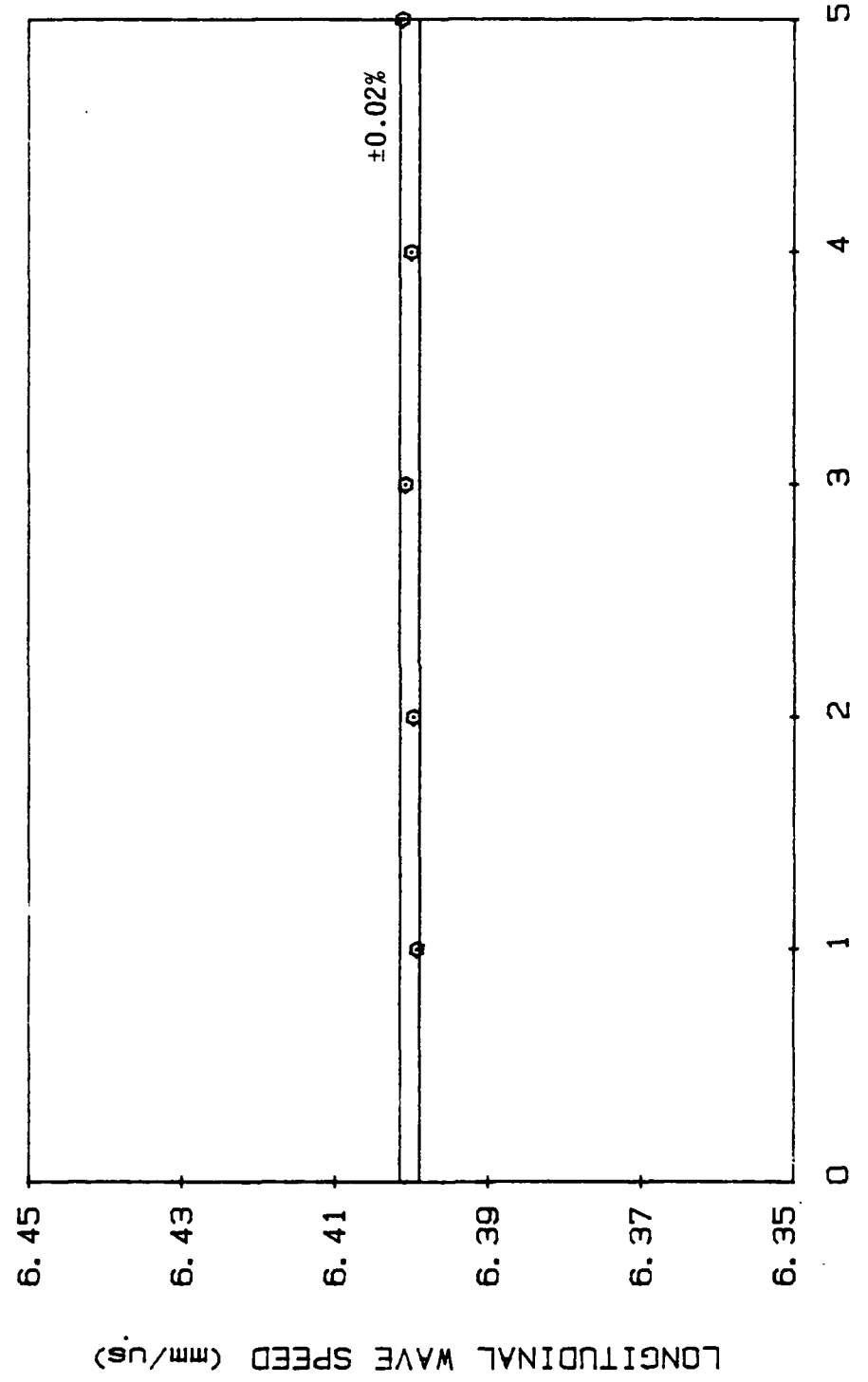

Figure 23. Wave speed repetition test for aluminum without removing each time.

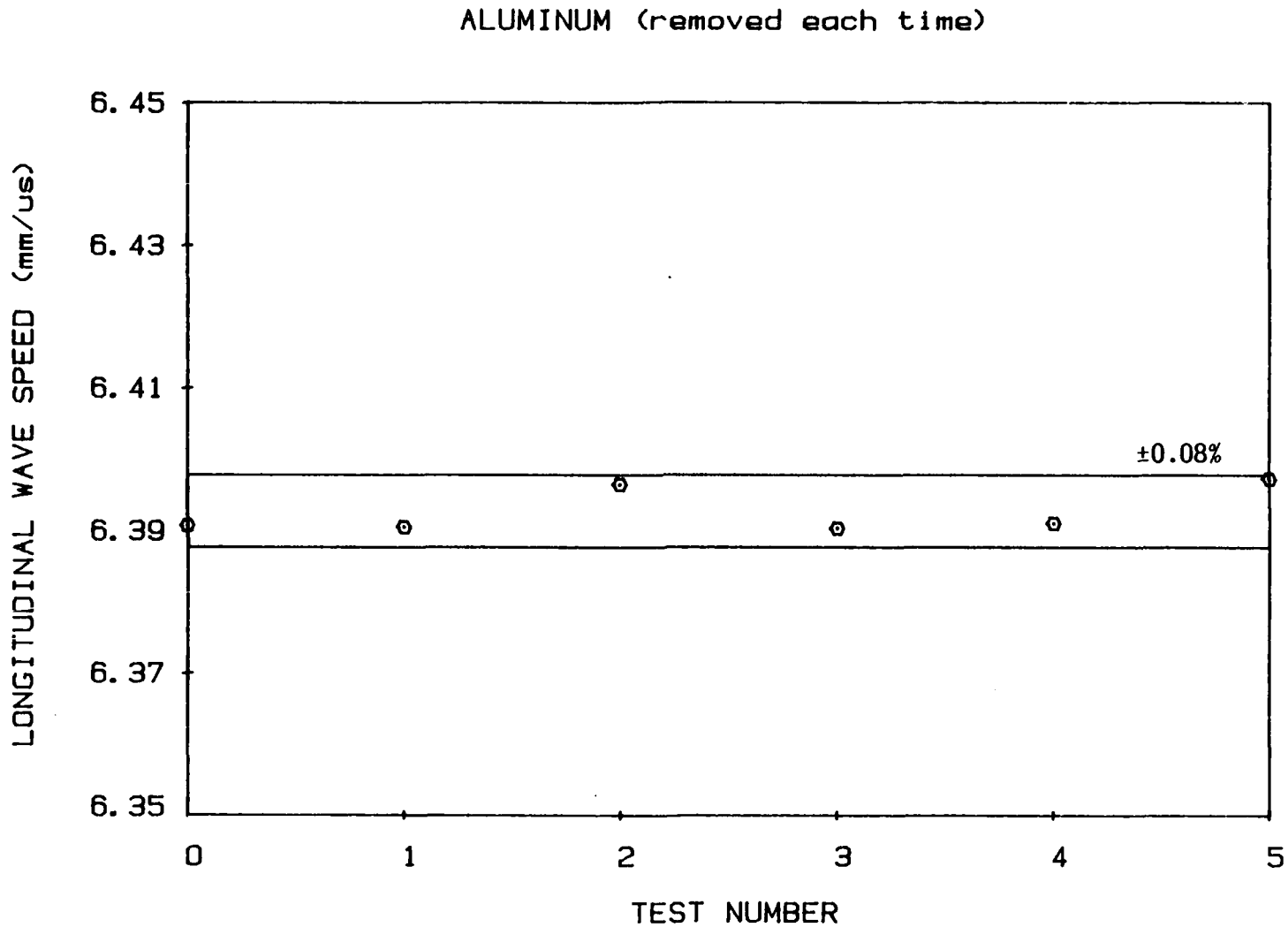

Figure 24. Wave speed repetition test for aluminum simulating actual testing sequence.

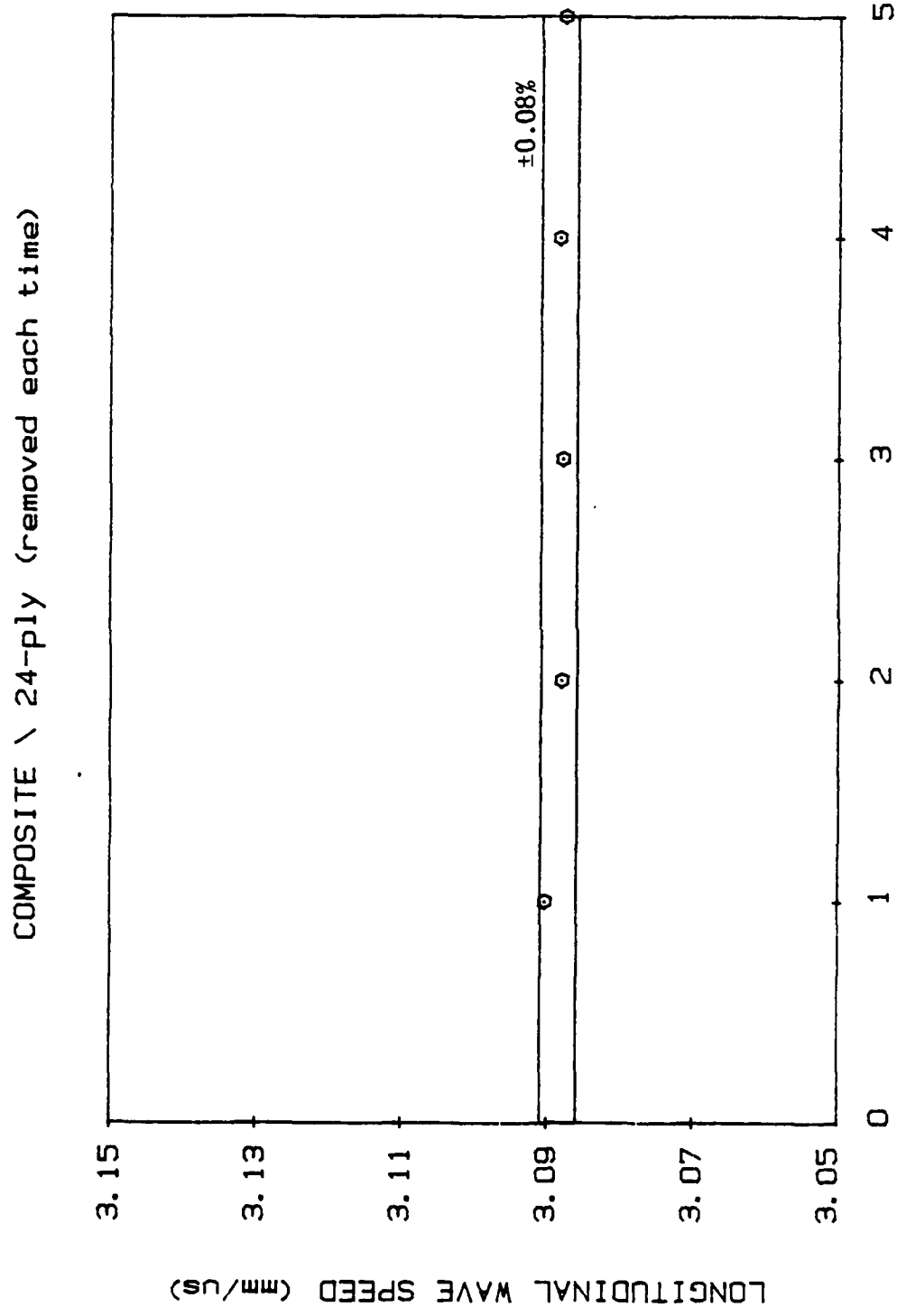

Figure 25. Wave speed repetition test for composite simulating actual testing sequence.

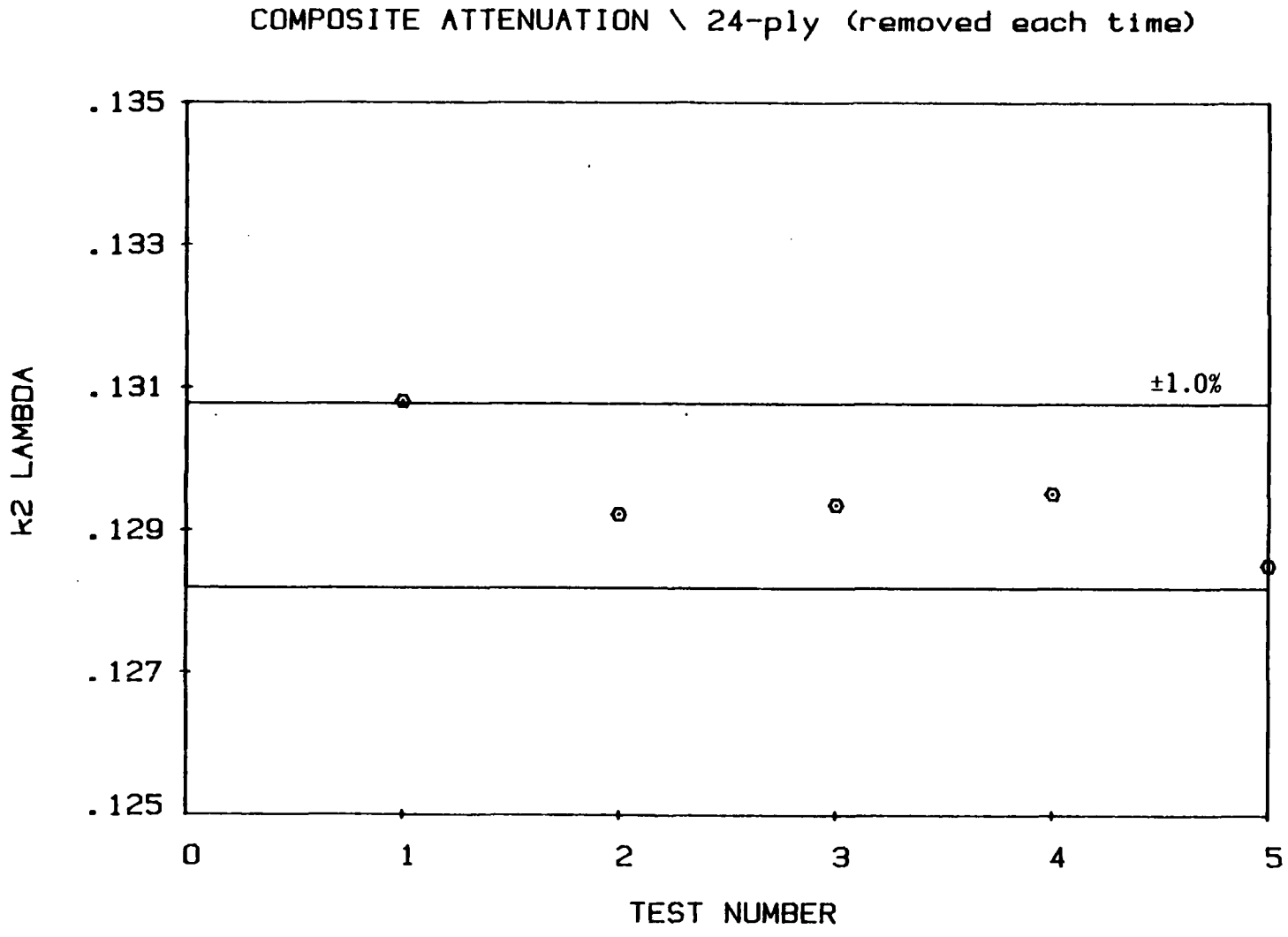

Figure 26. Attenuation repetition test for composite simulating actual testing sequence.

point where the wave speed and attenuation can be measured with a precision of ±0.1% and ±1.0%, respectively.

RESULTS AND DISCUSSION

At the end of each load step the wave speed and attenuation were measured at each position using 2.25, 5.0, and 7.5 MHz transducers. The results are presented in two parts. The wave speed data are explained in the first section and then the attenuation results follow.

Wave Speed

Before examining the results of this section the original goal of this investigation should be mentioned. First, since the level of precision for this technique is much higher than those of earlier methods it was hoped that the detection of damage growth at very low load levels could be detected. Much of the original work for this thesis concerned only the measurement of longitudinal wave speed and its direct correlation with stiffness. Test results not reported here, indicated that the wave speed through the thickness direction was not affected by damage. However, at higher load steps a rather disturbing observation was made: the wave speed increased. Actually, the wave was interacting with the damage in the interior and becoming more and more scattered. Since the second reflection was spreading (explained previously) it gave the perception that it was returning faster from the back surface. For completeness, a few of the wave speed results are presented here, but, as will be observed, no change

within the experimental error could be detected.

Figure 27 first shows the wave speed versus frequency for three positions (see Figure 19) along specimen A3 prior to loading. The wave speed exhibits a slight dependence upon frequency. Next, Figures 28-31 are the plots of wave speed versus stress level for each position (i.e., the stress at which the specimen had been previously loaded; all measurements were taken under zero load conditions). Figure 32 displays the final damage states for each position. Position 1's final damage state explains the large increase in wave speed at the last stress level as indicated by Figure 28 and 29. The second reflection has become so scattered that an accurate measurement of wave speed is impossible. Positions 2 and 3 show no consistent trend regarding their final damage states.

Figure 33 shows the wave speed data at position 1 for the other geometry tested, namely, $[0_6/90_4/0_2]s$, specimen B1. Here, the wave speed is slightly more dependent upon frequency than it was for specimen A3.

In summary, no definitive dependence of the through-the-thickness wave speed on damage could be established.

Attenuation

Having given up on the wave speed as an indicator of damage we now turned our attention to attenuation. During previous tests involving only wave speed measurement it was

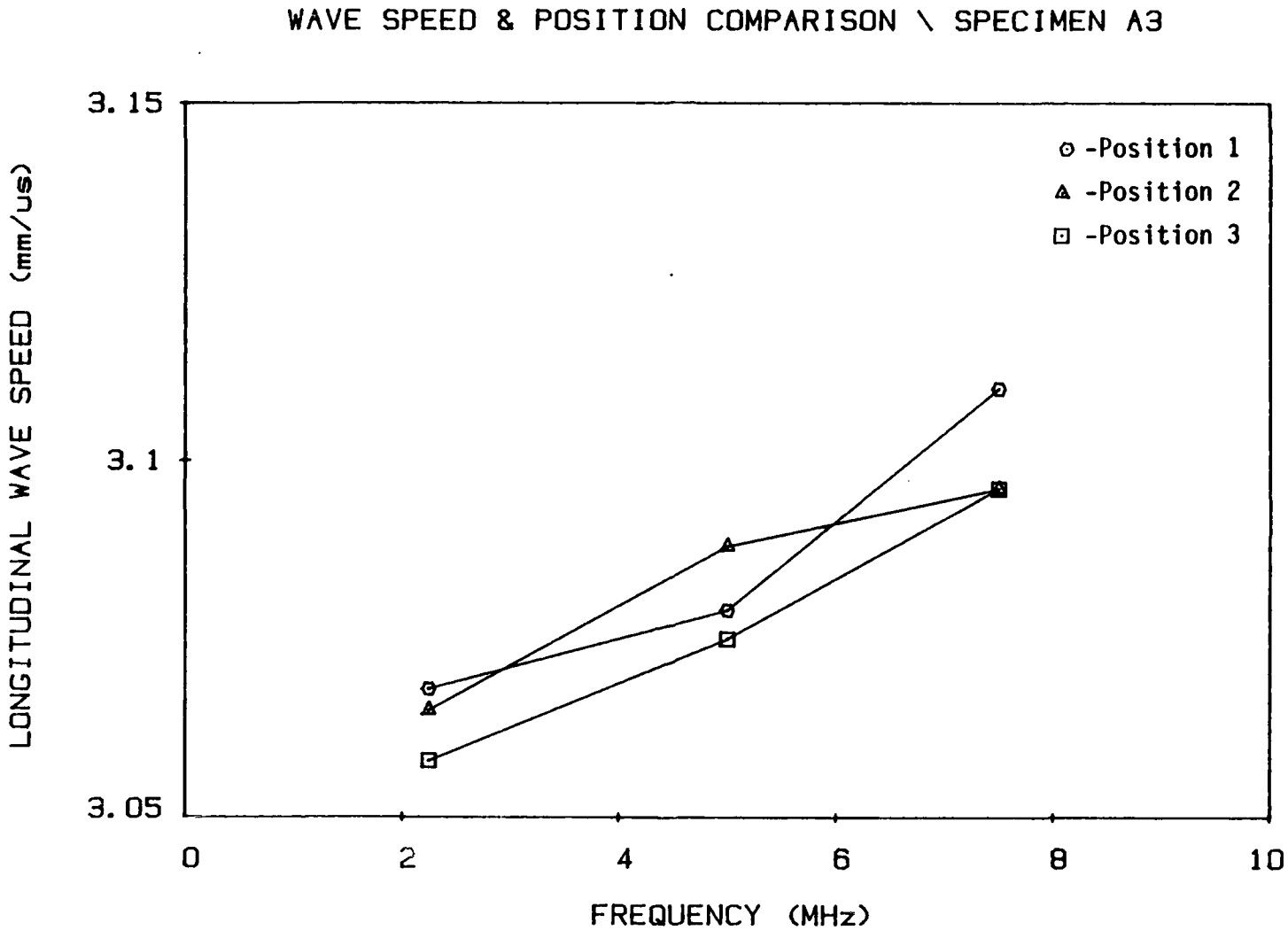

Figure 27. Longitudinal wave speed versus frequency for three positions along A3.

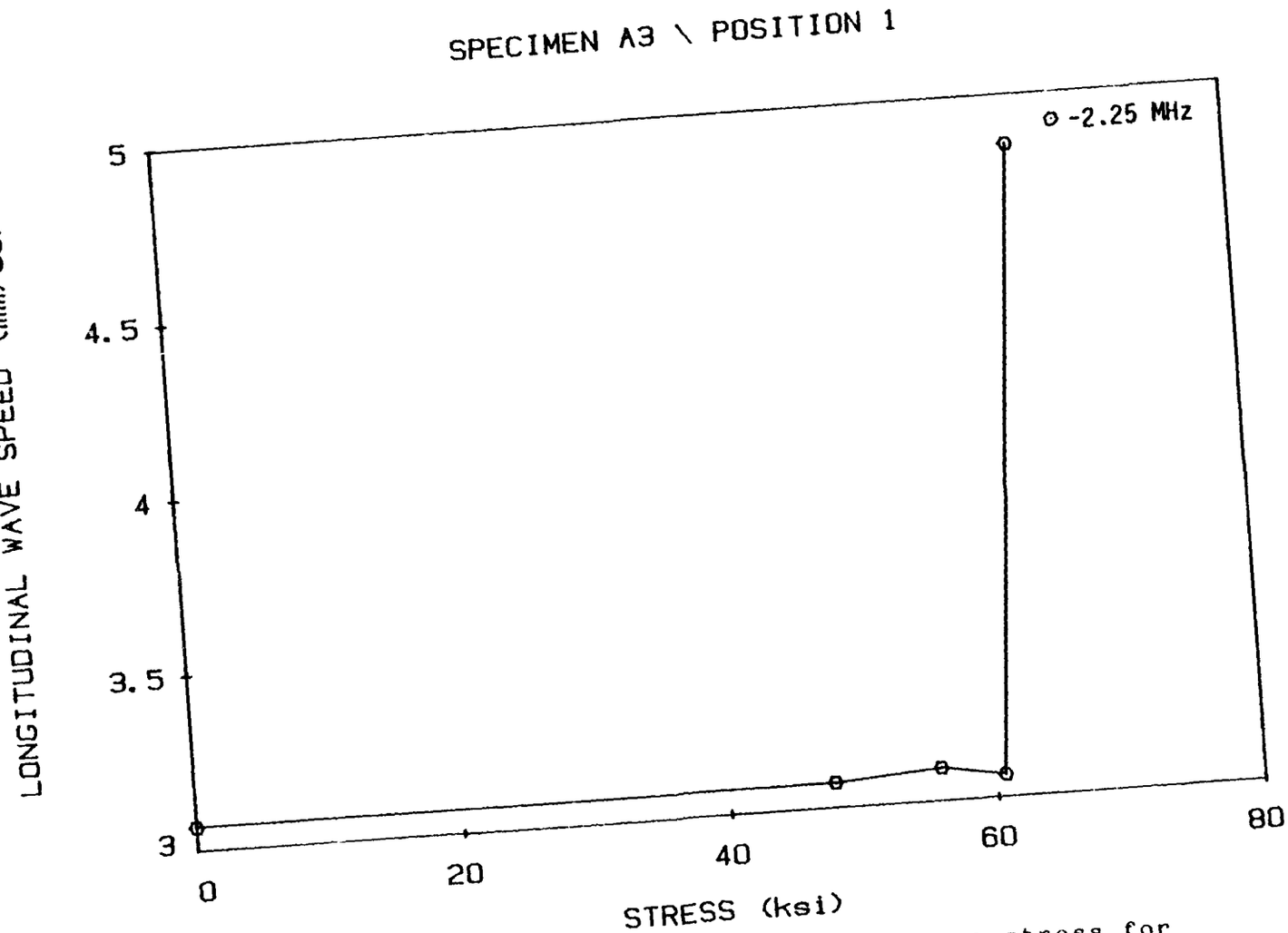

Figure 28. Longitudinal wave speed versus stress for specimen A3, position 1, at 2.25 MHz.

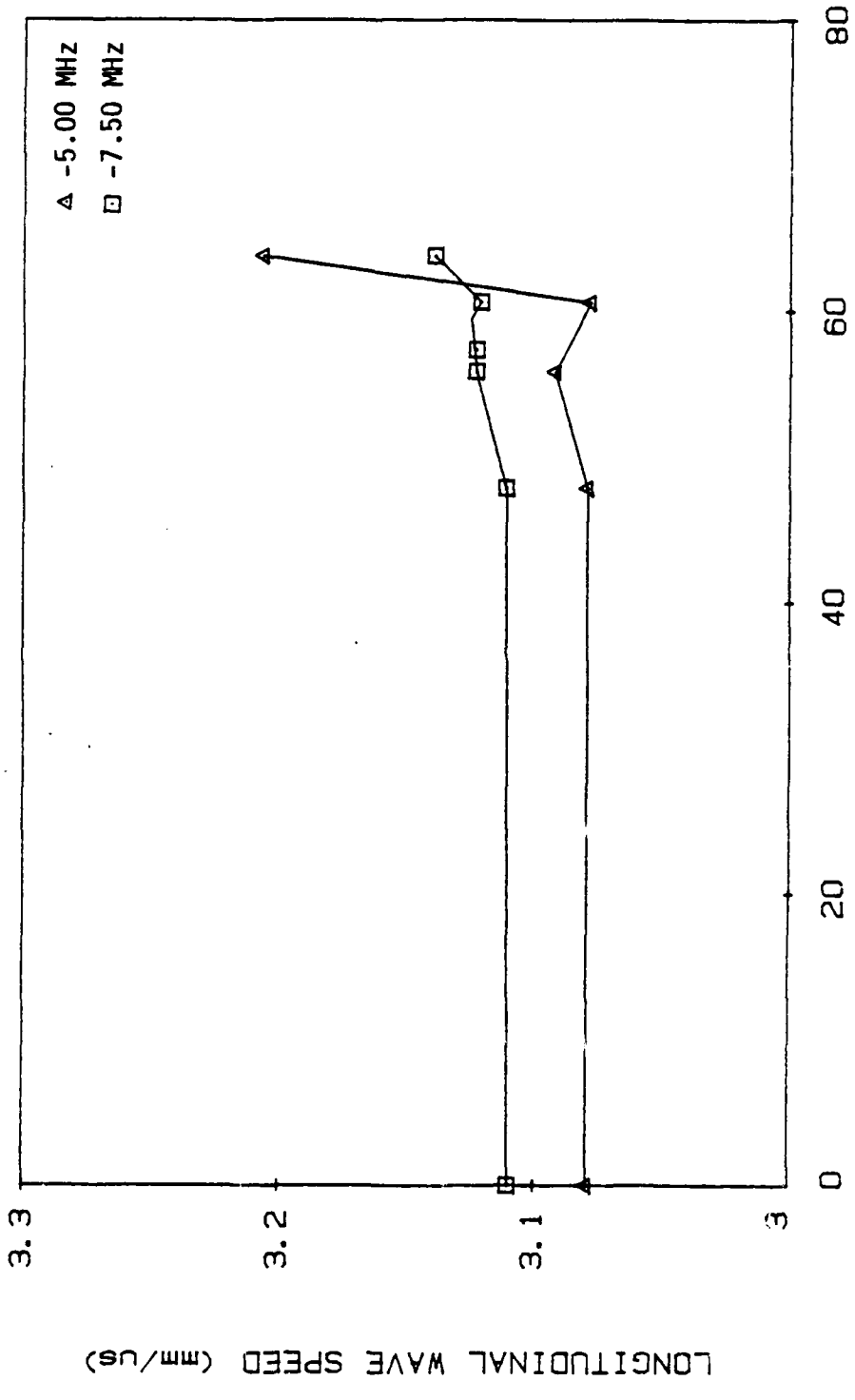

Figure 29. Longitudinal wave speed versus stress for specimen A3, position 1, at 5.0 and 7.5 MHz.

AD-A175 004 RESEARCH ON CHARACTERIZATION OF DAMAGE STATES IN CONTINUOUS FIBER COMPOSI (U) TEXAS A AND M UNIV COLLEGE STATION MECHANICS AND MATERIALS CE V K KINRA UNCLASSIFIED MAY 86 MM-5024-86-12 AFOSR-TR-86-2182 F/G 11/4 NL 2/2

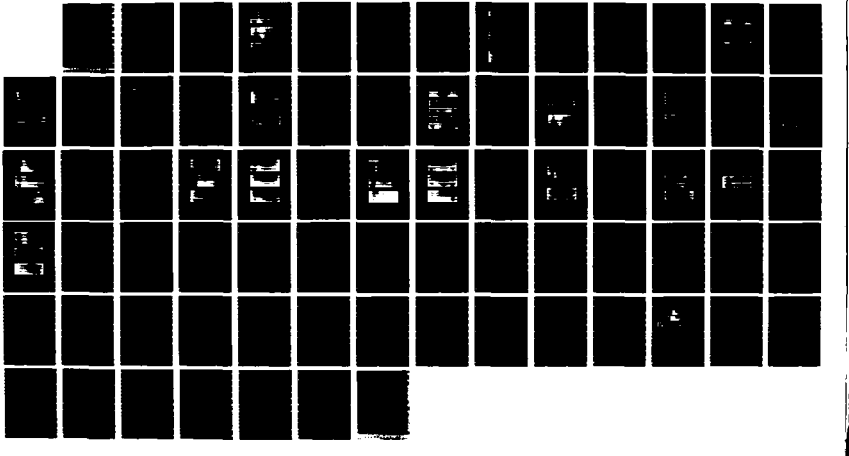

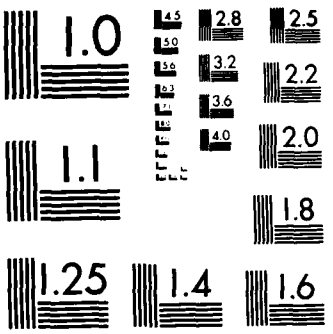

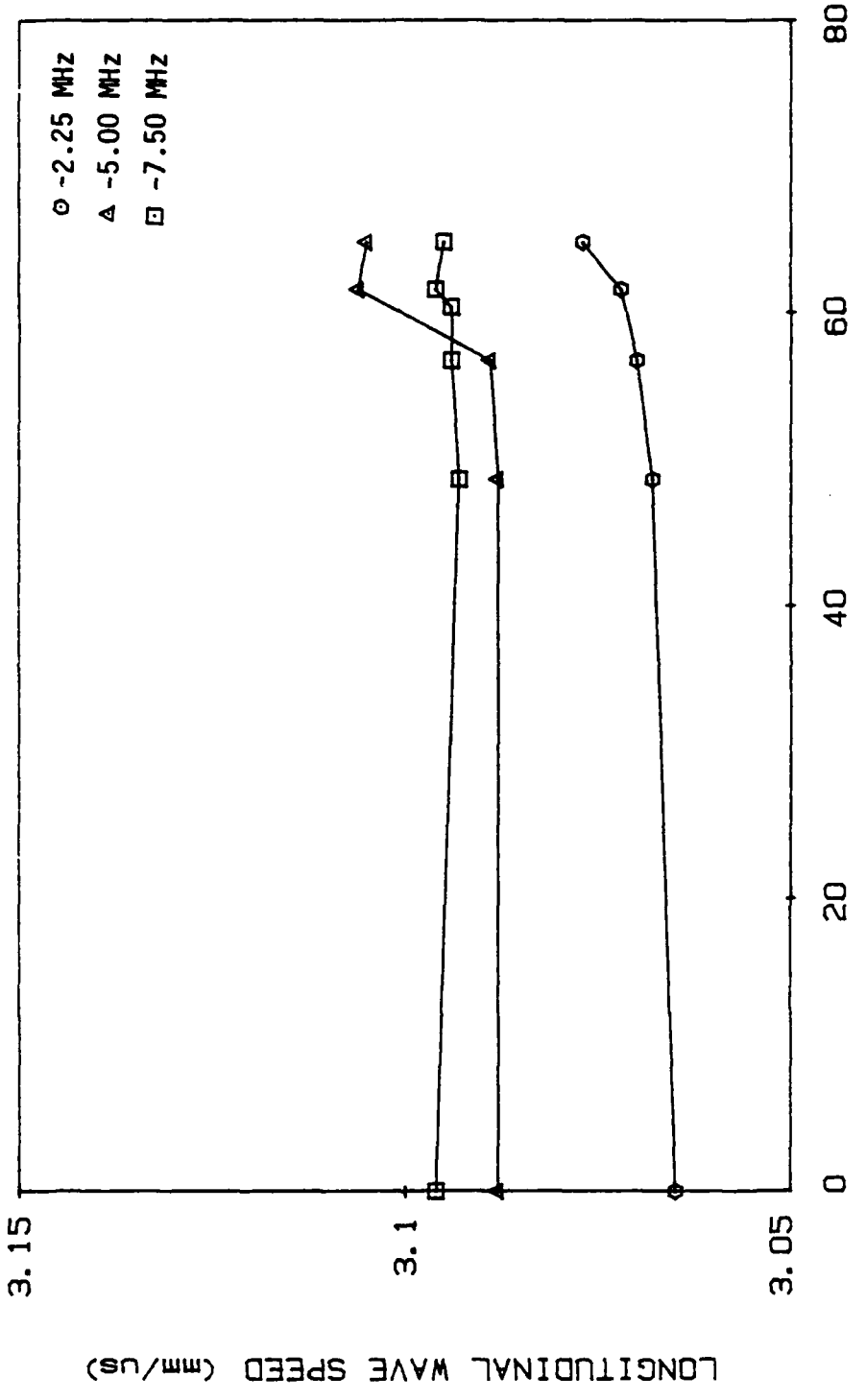

Figure 30. Longitudinal wave speed versus stress for specimen A3, position 2, at 2.25, 5.0, and 7.5 MHz.

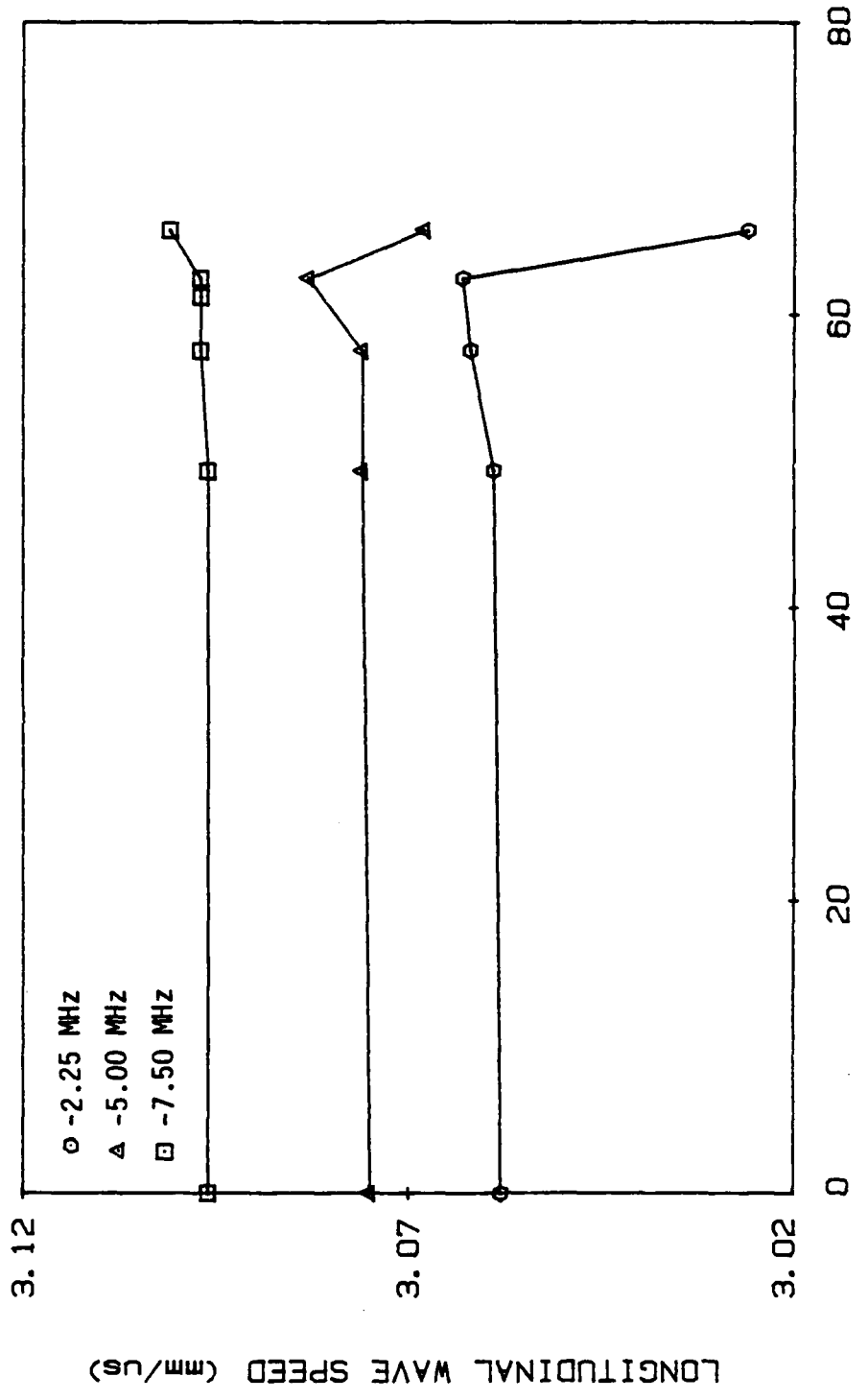

Figure 31. Longitudinal wave speed versus stress for specimen A3, position 3, at 2.25, 5.0, and 7.5 MHz.

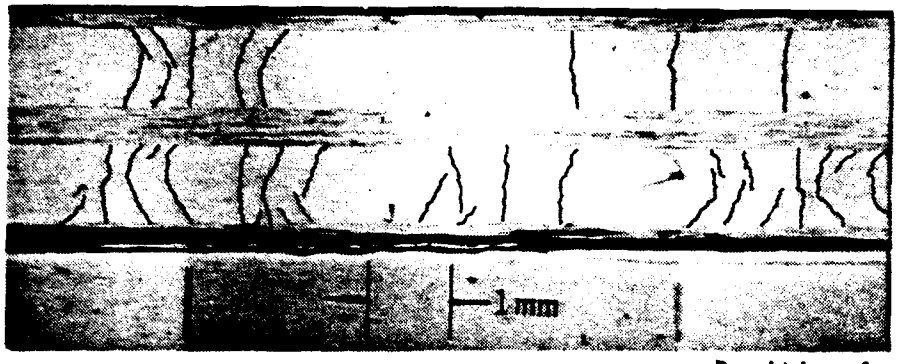

Position 1

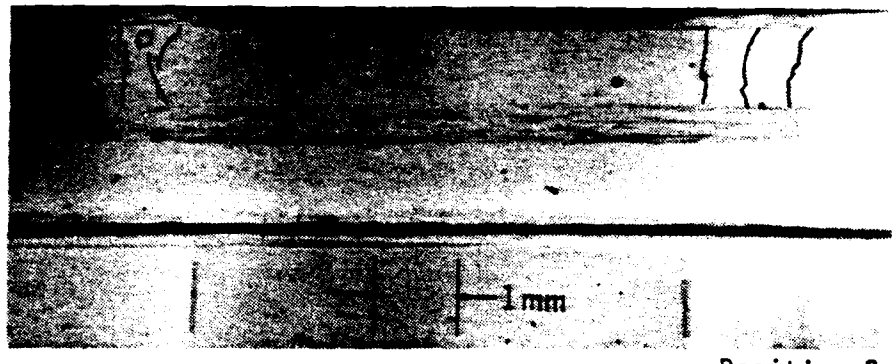

Position 2

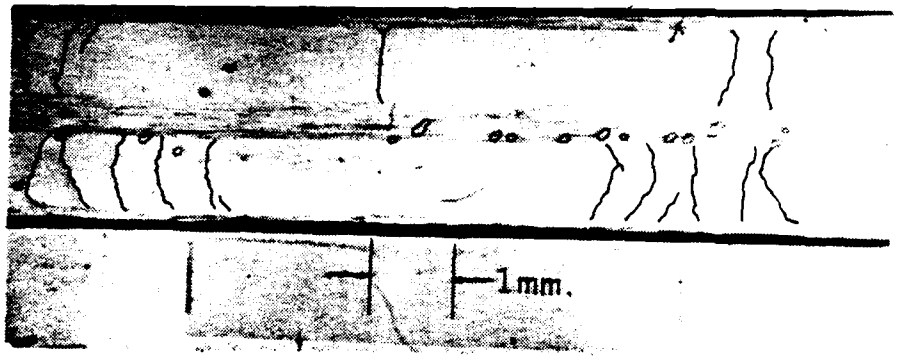

Position 3

Figure 32. Final damage states for specimen A3 at positions 1, 2, and 3.

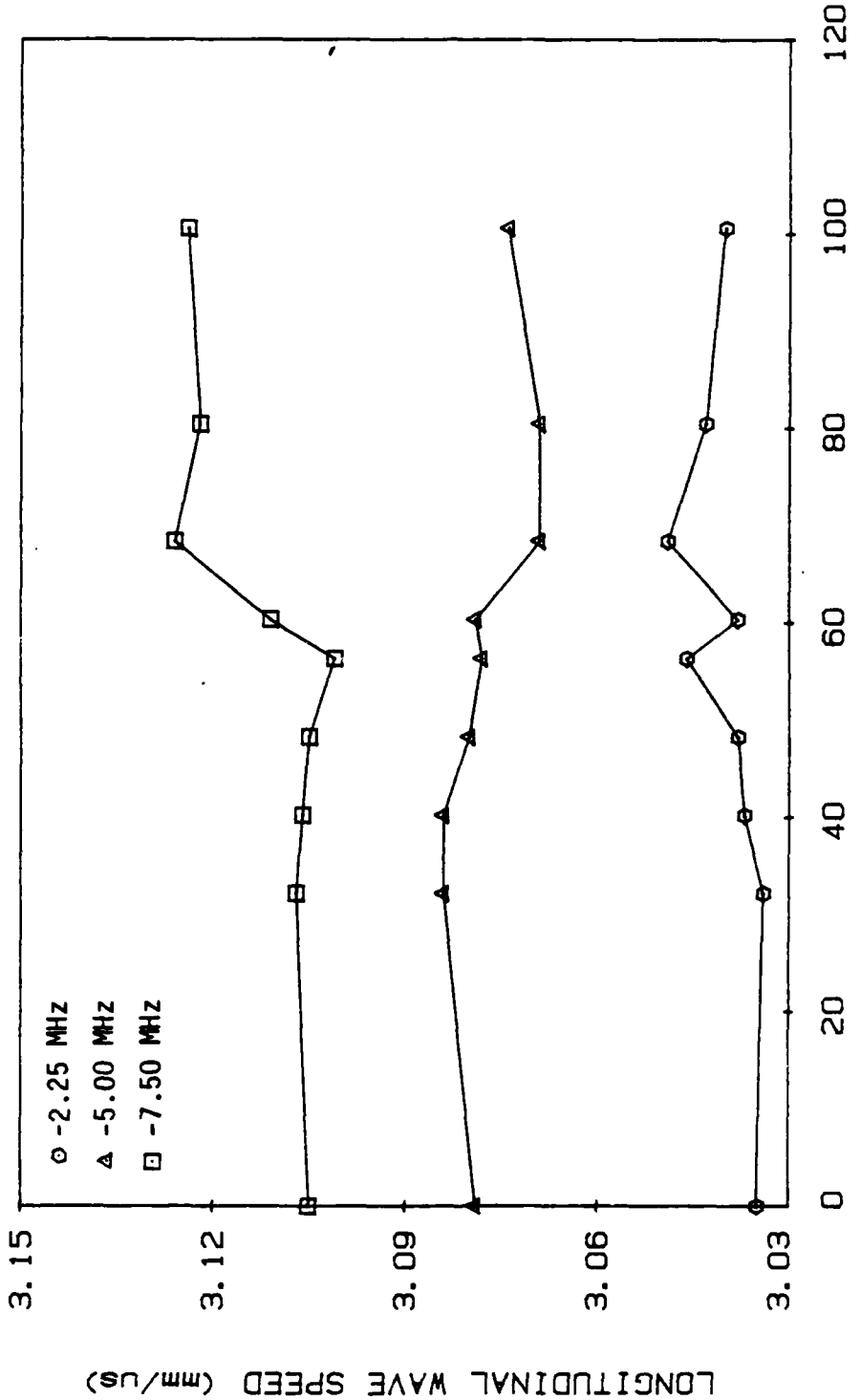

Figure 33. Longitudinal wave speed versus stress for specimen B1, position 1, at 2.25, 5.0, and 7.5 MHz.

consistently noted that as the damage increased within the specimen the amplitude of the second reflection would decrease. At first, a canonical approach was taken to correlate damage to attenuation. We wanted to determine the effect of a single isolated transverse crack and then apply this information to higher damage states. Much of the work was aimed at capturing one crack in the insonified area. Unfortunately, efforts to measure experimentally the scattering cross-section of a single crack failed; the reasons are explained later. However, results do indicate a definite trend in attenuation with frequency at higher damage states. In the following, the attenuation of the undamaged specimen was .btracted from that of the damaged specimen; thus, the difference is due only to the damage state.

Specimen A2 is a good indicator of the problems associated with trying to measure the effect of one crack. Figure 34 depicts how one crack under the transducer can be misleading. Each line represents a different position on the specimen, each having one crack in a different area of the transducer window. The cracks associated with positions 1 and 3 (Figures 35a and 35c) are located near the edge of the window while the crack associated with position 2 is in the center (Figure 35b). It is obvious that crack position under the transducer is affecting the attenuation results. Two possible explanations for the above problem are: 1) It is assumed that the compressional wave that was launched

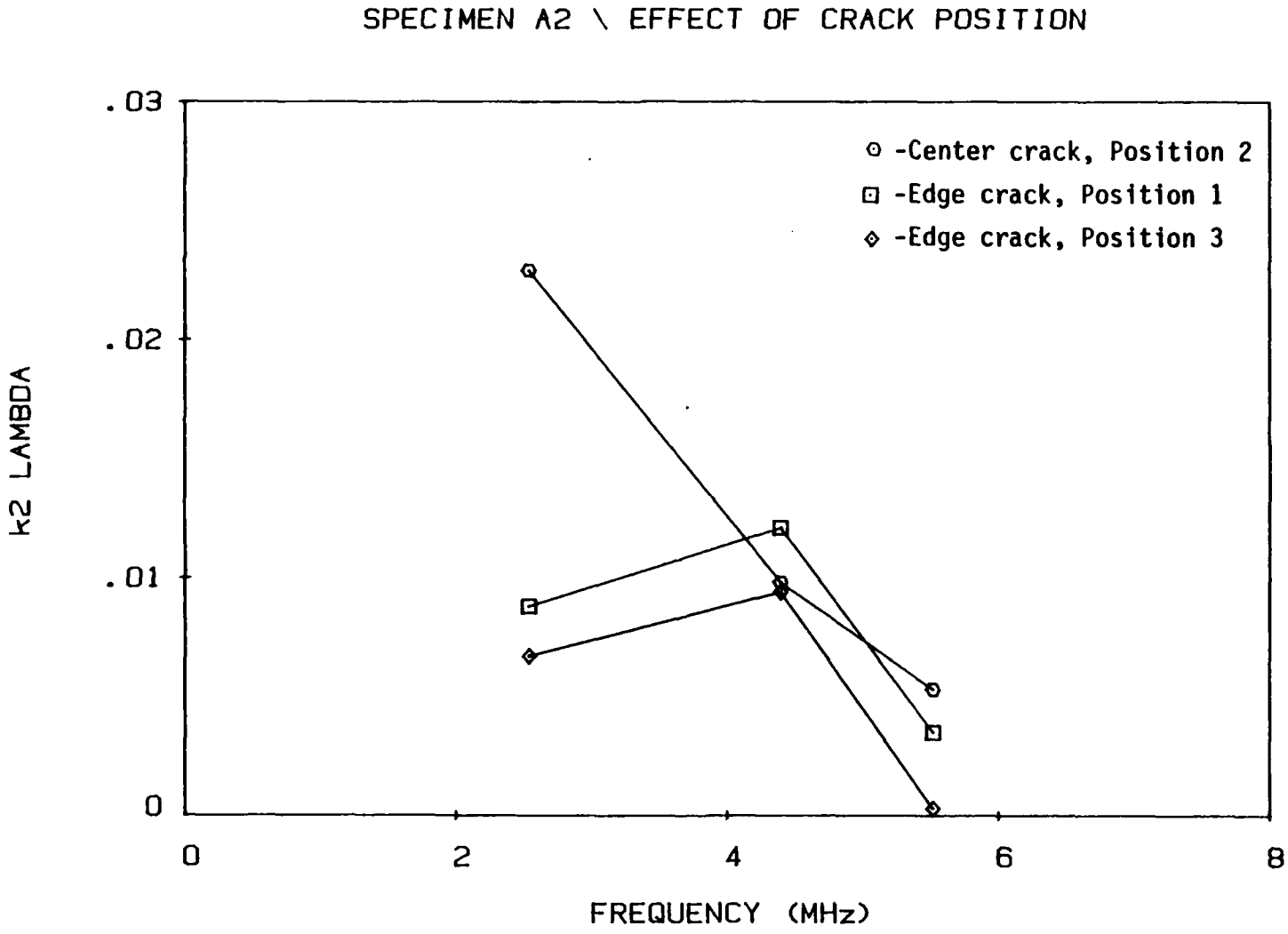

Figure 34. Effect of crack position relative to the transducer window for specimen A2.

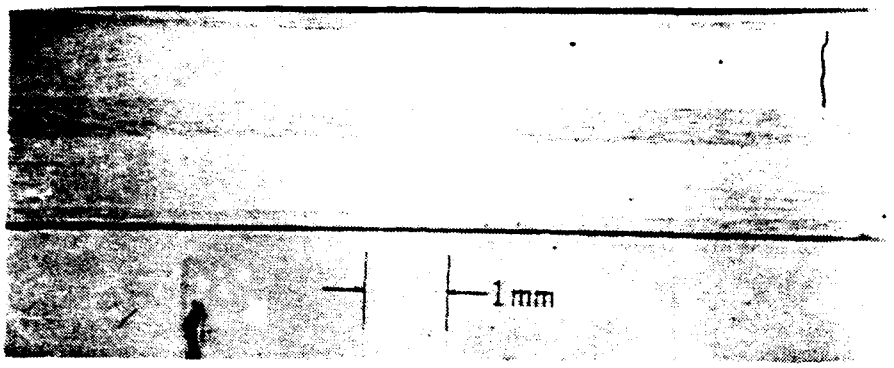

Figure 35a. Crack location for position 1, specimen A2.

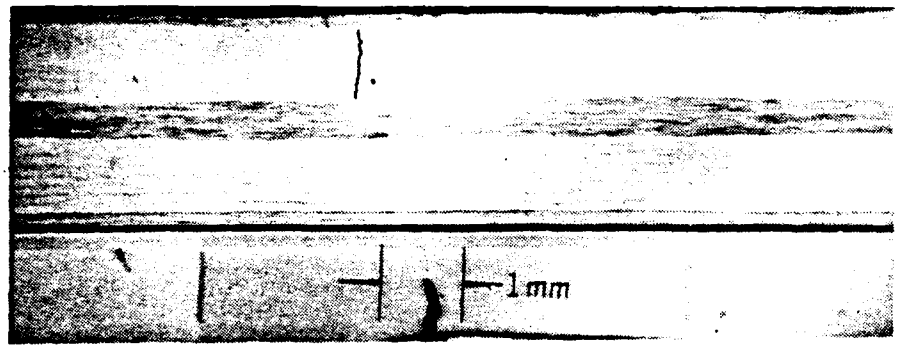

Figure 35b. Crack location for position 2, specimen A2.

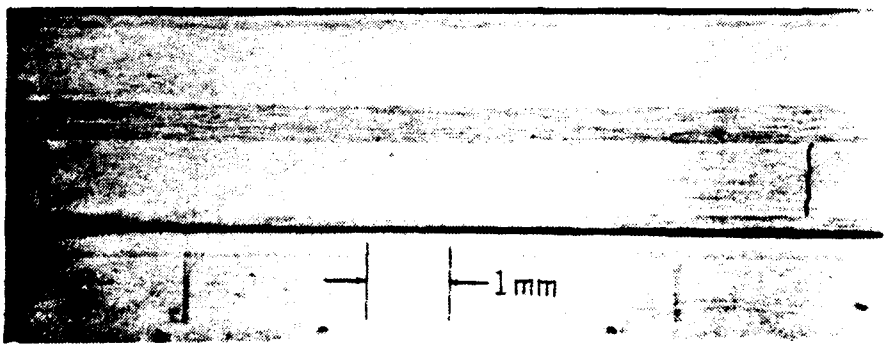

Figure 35c. Crack location for position 3, specimen A2.

from the transducer was of constant amplitude across the face of the transducer. If the amplitude was not constant, perhaps peaking in the center [59], then cracks near the edge would have less energy to scatter making them appear to have a smaller effect, and 2) When the wave and crack interact, the energy from a center-crack would see a larger decrease than a crack near the edge (Figure 36). This problem was again identified with specimen A3. Figure 37 is another plot of the effect of crack position, but this time there were groups of cracks instead of a single one. Figures 38a, 38b, and 38c indicate the position of the crack groups. From Figures 34 and 37 it is obvious that when the crack appears in the center the attenuation response is similar (i.e., attenuation decrease with increasing frequency), but the edge cracks give results that are inconsistent.

The attention is now turned toward the multiple crack problem. The preceeding figures are the plots of attenuation versus frequency for three positions along each specimen. Each curve in the figures indicates a higher load step. The numbered load steps indicate steps at which new cracks appeared within the insonified area. After each plot of $k_2\lambda$ versus frequency there is a set of photographs (damage states, DS) that correspond to the numbered load steps. Figures 39-44 are the plots of $k_2\lambda$ versus frequency and corresponding damage states for specimen A2. Unfortunately, for this particular layup, $[0_2/90_8/0_2]s$, it was

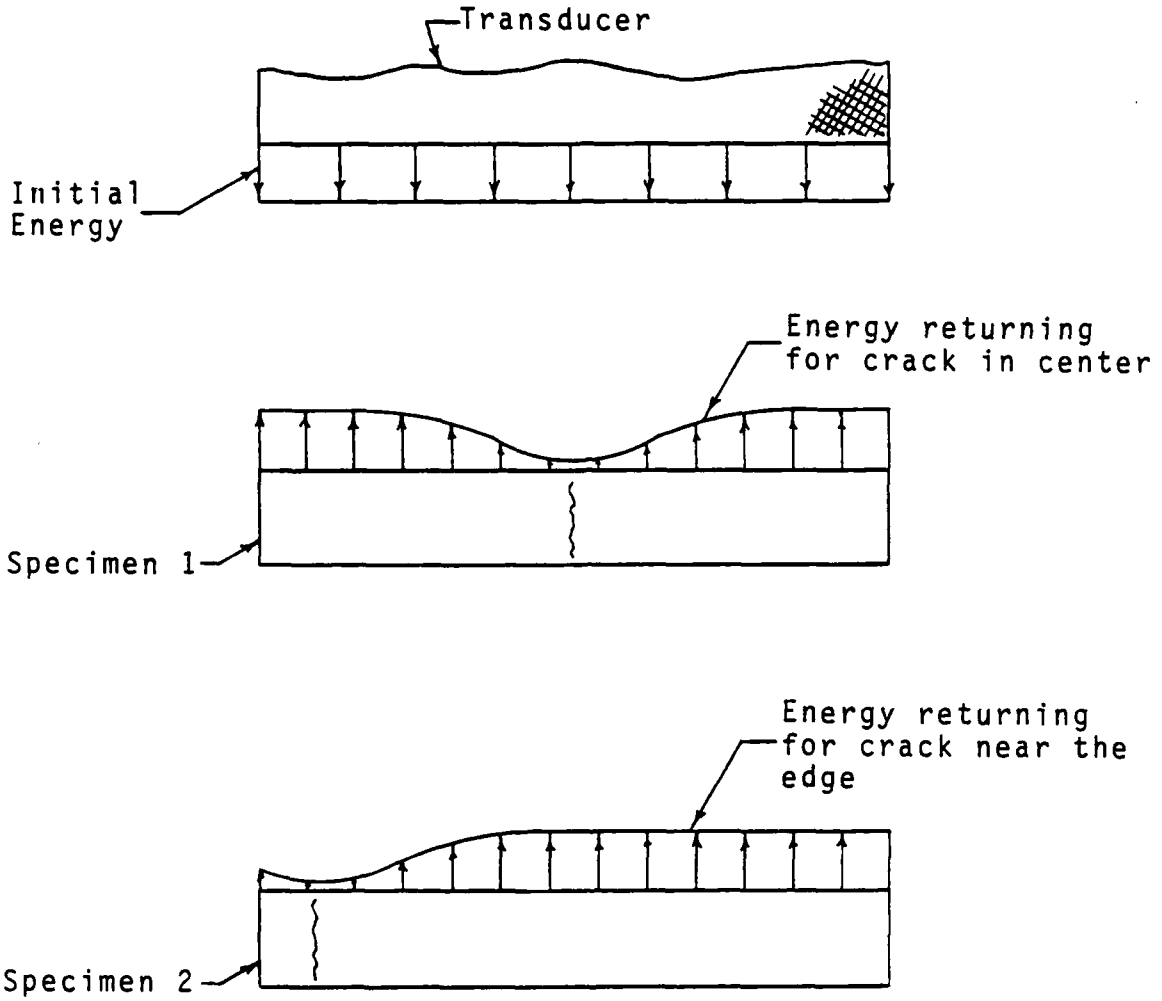

Figure 36. Effect of crack position on the energy returning to the transducer.

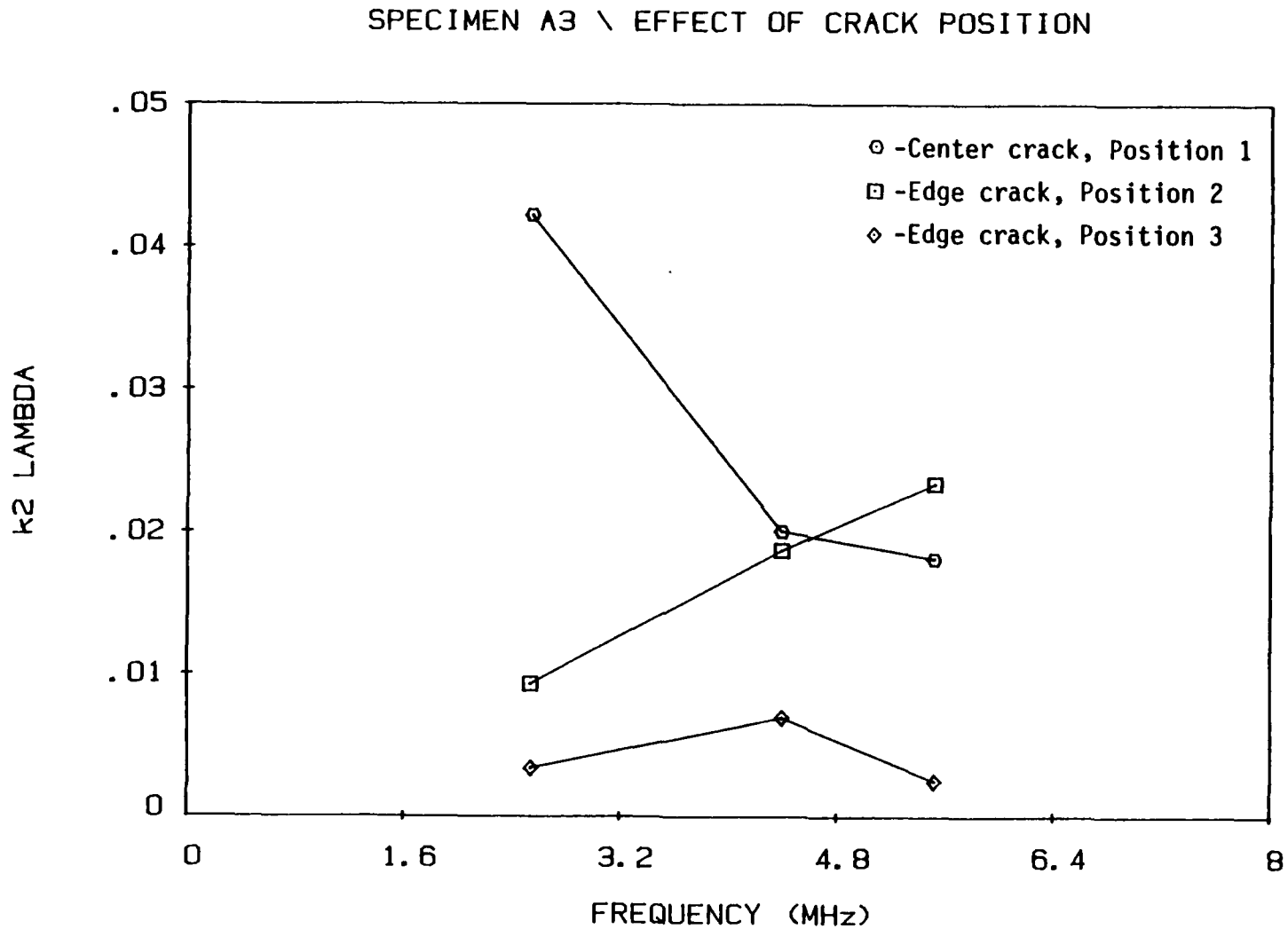

Figure 37. Effect of crack position relative to the transducer window for specimen A3.

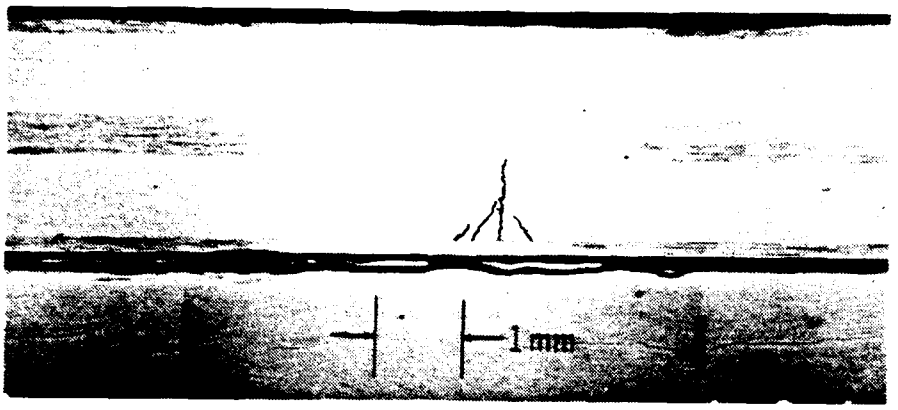

Figure 38a. Crack location for position 1, specimen A3.

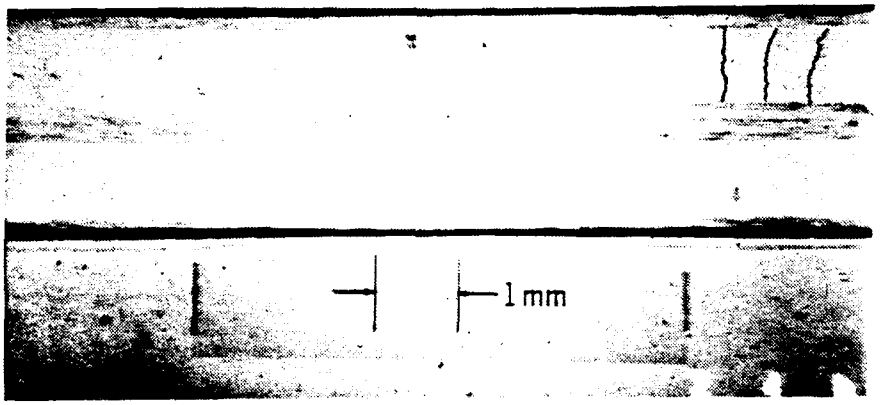

Figure 38b. Crack location for position 2, specimen A3.

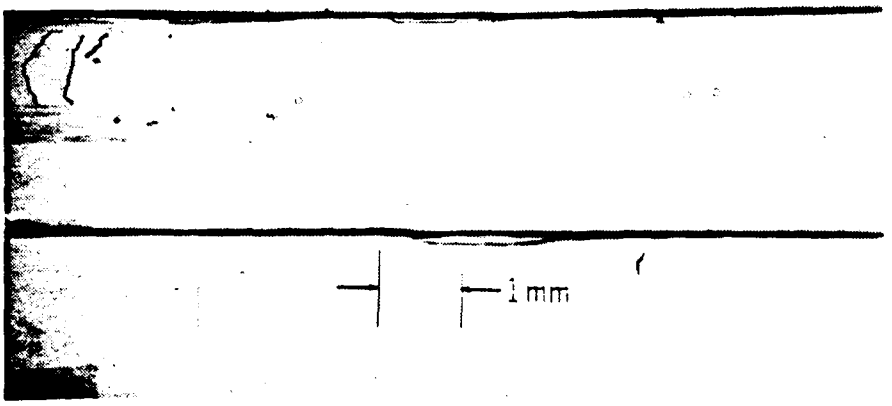

Figure 38c. Crack location for position 3, specimen A3.

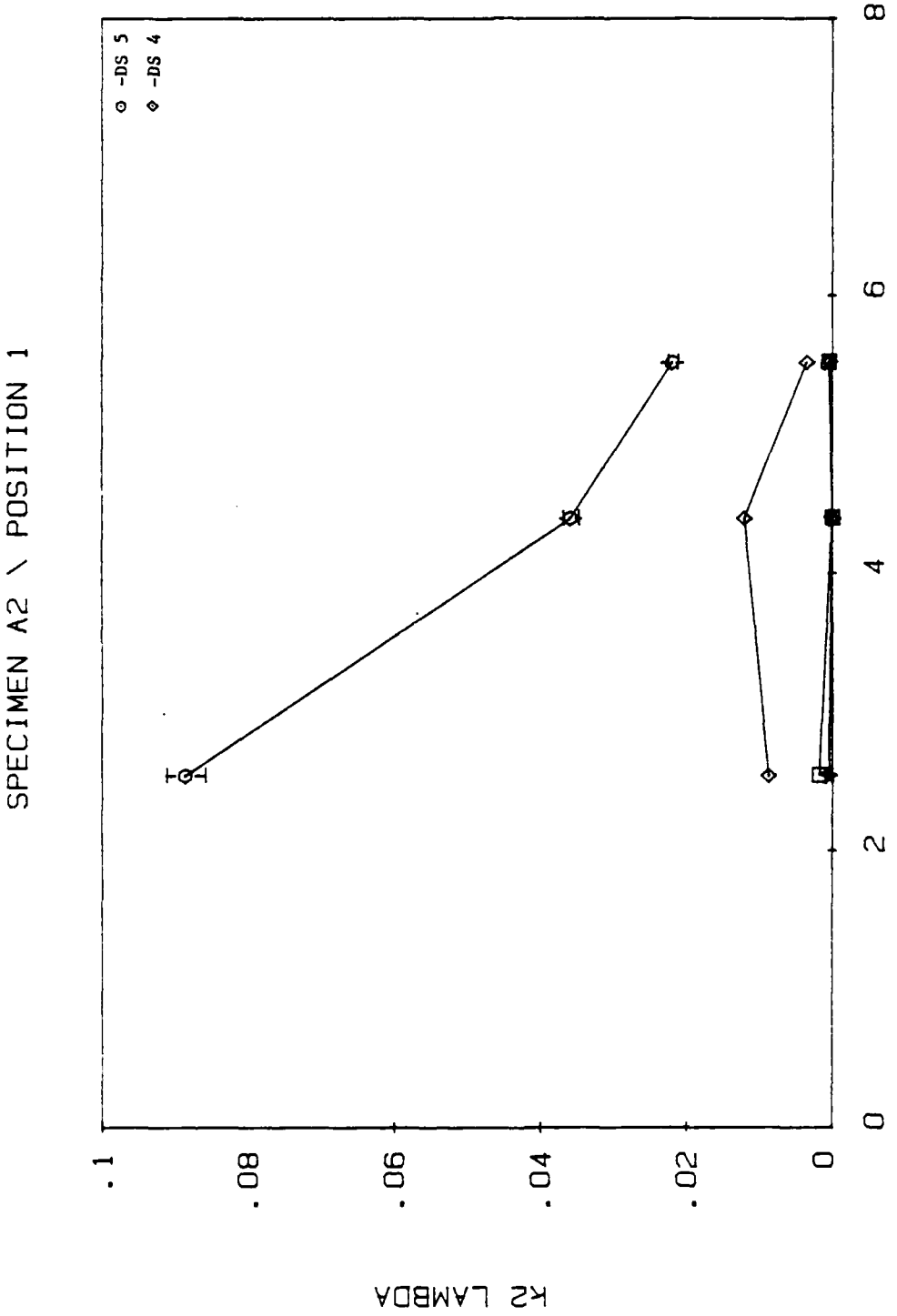

Figure 39. Attenuation versus frequency for each load step at position 1, specimen A2.

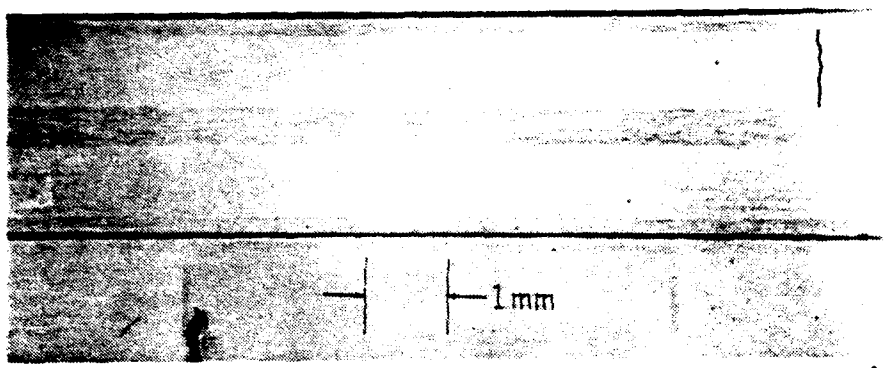

Damage state 4

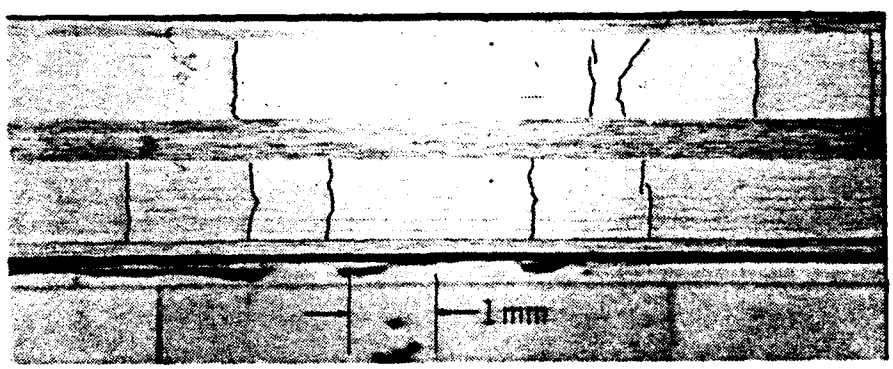

Damage state 5

Figure 40. Damage states for position 1 at load steps 4 and 5, specimen A2.

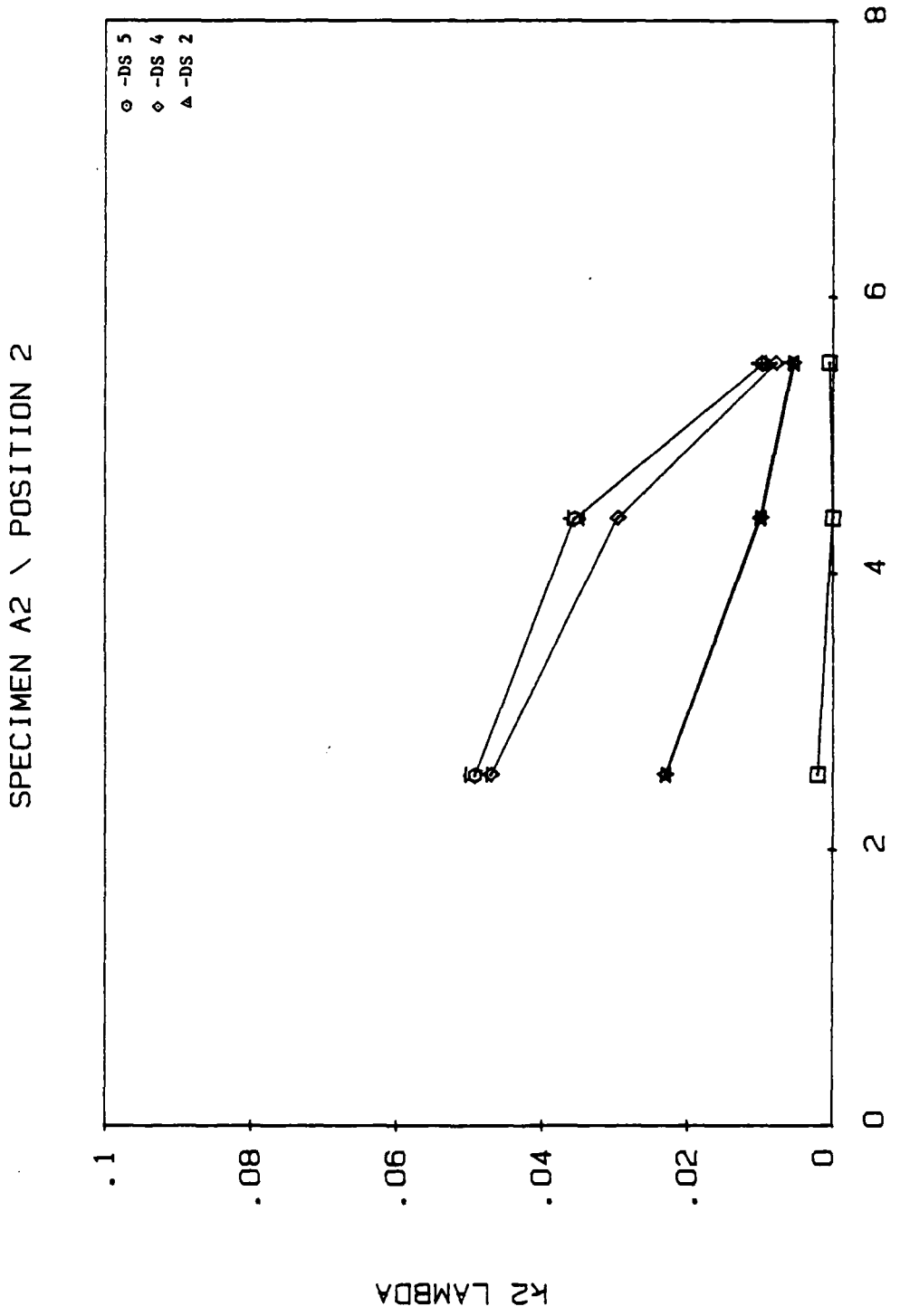

Figure 41. Attenuation versus frequency for each load step at position 2, specimen A2.

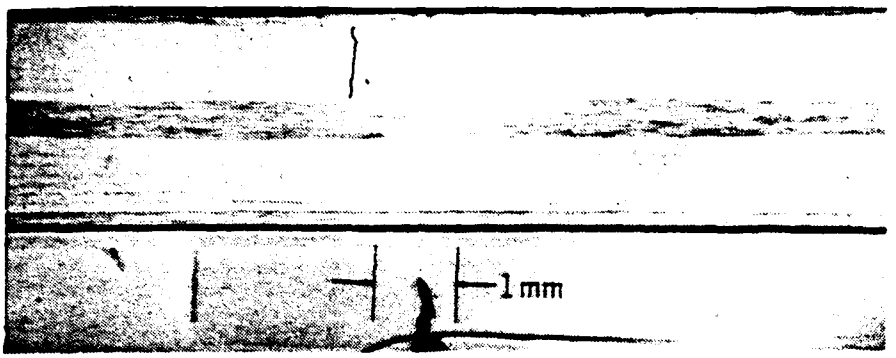

Damage state 2

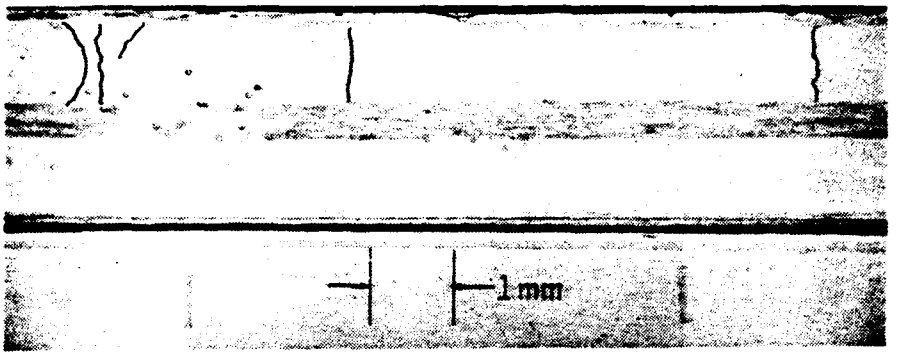

Damage state 4

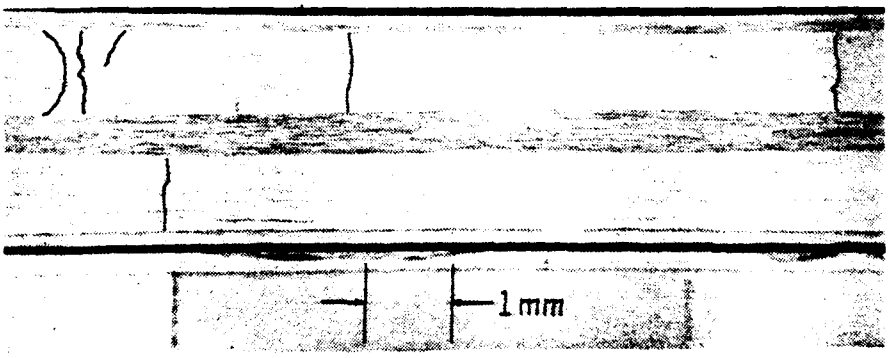

Damage state 5

Figure 42. Damage states for position 2 at load steps 2, 4, and 5, specimen A2.

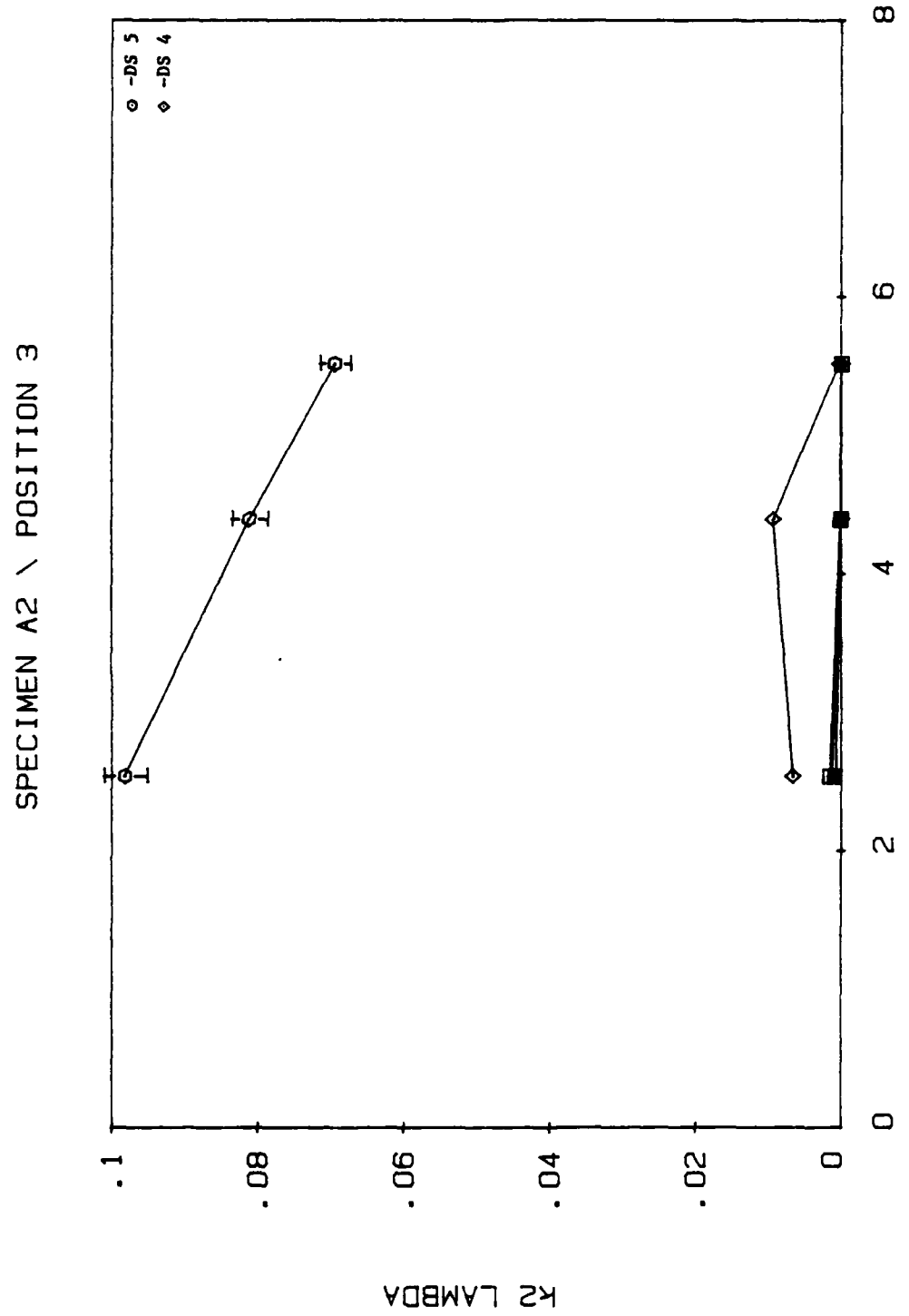

Figure 43. Attenuation versus frequency for each load step at position 3, specimen A2.

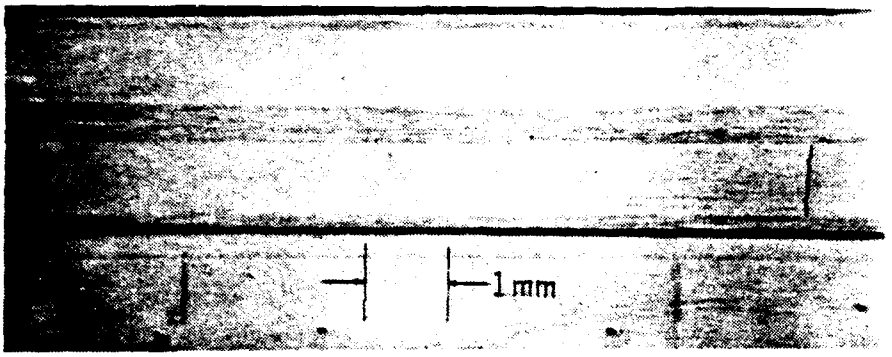

Damage state 4

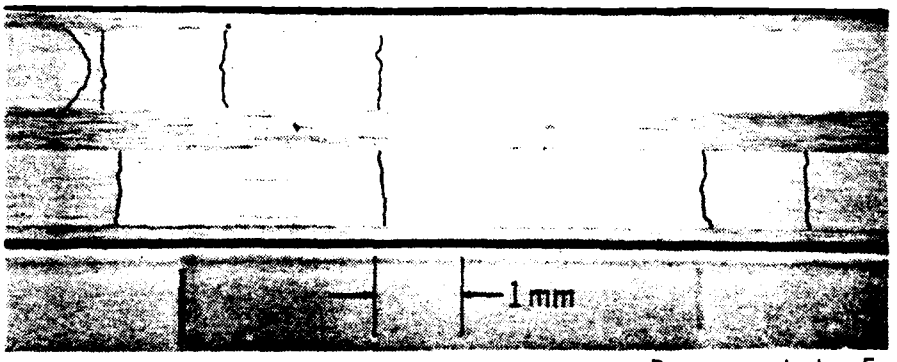

Damage state 5

Figure 44. Damage states for position 3 at load steps 4 and 5, specimen A2.

difficult to capture a steady increase in damage growth during loading and hence the fifth load step shows a sudden jump in attenuation. From position 1 the last load step shows the same trend in attenuation response as that for a single central crack, namely, the attenuation decreases with increasing frequency. The damage for position 1 at the last load step (Figure 40, Damage state 5) is evenly distributed. On the other hand, position 2 shows the effect of not having an even damage distribution (Figure 42, Damage state 5). Figures 43 and 44 are the attenuation and corresponding damage states for position 3. Again, the same trend in attenuation is observed as the damage state becomes more balanced at the final load step.

It was considered desirable to repeat the same series of tests for another specimen of the same geometry, A3. The attenuation plots and corresponding damage states are recorded in Figures 45-50. The trend of attenuation decrease with increasing frequency for evenly distributed damage cases is apparent and thus reconfirms the previous results.

The next step was to examine the effect of scaling of crack length. For this, a 24-ply specimen with layup geometry $[0_6/90_4/0_2]s$-B1 was tested. The damage growth in this specimen was much more gradual than that in the previous one, allowing for a complete depiction of damage growth versus attenuation changes. Figures 51-53 show the attenuation results obtained and the corresponding damage

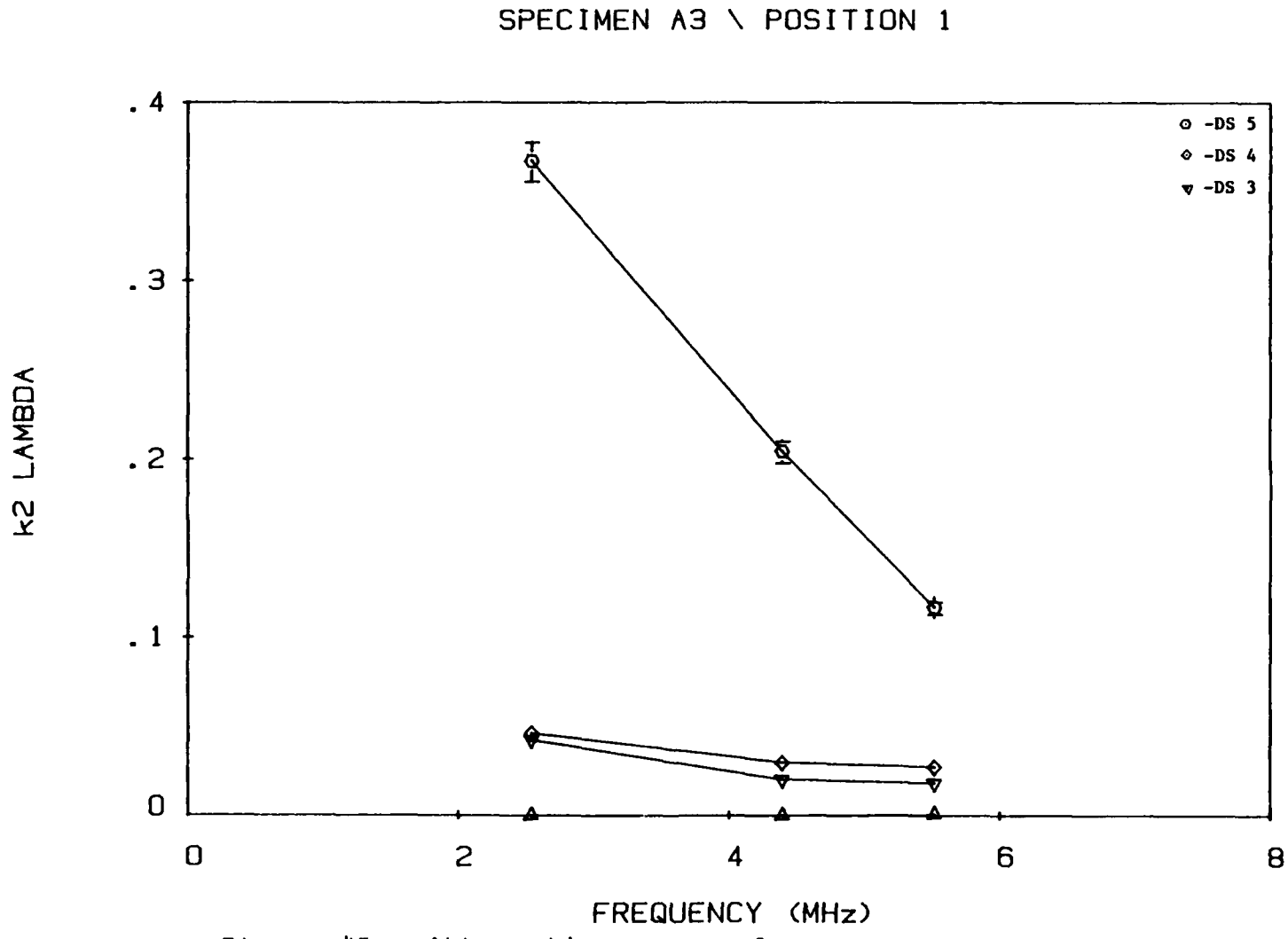

Figure 45. Attenuation versus frequency for each load step at position 1, specimen A3.

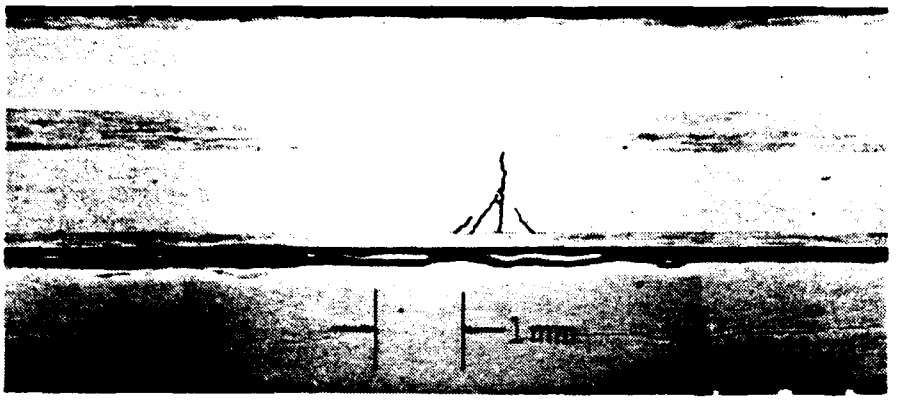

Damage state 3

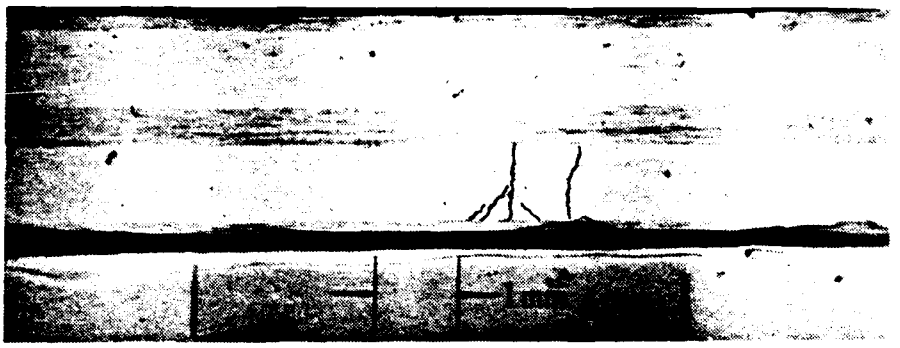

Damage state 4

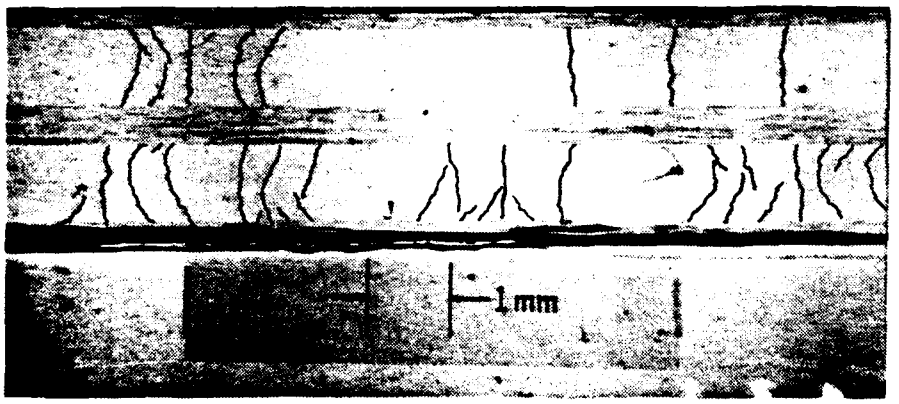

Damage state 5

Figure 46. Damage states for position 1 at load steps 3, 4, and 5, specimen A3.

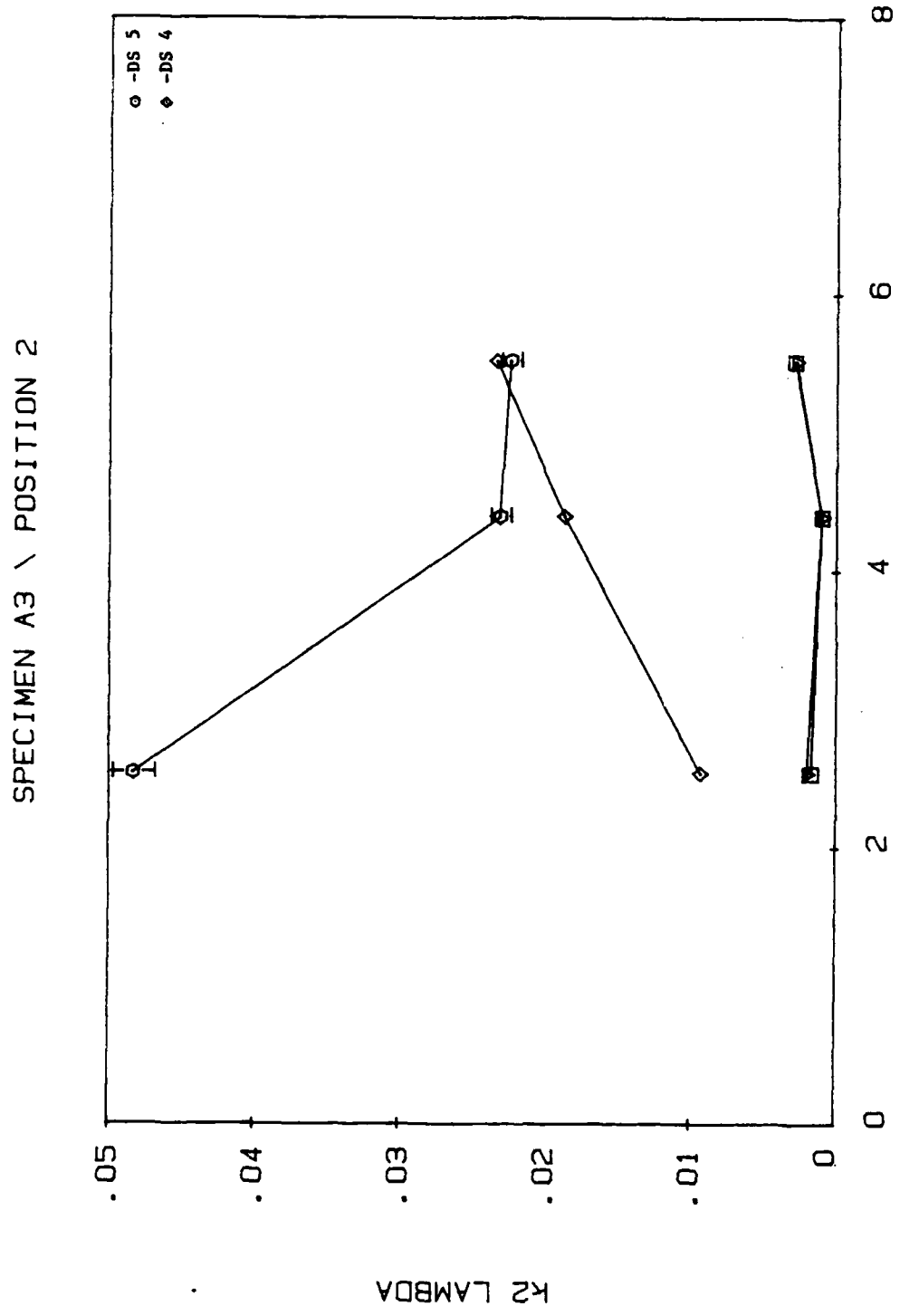

Figure 47. Attenuation versus frequency for each load step at position 2, specimen A3.

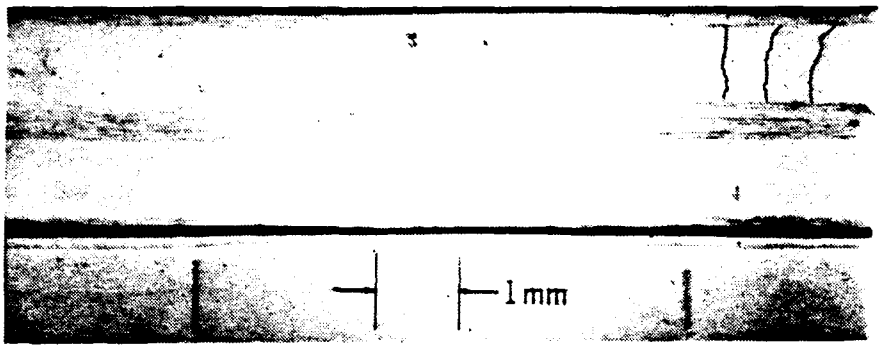

Damage state 4

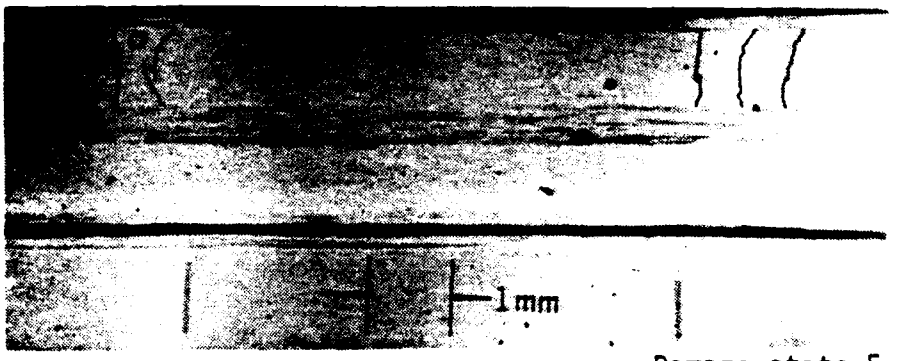

Damage state 5

Figure 48. Damage states for position 2 at load steps 4 and 5, specimen A3.

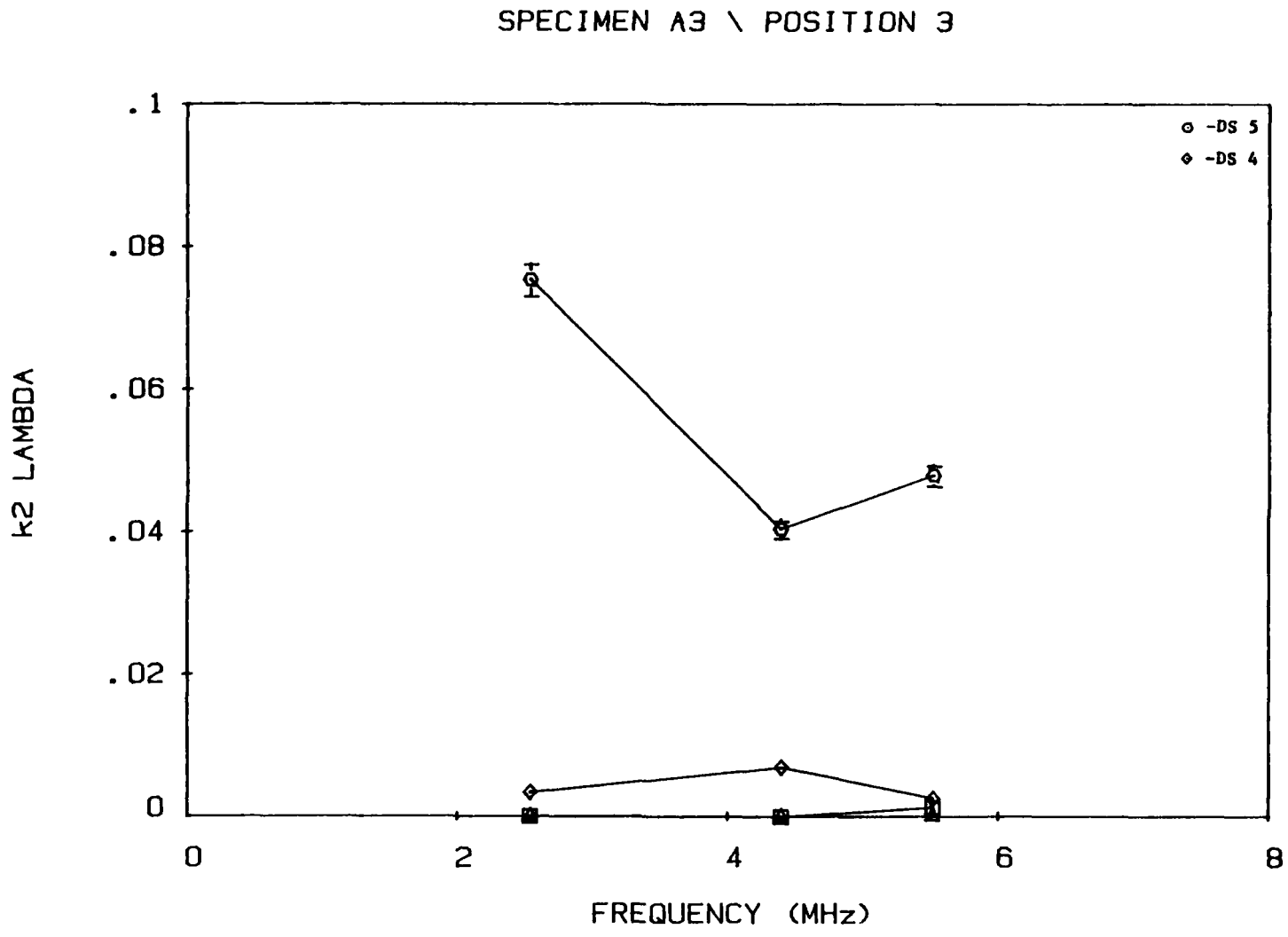

Figure 49. Attenuation versus frequency for each load step at position 3, specimen A3.

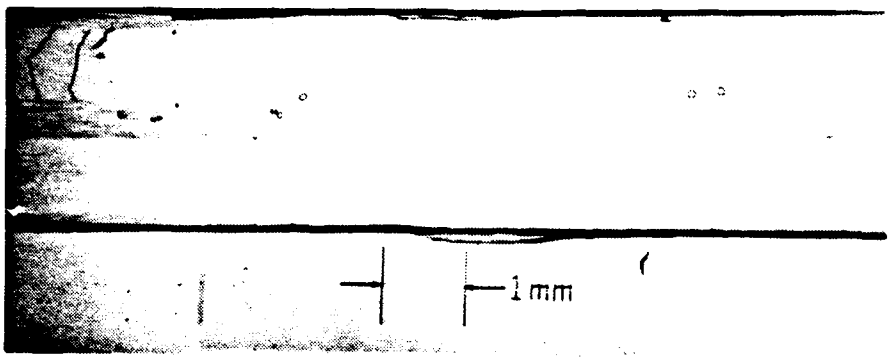

Damage state 4

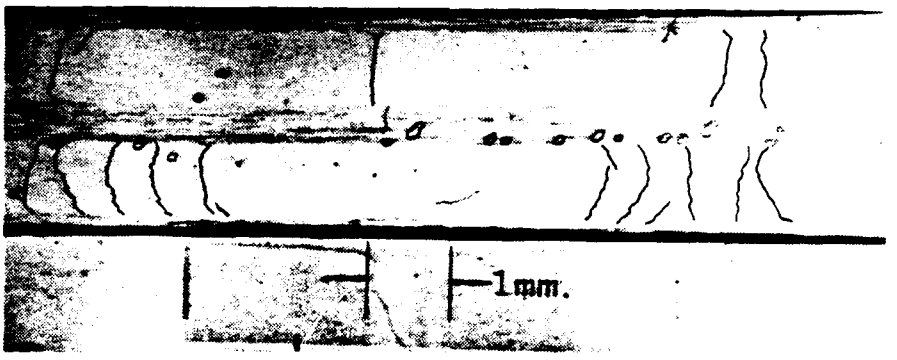

Damage state 5

Figure 50. Damage states for position 3 at load steps 4 and 5, specimen A3.

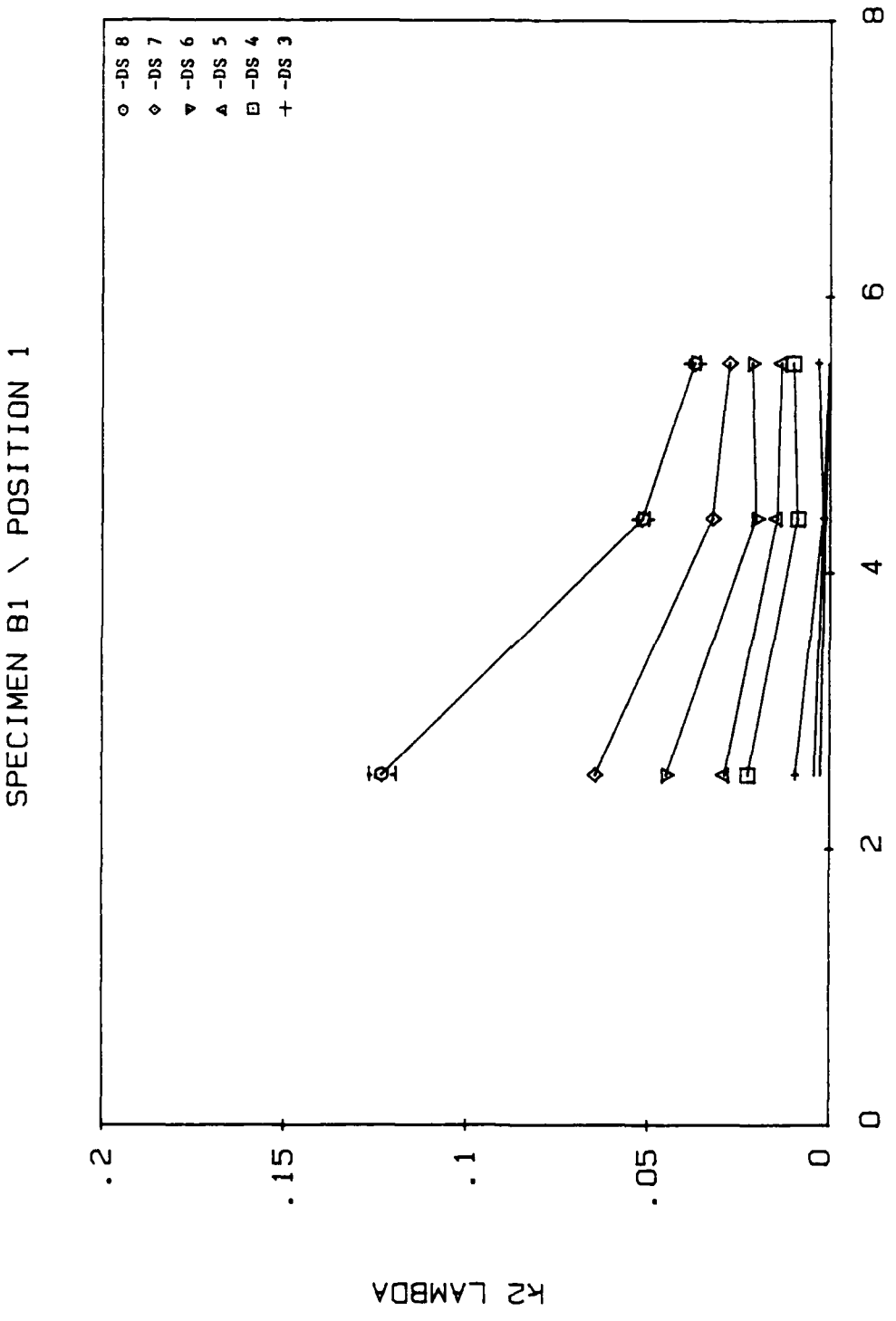

Figure 51. Attenuation versus frequency for each load step at position 1, specimen B1.

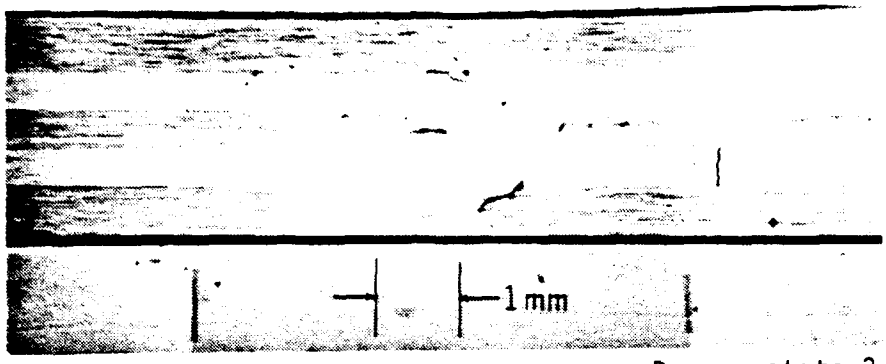

Damage state 3

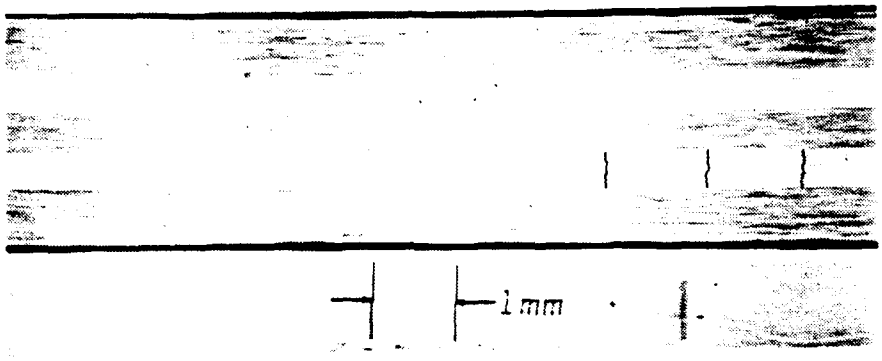

Damage state 4

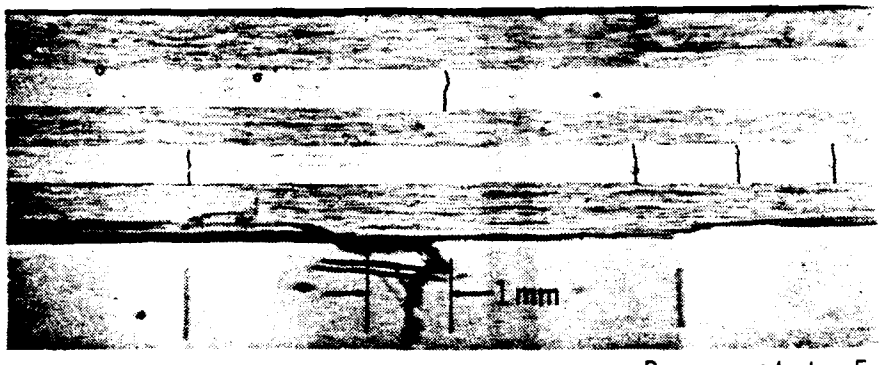

Damage state 5

Figure 52. Damage states for position 1 at load steps 3, 4, and 5, specimen B1.

Damage state 6

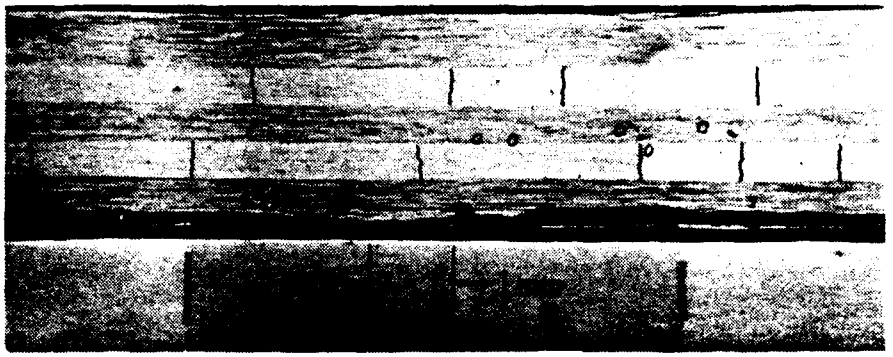

Damage state 7

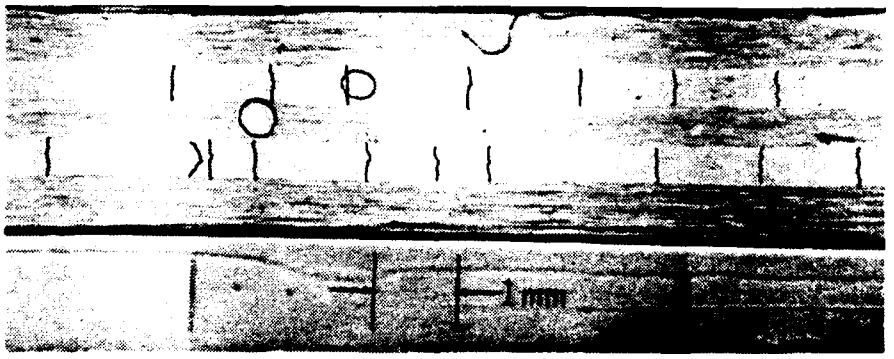

Damage state 8

Figure 53. Damage states for position 1 at load steps 6, 7, and 8, specimen B1.

pictures at each load step for position 1. The results indicate the same trend in attenuation as before. Similar results were obtained for positions 2 and 3 (Figures 54-59). Another specimen, B2, of the same layup was tested and the results from B1 were reconfirmed (Figures 60-66).

To check if the results were consistent when going from the 8-90° ply groups to the 4-90° ply groups a method for comparison was required. It was hoped that we could compare the effect of one crack on attenuation, but since crack position led to erroneous results this was impossible. The other alternative was to compare the higher damage states. Since at this point in the investigation the only visible damage is transverse matrix cracking we chose to use the total crack length, a * N, as a means for comparison (a is the crack length in the direction of the wave propagation-Figure 67, and N is the number of cracks within the transducer window). From the previous results presented, it is fairly well established that one cannot begin to correlate crack length with attenuation changes until the cracks have become evenly distributed within the transducer viewing area. Unfortunately, in the case of the $[0_2/90_8/0_2]$ specimens the cracks did not become evenly distributed until the last load step. This would provide only one point on an attenuation versus crack length plot. Also, specimen A3's final damage state contained many curved cracks. It may be conjectured that curved cracks will attenuate the wave more than the straight cracks, but

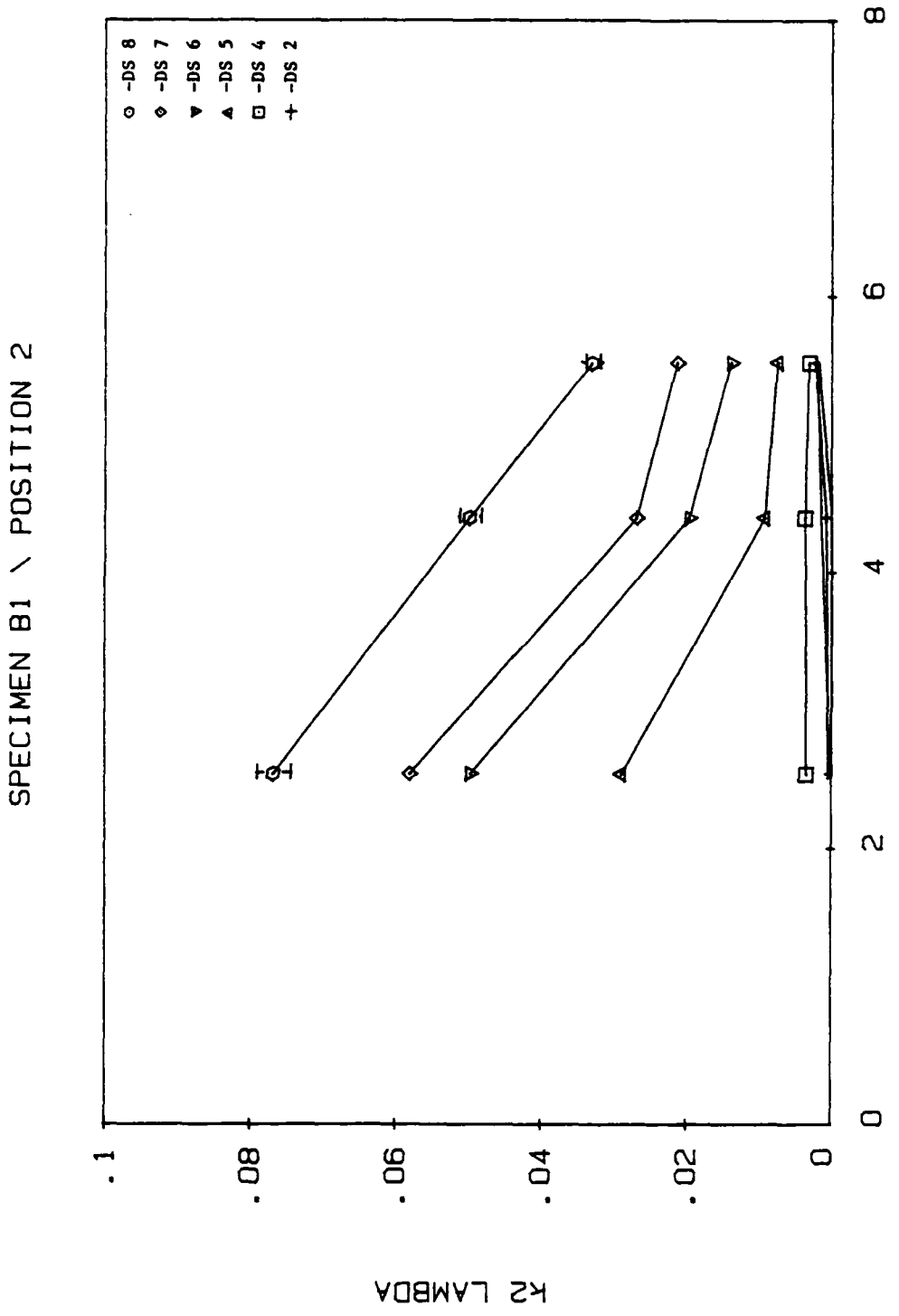

Figure 54. Attenuation versus frequency for each load step at position 2, specimen B1.

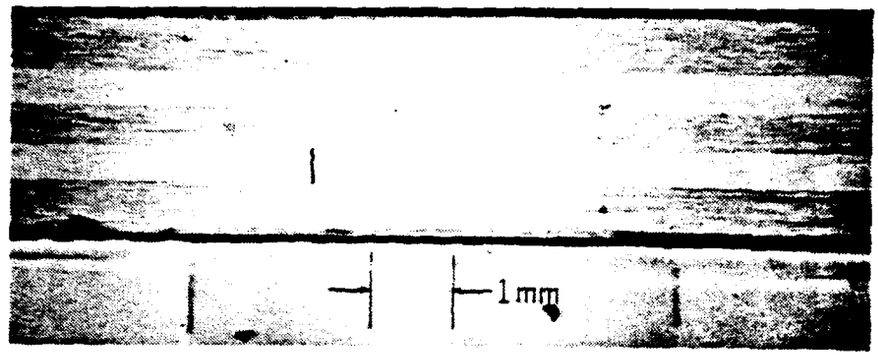

Damage state 2

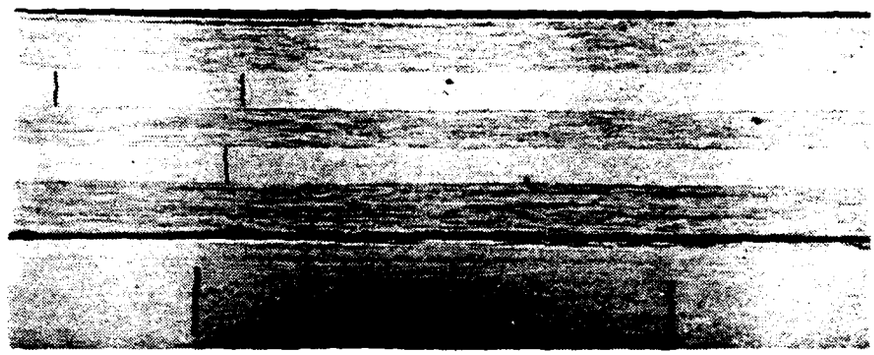

Damage state 4

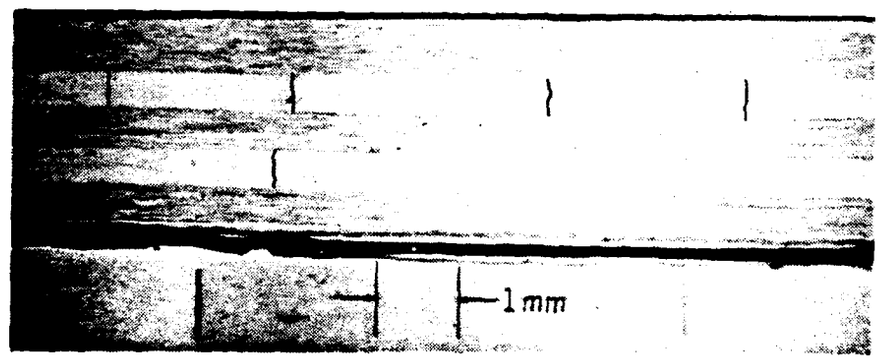

Damage state 5

Figure 55. Damage states for position 2 at load steps 2, 4, and 5, specimen B1.

Damage state 6

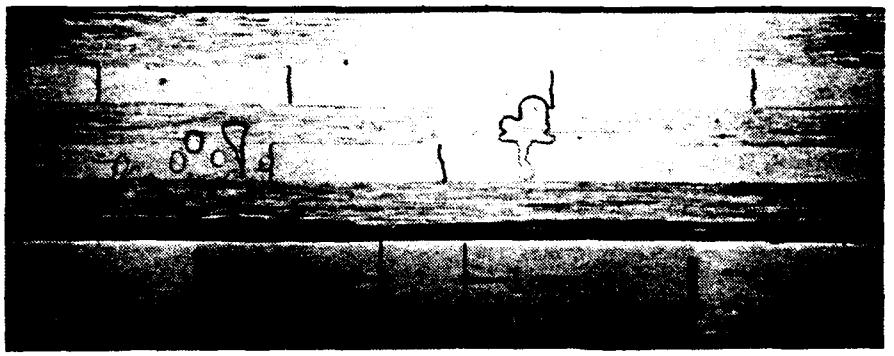

Damage state 7

Damage state 8

Figure 56. Damage states for position 2 at load steps 6, 7, and 8, specimen B1.

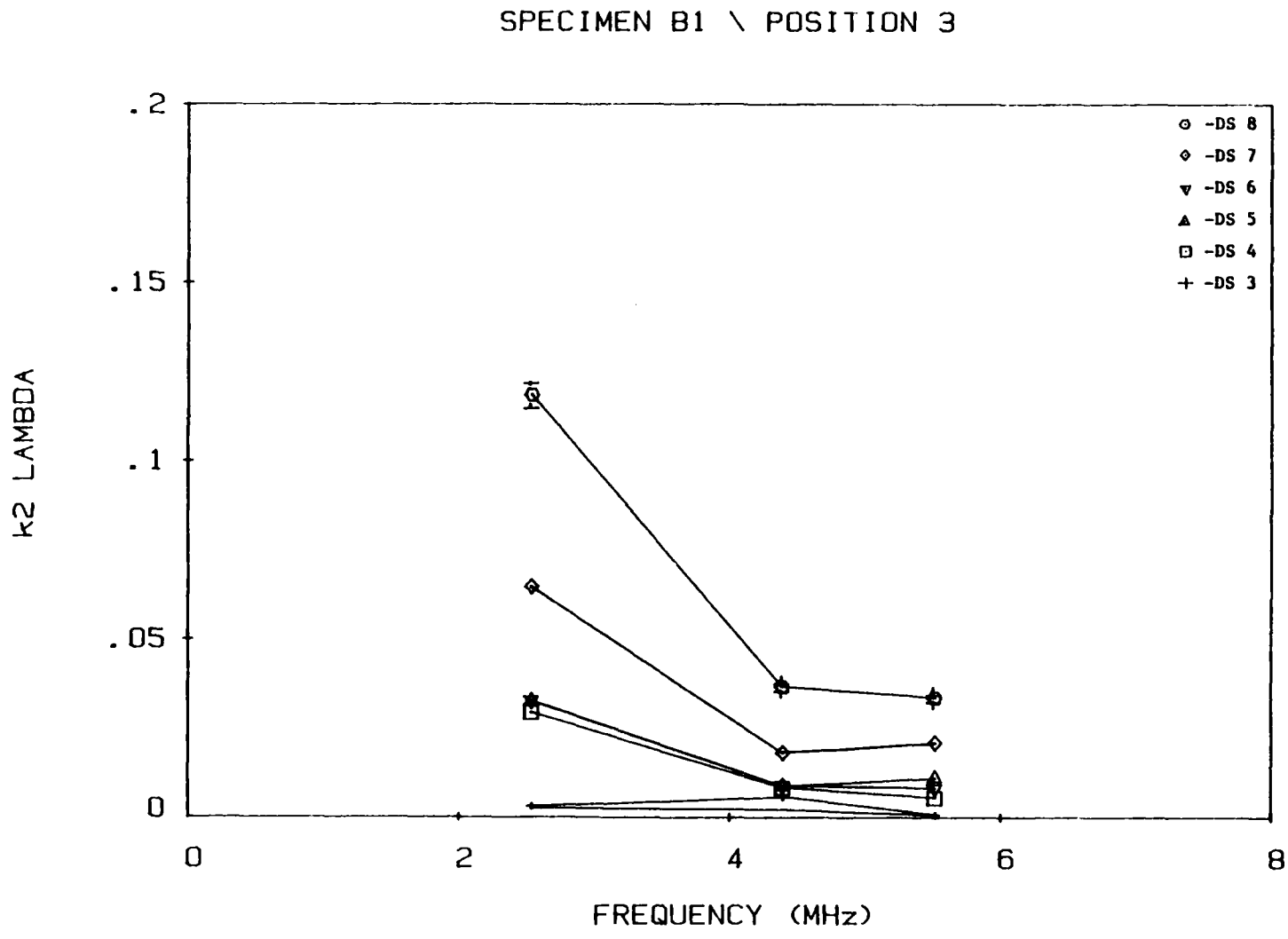

Figure 57. Attenuation versus frequency for each load step at position 3, specimen B1.

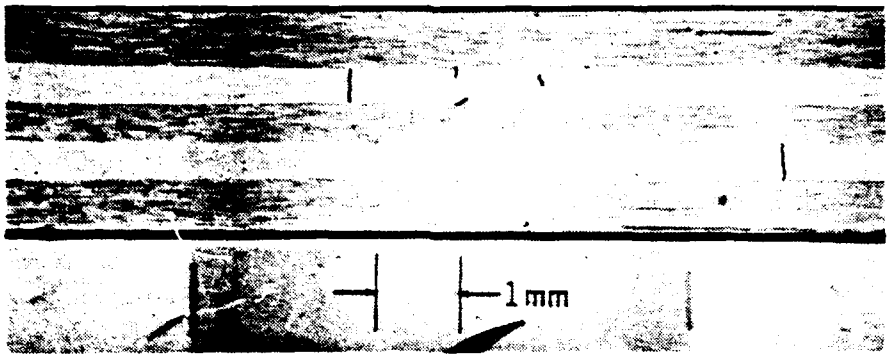

Damage state 3

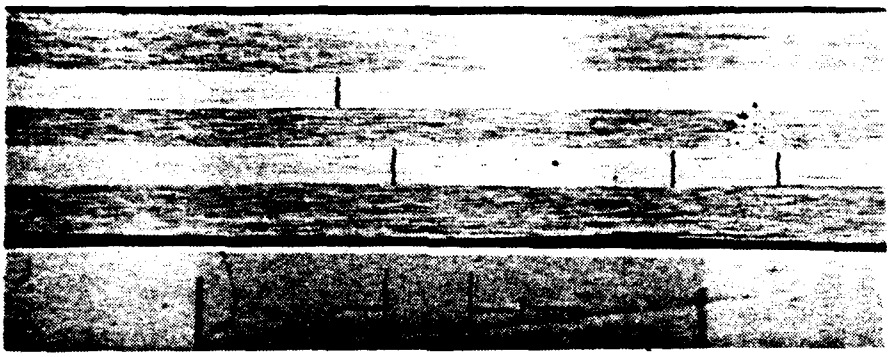

Damage state 4

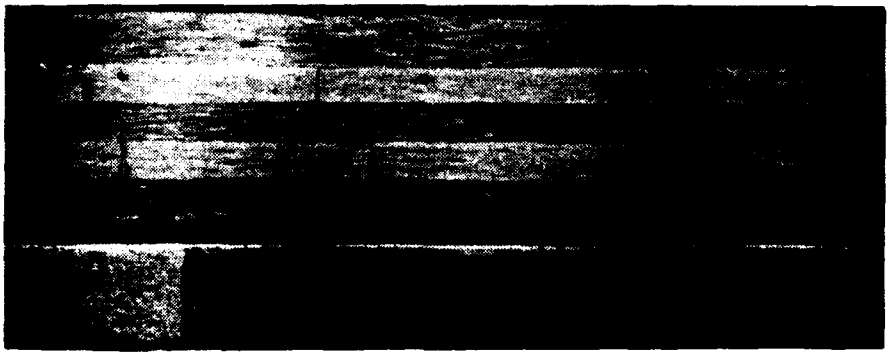

Damage state 5

Figure 58. Damage states for position 3 at load steps 3, 4, and 5, specimen B1.

Damage state 6

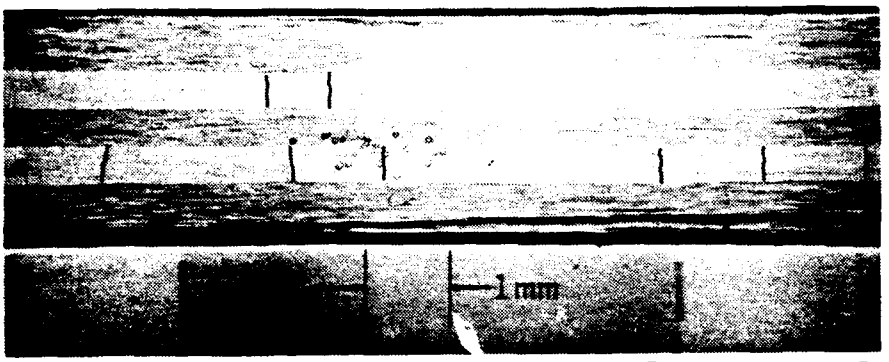

Damage state 7

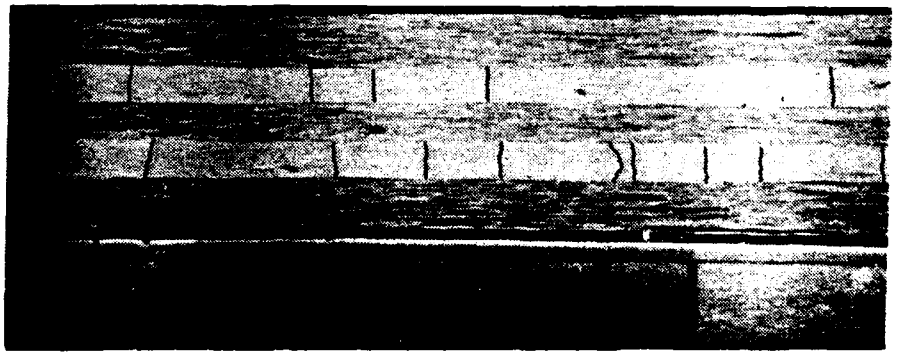

Damage state 8

Figure 59. Damage states for position 3 at load steps 6, 7, and 8, specimen B1.

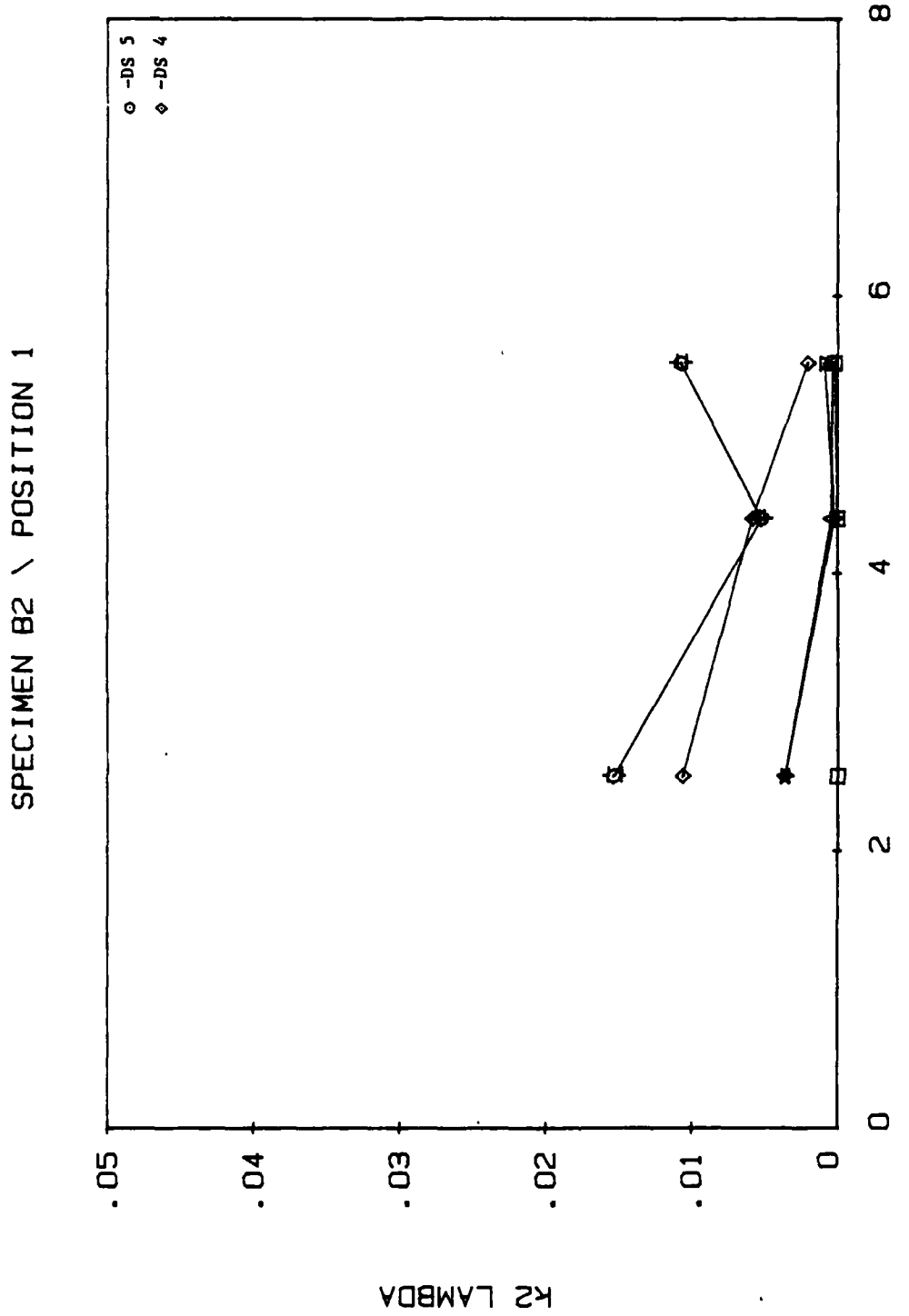

Figure 60. Attenuation versus frequency for each load step at position 1, specimen B2.

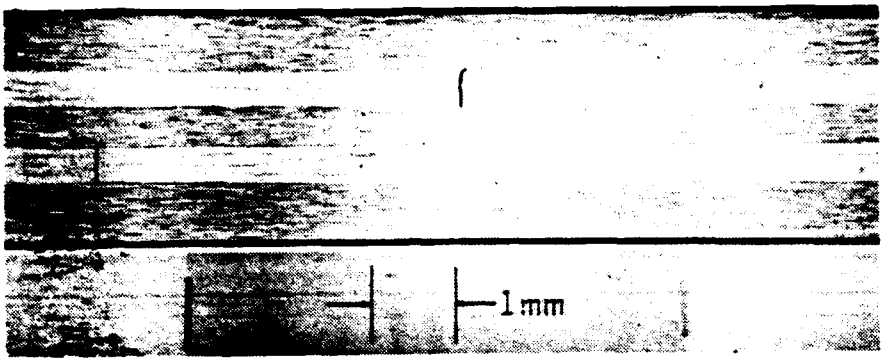

Damage state 4

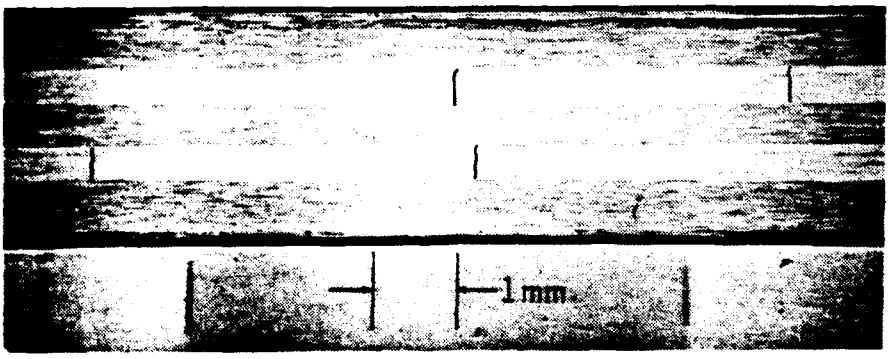

Damage state 5

Figure 61. Damage states for position 1 at load steps 4 and 5, specimen B2.

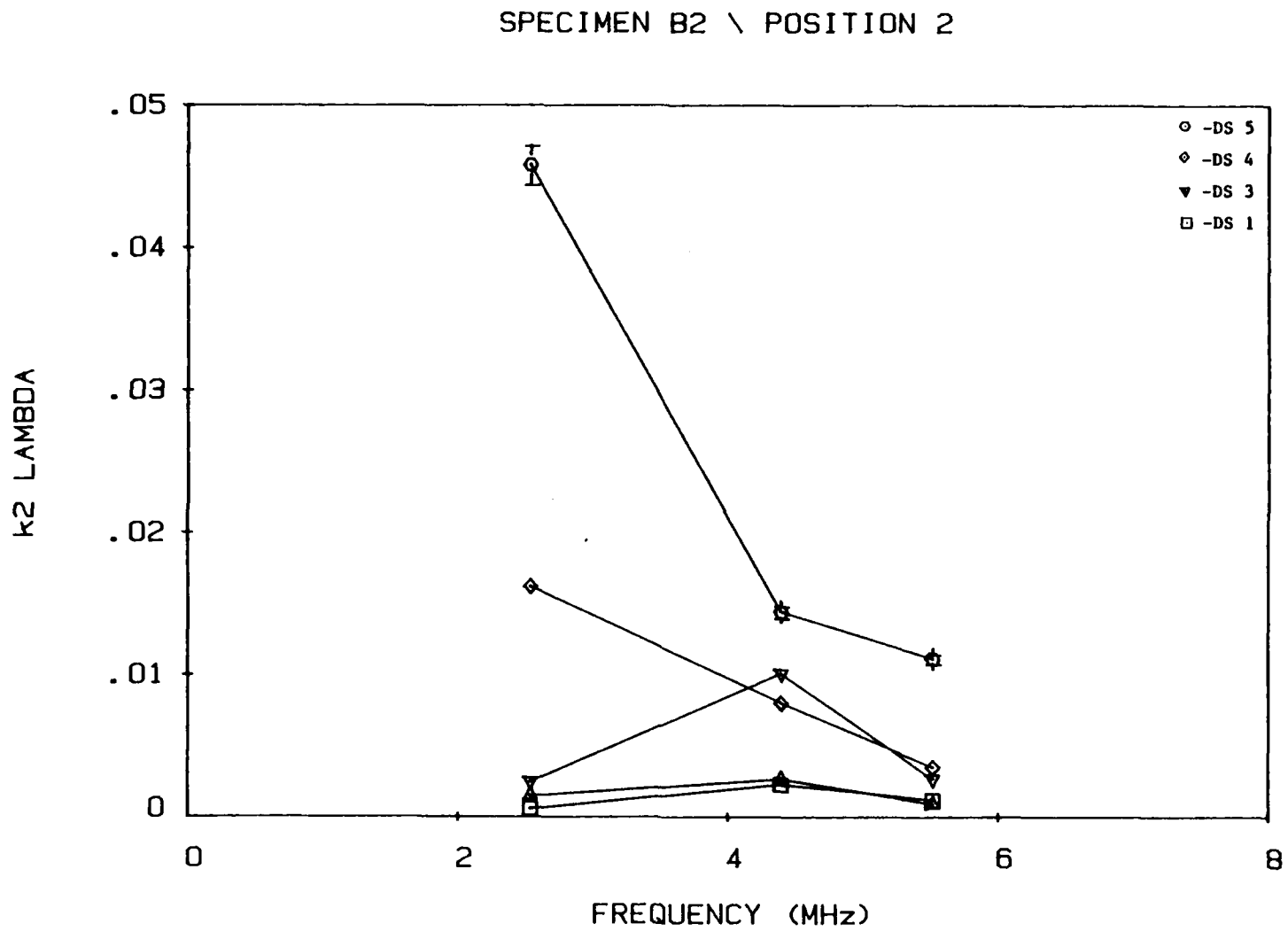

Figure 62. Attenuation versus frequency for each load step at position 2, specimen B2.

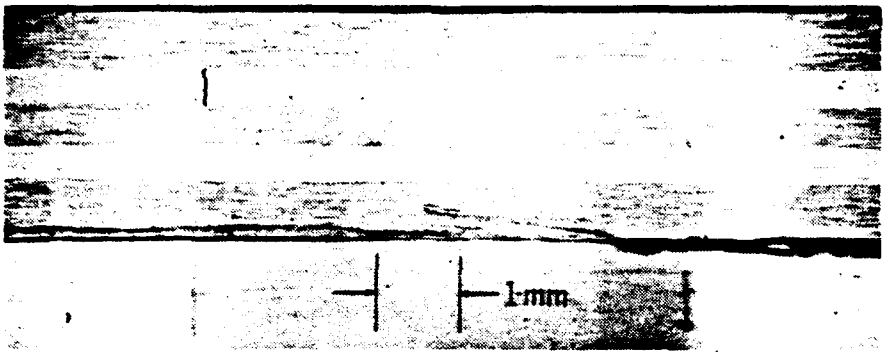

Damage state 1

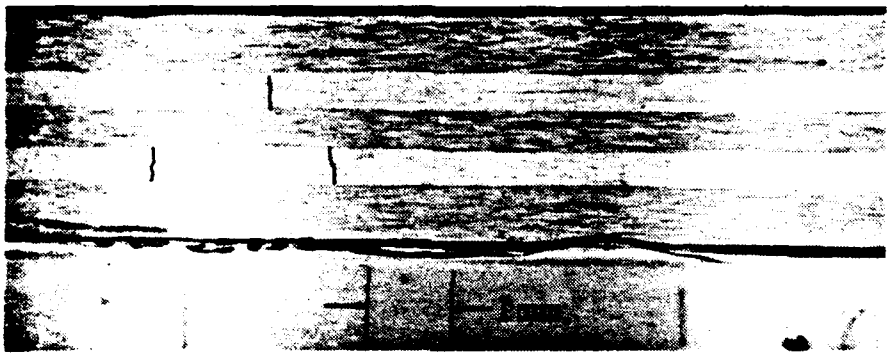

Damage state 3

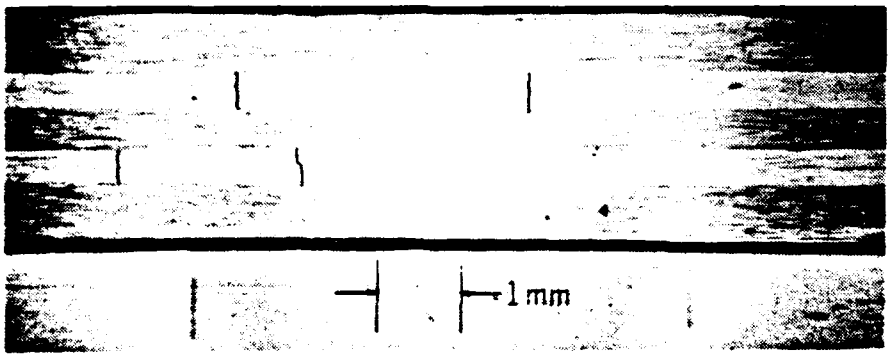

Damage state 4

Figure 63. Damage states for position 2 at load steps 1, 3, and 4, specimen B2.

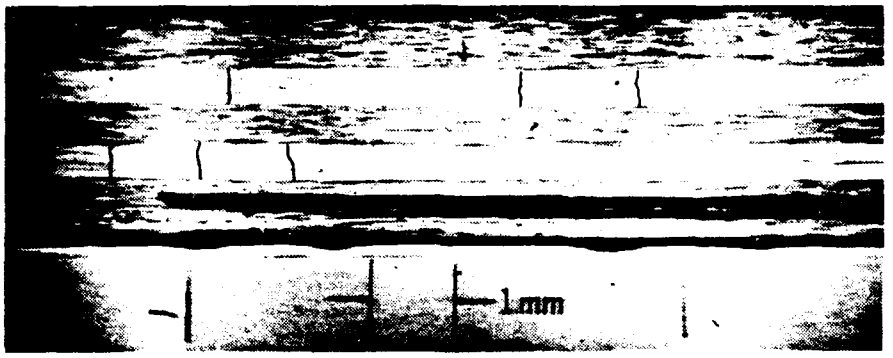

Damage state 5

Figure 64. Damage state for position 2 at load step 5 specimen B2.

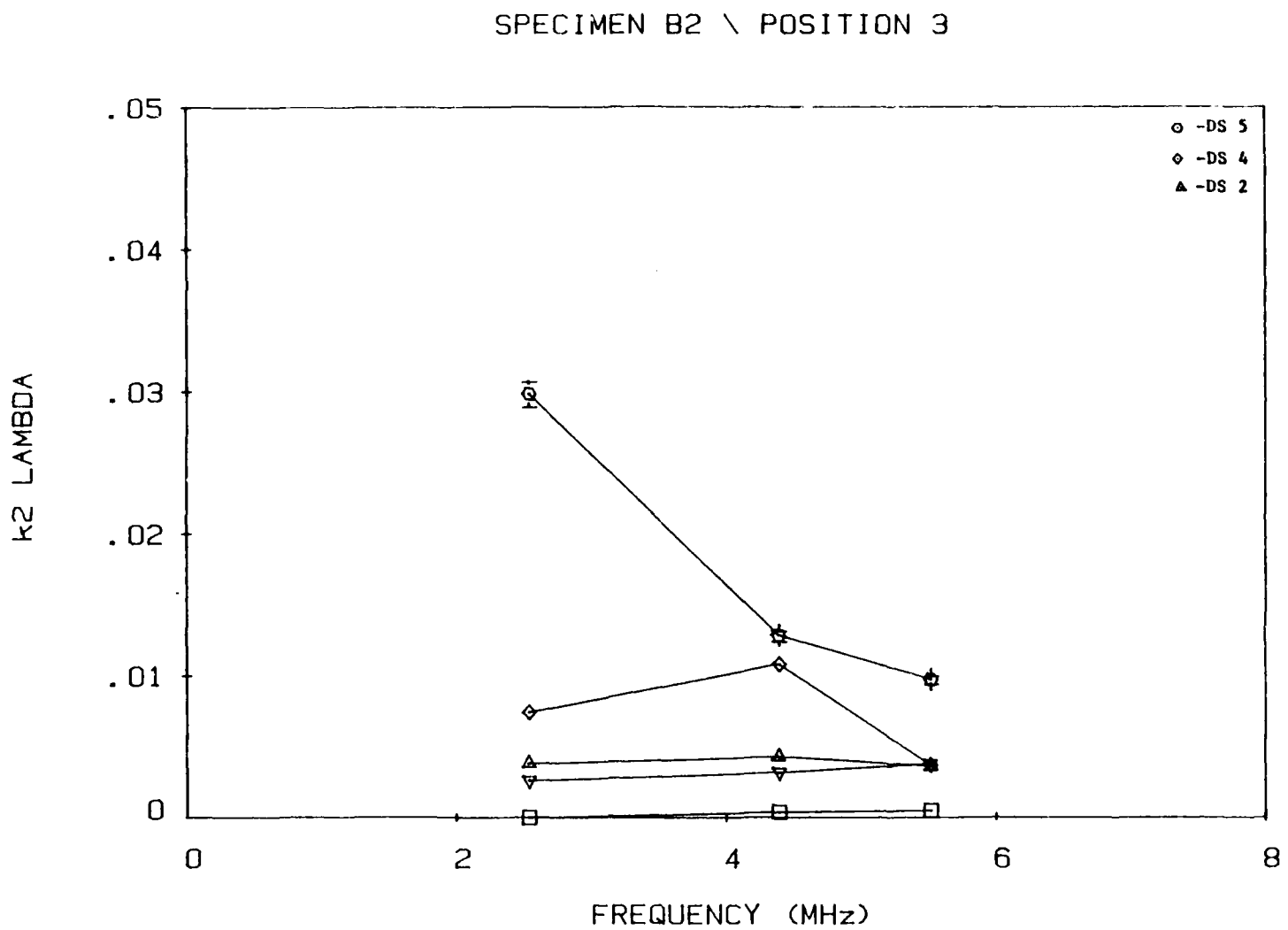

Figure 65. Attenuation versus frequency for each load step at position 3, specimen B2.

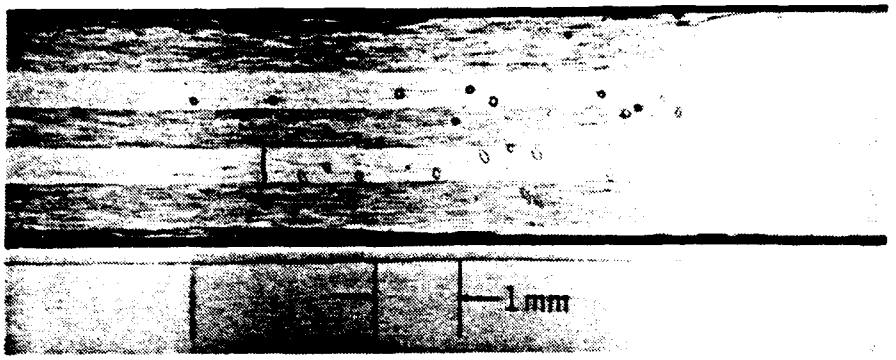

Damage state 2

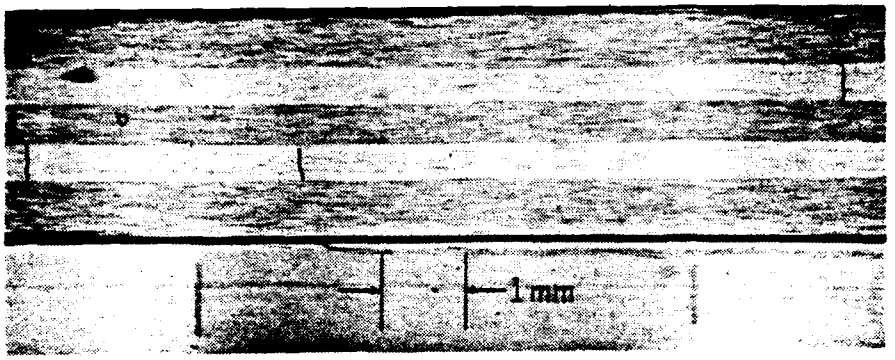

Damage state 4

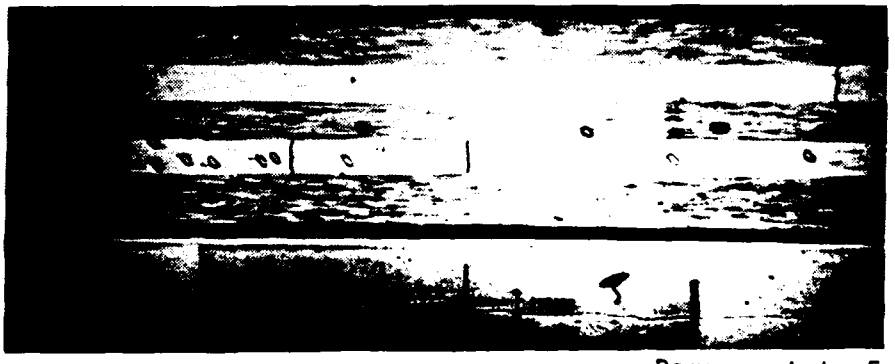

Damage state 5

Figure 66. Damage states for position 3 at load steps 2, 4, and 5, specimen B2.

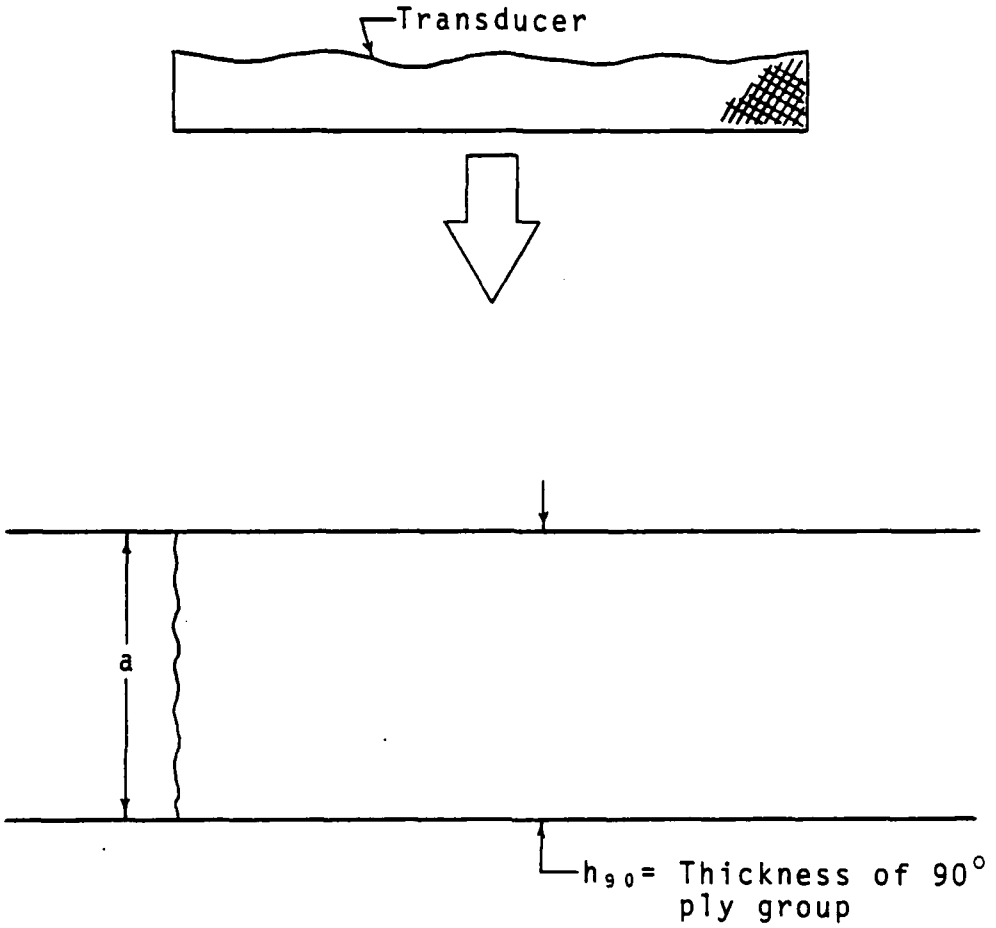

$$a = h_{90}$$

Figure 67. Definition of crack size, a.

since the relation between the attenuation of straight and curved cracks is not clearly understood a comparison of the two would be misleading. It was for the above reasons that any sort of comparison technique between the 8-90° ply group and the 4-90° ply group specimens was abandoned.

However, as shown earlier, specimen B1 did exhibit a steady growth in crack number as the loading increased. Figures 68-70 are the plots of $k_2\lambda$ versus crack length at 2.25, 5.0, and 7.5 MHz, respectively. Each line represents the data from a different position along B1. The data for each position are listed in Table 2. The scatter at the start of each plot is probably due to the uneven distribution of cracks in the beginning. What is important in the plots is the amount of scatter at the end. Since at each position the cracks have become evenly distributed and almost equal in total crack length one would assume that the values of $k_2\lambda$ would become similar as more cracks appear. From Figure 68 the data at 2.25 MHz indicate a variance in $k_2\lambda$ of approximately 100% at the larger crack lengths. At 5.0 MHz, Figure 69, the scatter is reduced to about 40%, and at 7.5 MHz, Figure 70, the attenuations fall within 10% of each other at the higher damage states. These figures indicate that even though larger attenuation changes were recorded at 2.25 MHz the values obtained may not give an accurate description of the actual damage that was present. However, as the frequency is reduced the data seem to give a better representation of the damage state.

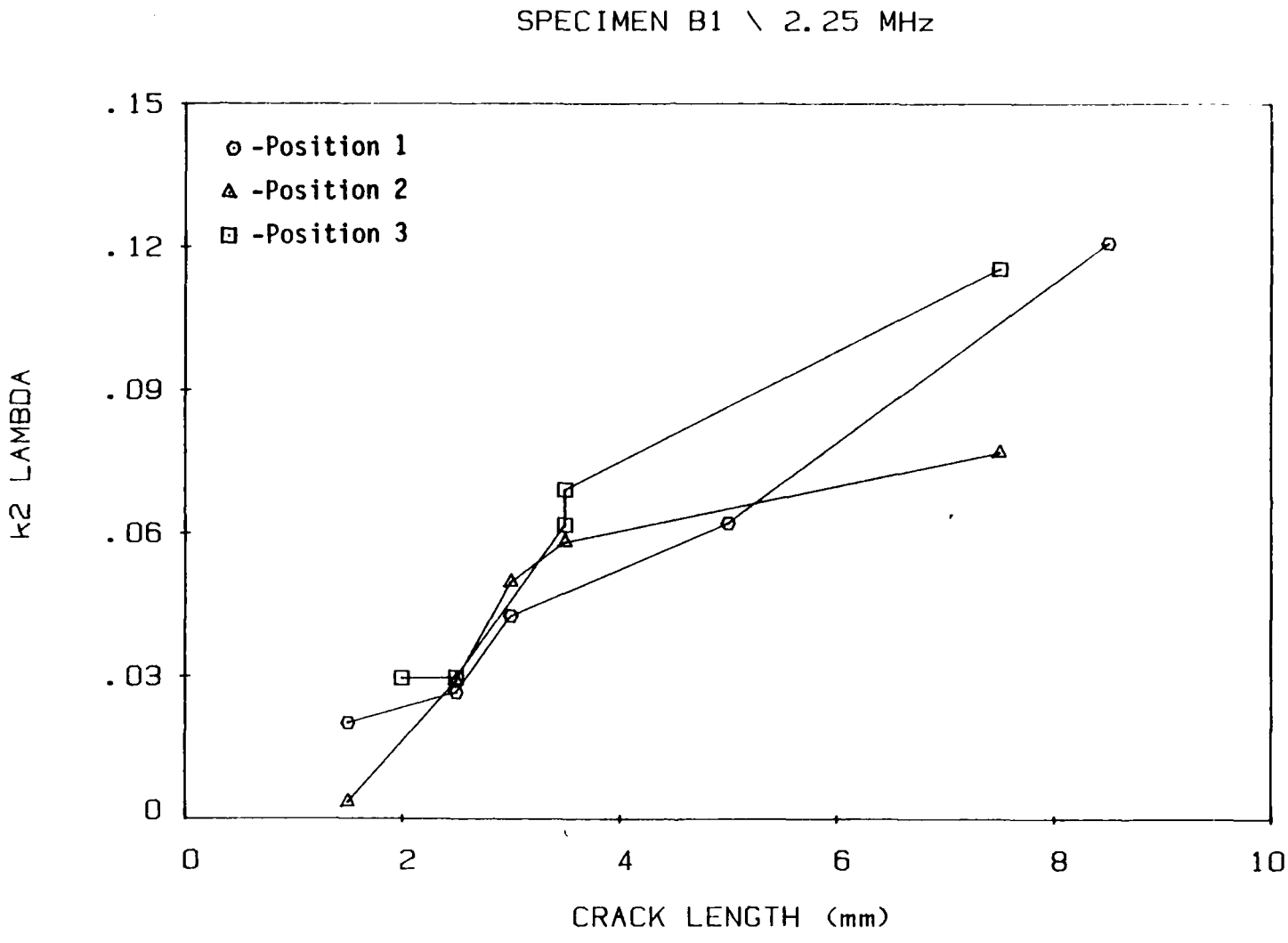

Figure 68. Attenuation versus crack length for specimen B1 at 2.25 MHz.

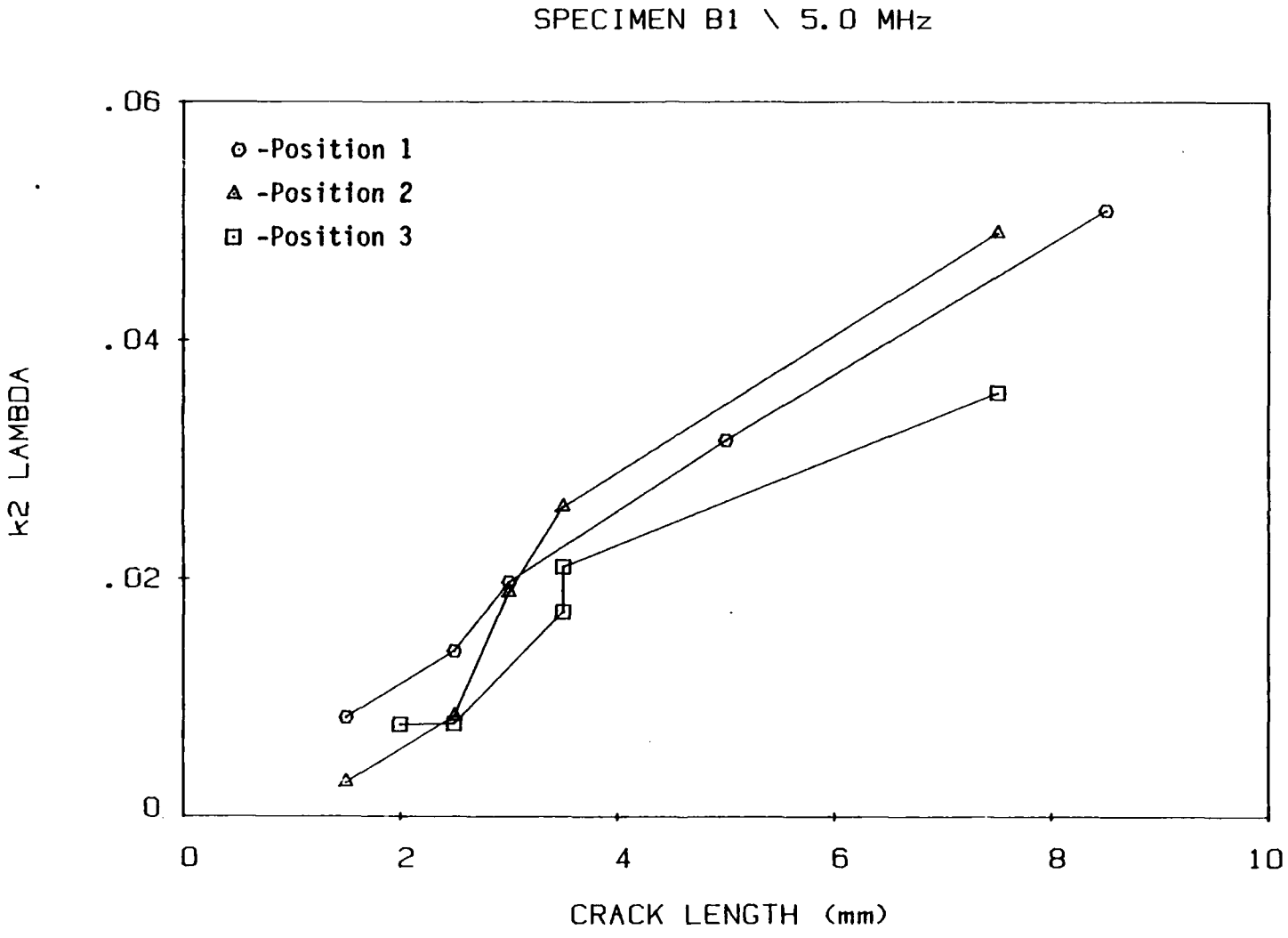

Figure 69. Attenuation versus crack length for specimen B1 at 5.0 MHz.

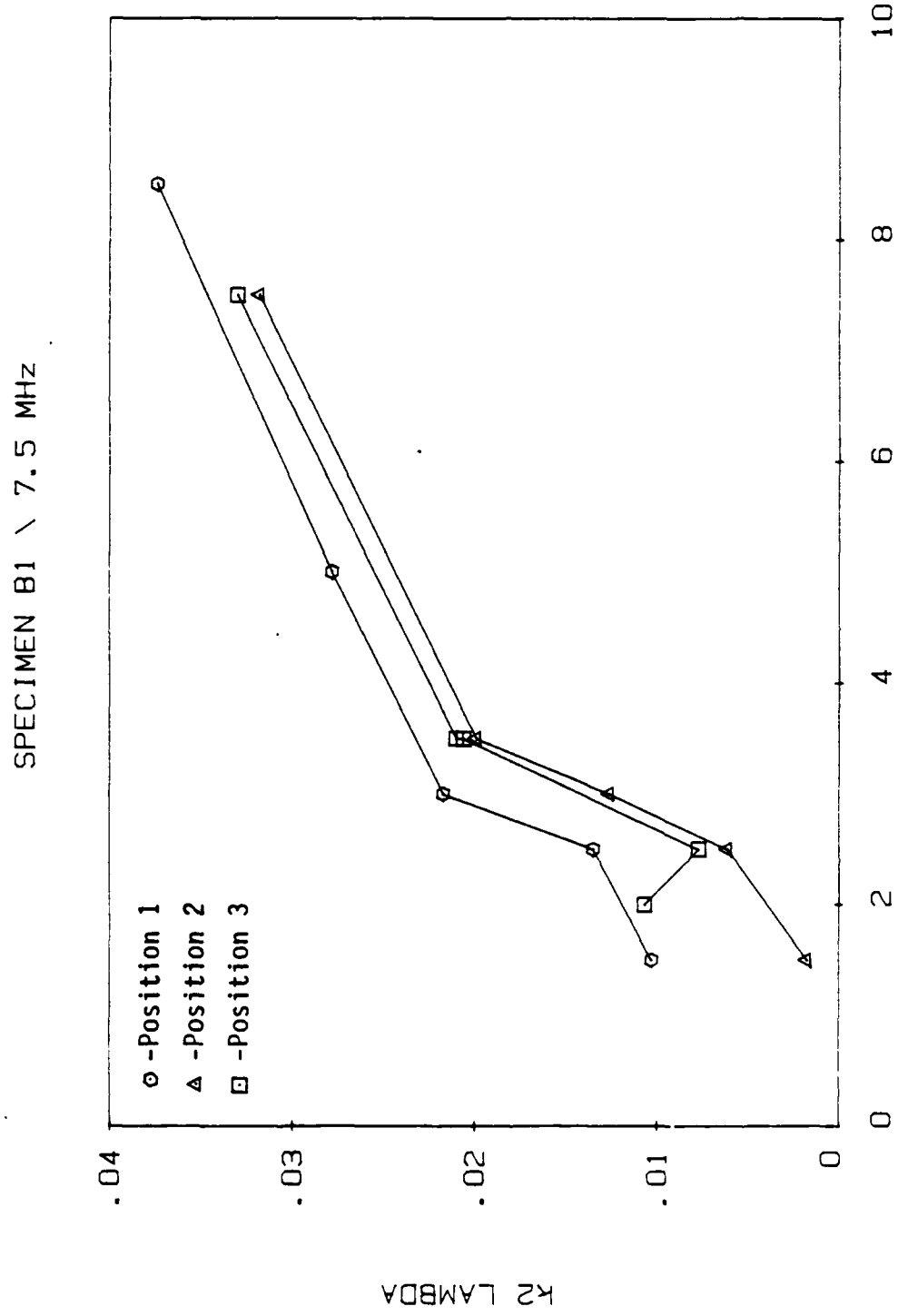

Figure 70. Attenuation versus crack length for specimen B1 at 7.5 MHz.

Table 2. Specimen B1 / Crack Length Data

Position	Load Step	Crack Length (mm)	Change in k2 Lambda measured at 2.25 MHz	5.0 MHz	7.5 MHz
1	4	1.5	.0202	.0084	.0103
	5	2.5	.0266	.0139	.0135
	6	3.0	.0426	.0197	.0217
	7	5.0	.0621	.0316	.0278
	8	8.5	.1208	.0509	.0374
2	4	1.5	.0036	.0029	.0018
	5	2.5	.0290	.0085	.0061
	6	3.0	.0497	.0189	.0126
	7	3.5	.0581	.0260	.0199
	8	7.5	.0769	.0490	.0318
3	4	2.0	.0296	.0078	.0107
	5	2.5	.0297	.0078	.0077
	6	3.5	.0617	.0172	.0206
	7	3.5	.0691	.0210	.0210
	8	7.5	.1154	.0356	.0330

A possible explanation is that the wavelength, λ, of the investigating pulse is becoming comparable to the actual crack length, a. For specimen B1, a=0.5 mm. The wavelength at 2.25 MHz, λ_2, through this particular composite specimen is 1.36 mm. At 5.0 MHz λ_5=0.61 mm, and at 7.5 MHz λ_7=0.41 mm.

CONCLUSIONS

The first sections of this thesis mainly concern technique development and implementation. Although not titled as 'results' the data obtained for these sections served as starting points for each new test. As in the development of any new technique many unexpected problems arise that have to be studied, explained, and eliminated if possible. Therefore, one of the major results would be the production of a reliable measurement system. The wave speed and the attenuation can be measured with a precision of ±0.1% and ±1.0%, respectively.

Two composite layup geometries were studied: 1) $[0_2/90_8/0_2]s$, and 2) $[0_6/90_4/0_2]s$. The specimens were monotonically loaded and at each step the wave speed and attenuation were measured at 2.25, 5.0, and 7.75 MHz. No definitive conclusions can be made regarding the influence of damage on wave speed.

For attenuation, the problem of crack position within the transducer window proved to be significant. The results show that only at higher load levels, where the transverse cracks are evenly distributed, can the attenuation values be expected to exhibit a reproducible trend with frequency (i.e., attenuation decrease with increasing frequency).

The attenuation data at 2.25 MHz consistently indicated a larger increase with increasing damage than the 5.0 or 7.5 MHz data. However, when the results were compared with

the total crack length it was observed that the 7.5 MHz results gave a better depiction of the actual damage in the composite.

RECOMMENDATIONS

The reason for choosing the layup geometries tested was to establish a relationship between crack size, a, and its corresponding attenuation. It was hoped that these data could be extended to the multiple crack problem. Since this information was unattainable due to the problems previously discussed it is recommended that new specimens be made that contain smaller 90° ply groups. Even though a single crack may not be detected the damage growth would probably be more consistent.

Also, a more precise specimen holder needs to be manufactured. From experience, it is believed that reproducing the exact specimen position from test to test is the most critical source of error.

REFERENCES

1. K.L. Reifsnider and R. Jamison,"Fracture of Fatigue-Loaded Composite Laminates," Int. J. of Fatigue, Oct., 1982, p.187-197.

2. J.D. Achenbach, Wave Propagation in Elastic Solids, North-Holland Publishing Company, New York, N.Y., 1973, p.30.

3. H. Kolsky, Stress Waves in Solids, Dover Publications, Inc., New York, 1963, p.17.

4. W.M. Pless, S.M. Freeman, and C.P. Bailey,"Advanced Methods for Damage Analysis in Graphite-Epoxy Composites," 14th National SAMPE Technical Conference, Oct.12-14, 1982.

5. K.L. Reifsnider, H.G. Henneke, W.W. Stinchcomb, and J.C.Duke, "Damage and NDE of Composite Laminates," Mechanics of Composite Materials, Engineering Science and Mechanics Dept., Virginia Polytechnic Institute, Virginia, 1983, pp.399-420.

6. G.P. Sendeckyj,"NDE Techniques for Composite Laminates," AGARD Conference Proceedings No. 355, Papers presented at the 56th meeting of the Structures and Materials Panel in London, United Kingdom, April 12-14, 1983, p2-1.

7. D.O. Stalnacker and W.W. Stichcomb,"Load History-Edge Damage Studies in Two Quasi-Isotropic Graphite Epoxy Laminates," American Society for Testing and Materials, ASTM STP-674, R.B. Pipes, Ed., 1979, p.622-641.

8. W.E. Dance and J.B. Middlebrook,"Neutron Radiographic Nondestructive Inspection for Bonded [illegible] Structures," Nondestructive Evaluation [illegible] Criticality for Composite Materials, American Society for Testing and Materials , ASTM 696, R.B. [illegible], Ed., 1979, pp.57-71.

9. T.S. Jones and E.G. Henneke,"Detection of Damage in Composite Materials by Vibrothermography," Non-destructive Evaluation and Flaw Criticality for Composite Materials, American Society for Testing and Materials, ASTM 696, R.B. Pipes, Ed., 1979, pp.83-95.

10. G.E. Maddux and G.P. Sendeckyj,"Holographic Techniques for Defect Detection in Composite Materials,"

Nondestructive Evaluation and Flaw Criticality for Composite Materials, American Society for Testing and Materials, ASTM 696, R.B. Pipes, Ed., 1979, pp.83-95.

11. J.A. Charles,"Liquid Crystals for Flaw Detection in Composites," Nondestructive Evaluation and Flaw Criticality for Composite Materials, American Society for Testing and Materials, ASTM 696, R.B. Pipes, Ed., 1979, pp.72-82.

12. C.D. Bailey, S.M. Freeman, and J.M. Hamilton,"Acoustic Emission Monitors Damage Progression in Graphite Epoxy Composite Structures," Materials Evaluation, Vol.38, Aug., 1980, p.21.

13. R.S. Williams and K.L. Reifsnider,"Real-Time Nondestructive Evaluation of Composite Materials During Fatigue Loading," Materials Evaluation, Vol. 35, Aug., 1977, p. 50.

14. A. Arora and Tangri,"Acoustic Emission: A Means of Measuring Crack Growth at Elevated Temperatures," Experimental Mechanics, Vol. 21, No. 7, July, 1981, p.261.

15. Joachim Block,"Monitoring of Defect Progression by Acoustic Emission," AGARD Conference Proceedings No. 355, Papars presented at the 56th meeting of the Structures and Materials Panel in London, United Kingdom, April 12-14, 1983, p3-1.

16. David A. Ulman, Edmund Henneke, J.C. Duke, K.L. Reifsnider, and W.W. Stinchcomb,"Nondestructive Evaluation in Metal Matrix Composites," Dept. of Engineering and Mechanics, Virginia Polytechnic Institute, Virginia, Final Report, June 1, 1982.

17. J.H. Williams and D.M. Egan,"Acoustic Emission Spectral Analysis of Fiber Composite Failure Mechanisms," Materials Evaluation, Vol. 37, No. 1, Jan., 1979, p.43.

18. Robert A. Blake,"Digital Nondestructive Evaluation of Composite Materials," Micro-Delcon, Newark, Delaware, March, 1982.

19. Robert A. Blake,"Digital Dot Matrix C-Scan," Center for Composites, University of Delaware, Newark, Delaware, 1982.

20. Robert A. Blake,"Ultrasonic Image Histogram Evaluation and Enhancement," IEEE 1983 Proceedings of the Sixth Annual Micro-Delcon Conference, Newark, Delaware.

21. Robert A. Blake and Hans S. Hartmann,"Computer-Aided Ultrasonic Evaluation of Fiber FP Metal Matrix Composites," Composites Technology Review, Vol. 6, No.3, Sept., 1984, pp.118-123.

22. F.H. Chang, J.R. Bell, A.H. Gardner, C.P. Fisher, and R.W. Haile,"A Laboratory Mock-Up Ultrasonic Inspection System for Composites," Materials Evaluation, Vol. 40, No. 7, June, 1982, pp.756-761.

23. F.H. Chang, J.R. Bell, A.H. Gardner, G.P. Handley, and C.P. Fisher,"In-Service Inspection of Advanced Composite Aircraft Structures," General Dynamics, Fort Worth Division, Report AFML-TR-79-4087, Feb., 1979.

24. Louis J. Kiraly and Erwin H. Meyn,"Ultrasonic Scanning System for Imaging Flaw Growth in Composites," Twenty-Eighth Int. Instrumentation Symposium, Instrument Society of America, Las Vegas, Nevada, May 3-6, 1982.

25. I.M. Daniel, S.W. Schramm, and T. Liber,"Fatigue Damage Monitoring in Composites by Ultrasonic Mapping," Materials Evaluation, Vol. 39, No. 9, August, 1981, pp.834-839.

26. T. Liber, I.M. Daniel, and S.W. Schramm,"Ultrasonic Techniques for Inspecting Flat and Cylindrical Composite Specimens," Nondestructive Evaluation and Flaw Criticality for Composite Materials, American Society for Testing and Materials, ASTM 696, R.B. Pipes, Ed., 1979, pp.5-25.

27. W.H.M. van Dreumel and J.L. Speijer,"Nondestructive Composite Laminate Characterization by Means of Ultrasonic Polar-Scan," Materials Evaluation, Vol. 39, No. 10, Sept., 1981, pp.922-924.

28. W.H.M. van Dreumel and J.L. Speijer,"Polar-Scan, A Nondestructive Test Method for the Inspection of Layer Orientation and Stacking Order in Advanced Fiber Composites," Materials Evaluation, Vol. 41, No. 9, Aug., 1983, pp.1060-1062.

29. A. Vary and K.J. Bowels,"Ultrasonic Evaluation of the Strength of Unidirectional Graphite/Polyamide Composites," Proceedings of the Eleventh Symposium on Nondestructive Testing, Columbus, and Southwest Research Institute, San Antonio, 1977, pp.242-258.

30. A. Vary,"A Review of Issues and Strategies in Nondestructive Evaluation of Fiber Reinforced

Composites," Proceedings of the Eleventh National SAMPE Technical Conference: New Horizons-Materials and Processes for the Eighties, Vol. 11, Society for the Advancement of Material and Process Engineering, Azusa, CA., 1979, pp.166-177.

31. A. Vary,"Correlations between Ultrasonic and Fracture Toughness Factors on Metallic Materials," Fracture Mechanics, American Society for Testing and Materials, ASTM STP-677, R.B. Pipes, Ed., 1979, pp.563-578.

32. A. Vary and K.J. Bowles,"An Ultrasonic-Acoustic Technique for Nondestructive Evaluation of Fiber Composite Quality," Polymer Engineering and Science, Vol. 19, No. 5, 1979, pp.373-376.

33. A. Vary and R.F. Lark,"Correlation of Fiber Composite Tensile Strength with the Ultrasonic Stress Wave Factor," J. of Testing and Evaluation, Vol. 7, No. 4, 1979, pp.185-191.

34. A. Vary,"Concepts and Techniques for Ultrasonic Evaluation of Material Mechanical Properties," Mechanics of Nondestructive Testing, Plenum Press, New York, 1980, pp.123-141.

35. A. Vary,"Ultrasonic Measurements of Material Properties," Research Techniques in Nondestructive Testing, Vol. 4, Academic Press, London, 1980, pp.159-204.

36. A. Vary and D.R. Hull,"Interrelation of Material Microstructure, Ultrasonic Factors and Fracture Toughness of a Two Phase Titanium Alloy," Materials Evaluation, Vol. 41, 1983, pp.309-314.

37. A. Vary,"Correlations Among Ultrasonic Propagation Factors and Fracture Toughness Properties of Metallic Materials," NASA Technical Memorandum, NASA TM X-71889, 1976.

38. J.H. Williams and B. Doll,"Ultrasonic Attenuation as an Indicator of Fatigue Life of Graphite Fiber Epoxy Composite," Materials Evaluation, Vol. 38, No. 5, May, 1980, pp.33-37.

39. J.H. Williams, H. Yuce, and S.S. Lee,"Ultrasonic and Mechanical Characterizations of Fatigue States of Graphite Epoxy Composite Laminates," Materials Evaluation, Vol. 40, No. 5, April, 1982, pp.560-565.

40. J.H. Williams and S.S. Lee,"Stress-Wave Attenuation in Thin Structures by Ultrasonic Through-Transmission,"

J. of Nondestructive Evaluation, Vol. 1, No. 4, 1980, pp.277-286.

41. J.H. Williams, Hamid Nayeh-Hashemi, and S.S. Lee, "Ultrasonic Attenuation and Velocity in AS/3501-6 Graphite Fiber Composite," J. of Nondestructive Evaluation, Vol. 1, No. 2, 1980, pp.137-148.

42. J.H. Williams and N.R. Lampert,"Ultrasonic Evaluation of Impact-Damaged Graphite Fiber Composite," Materials Evaluation, Vol. 38, No. 12, Dec., 1980, pp.68-72.

43. R. Truell and A. Hikata,"Fatigue and Ultrasonic Attenuation," Symposium on Nondestructive Testing, Los Angeles, CA., Sept. 17, 1956, American Society for Testing and Materials, ASTM STP-213, R.B. Pipes, Ed., 1957, pp.63-69.

44. Narayan R. Joshi and Robert E. Green,"Ultrasonic Detection of Fatigue Damage," Engineering Fracture Mechanics, Vol. 11, 1972, pp.577-583.

45. D.T. Hayford, E.G. Henneke, and W.W. Stinchcomb,"The Correlation of Ultrasonic Attenuation and Shear Strength in Graphite-Polyamide Composites," J. of Composite Materials, Vol. 11, Oct., 1977, pp.429-444.

46. E.G. Henneke, J.C. Duke, W.W. Stinchcomb, A. Govada, and A. Lemascon,"A Study of the Stress Wave Factor Technique for the Characterization of Composite Materials," NASA Contractor Report 3670, Grant NSG-3-172, Feb., 1983.

47. Ramish Talreja, Anil Govada, and E.G. Henneke, "Quantitative Assessment of Damage Growth in Graphite Epoxy Laminates Acoustic-Ultrasonic Measurements," Materials Response Group, Dept. of Engineering Science and Mechanics, Virginia Polytechnic Institute, Virginia, August, 1983.

48. R.P. Nimmer,"Progressive Matrix Damage in Laminated Fiber-Epoxy Flywheel Disks," General Electric Corperate Research and Developement, Schenectady, New York, March, 1980.

49. John H. Hemann and George Y. Baaklini,"The Effect of Stress on Ultrasonic Pulses in Fiber Reinforced Composites," NASA Contractor Report 3724, 1983.

50. R.D. Kriz and H.M. Ledbetter,"Elastic Representation Surfaces of Unidirectional Graphite/Epoxy Composites," Fracture and Deformation Division, National Bureau of Standards, Boulder, Colorado, 80303, USA, June, 1983.

51. R.D. Kriz and W.W. Stinchcomb,"Elastic Moduli of Transverse Isotropic Graphite Fibers and Their Composites," Experimental Mechanics, Vol. 19, No. 2, Feb., 1979, pp.41-49.

52. R.D. Kriz,"Monitoring Elastic Stiffness Degradation in Graphite/Epoxy Composites," Fracture and Deformation Division, National Bureau of Standards, Boulder, Colorado, 80803, USA, March, 1982.

53. V.K. Kinra and J.G. Eden,"Propagation of Elastic Waves in Unidirectional Fiber-Reinforced Composites," Dept. of Aerospace Eng., Texas A&M University, College Station, AFOSR Contract Report, MM4875-84-19, Aug., 1984.

54. M.P.J. Musgrave, Crystal Acoustics, Holden-Day Inc., San Francisco, CA., 1970.

55. T.R. Tauchert and A.N. Guzelsu,"An Experimental Study of Dispersion of Stress Waves in a Fiber-Reinforced Composite," J. of Applied Mechanics, Vol. 39, March, 1972, pp.98-102.

56. T.R. Tauchert,"Measurements of the Elastic Moduli of Laminated Composites Using an Ultrasonic Technique," J. of Composite Materials, Vol. 5, Oct., 1971, pp.549-552.

57. F.H. Chang, J.C. Couchman, and B.G.W. Yee,"Ultrasonic Resonance Measurements of Sound Velocity in Thin Composite Laminates,"J. of Composite Materials, Vol. 8, October, 1974, pp.356-363.

58. V.K. Kinra,"Ultrasonic Nondestructive Evaluation of Damage in Continuous Fiber Composites", Dept. of Aerospace Eng., Texas A&M University, College Station, AFOSR Contract Report, MM5024-85-7, April, 1985.

59. J. Krautkramer, H. Krautkramer, Ultrasonic Testing of Materials, Springer-Verlag Berlin Heidelberg, New York, N.Y., 1983, p.86.

VITA

John Gregory Eden was born July 7, 1961, in Ft. Worth, Texas, the son of Johnny and Janice Eden. He graduated from L.D. Bell High School, Hurst, Texas in 1979. Greg entered Texas A&M University in the fall of 1979 and received a Bachelor of Science Degree in Aerospace Engineering in May 1983. He will receive his Master of Science Degree in Aerospace Engineering in December, 1985. Greg has accepted a job at General Dynamics, Ft. Worth Division within the Advanced Methods Group.

Permanent mailing address: 441 Pleasantview
Hurst, Texas
76054

APPENDIX II

Title:

ULTRASONIC NONDESTRUCTIVE TESTING OF FIBER REINFORCED COMPOSITE MATERIALS

Authors:

* Vinay Dayal
** Dr. V.K. Kinra
*** J.G. Eden

ABSTRACT A fully computerized technique for the measurement of wavespeed and attenuation has been developed. The technique can be applied to a thin specimen . It has been used to measure damage in specimens made of Magnamite AS4/3502 Graphite/Epoxy. It has been observed that attenuation is a reliable measure of damage due to microcracks. To the best of our knowledge this is the first technique which can be used to interrogate very thin specimens.

INTRODUCTION It is well known that fiber-reinforced composite materials develop a complex damage state when subjected to mechanical or thermal loading. The residual strength or fatigue life depends upon the current state of damage. When the damage occurs, it has two effects upon the propagation of a mechanical wave through the composite:1.It affects the stiffness and, therefore, the speed of wave propagation; 2.It increases the attenuation of the wave. Thus the ultrasonic parameters,wavespeed and attenuation, are a measure of the damage of the composite.

A new technique of ultrasonic NDE of composites is presented here. Ultrasonic NDE has been around for years. However, none of the existing techniques work satisfactorily for thin laminates for the following reason: the wave reflection from laminate faces are too close in the time domain and interfere with each another. A new technique has been developed based on the following theorem of the theory of Fourier transforms: the closer two events are in the time domain, the farther apart are the corresponding events in the frequency domain. The technique developed here yields accurate measurements of wavespeed (or stiffness) and attenuation (or damping) of longitudinal and shear waves in the thickness direction.

The development of the technique and some results from its application to fiber-reinforced composite,Graphite/Epoxy AS4/3502 laminates, of a variety of stacking sequences are presented.

---

* Grad Student Aerospace Engg.,Texas A&M Univ.,Coll. St. TX 77843
** Assoc. Prof Aerospace Engg.,Texas A&M Univ.,Coll. St. TX 77843
*** Engineer,Adv.Methods Gr.,General Dynamics,Fort Worth TX 76101

THEORETICAL ANALYSIS Consider a plate of a linear viscoelastic material sandwiched between two half-spaces of perfectly elastic materials. Consider also, a finite duration pulse,ray 1,incident at the viscoelastic plate as shown in fig.1.

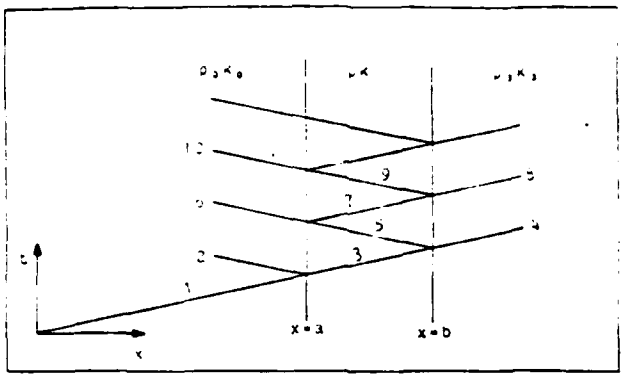

Fig.1 Pulse reflection and transmission by a plate.

Due to the mismatch in the acoustic impedence of the three materials, there will be an infinite series of reflected and transmitted pulses. These pulses contain information about the acoustic properties of the viscoelastic material.

Let the displacement field along the incident ray 1 be given by $u^{inc}=f(\omega t-k_0 x)$, where $f(s)\equiv 0$ for $s<0$ and ω and k_0 are circular frequency and wavenumber of the first half-space,respectively. The total reflected field is the sum of the following rays, with ($h=b-a$ and $s=\omega t+k_0 x$).

$u^2=R_{12}f(s-s_2)$; $s_2=2k_0a$

$u^6=T_{12}R_{23}T_{21}f(s-s_6)$; $s_6=2k_0a+2kh$

$u^{10}=T_{12}R_{23}R_{21}R_{23}T_{21}f(s-s_{10})$; $s_{10}=2k_0a+4kh$

where T_{ij}=Transmission coefficient from medium i to j

R_{ij}=Reflection coefficient from interface of media i&j with wave incident in medium i

The sum of these rays is

$$u^r=R_{12}f(s-2k_0a)+T_{12}R_{23}T_{21}\sum_{m=0}^{\infty}(R_{12}R_{23})^{m-1}f(s-s_m);\ s_m=2k_0a+m2kh \quad (1)$$

Similarly, the sum of the transmitted field can be written as

$$u^t=T_{12}T_{23}\sum_{m=0}^{\infty}(R_{21}R_{23})^m f(s-s_m);\quad s_m=a(k_0-k_3)+h[(2m+1)k-k_3] \quad (2)$$

It is to be noted here that k for a viscoelastic plate is a complex wavenumber.

If we consider a plate immersed in water then in the above analysis, the two half spaces are identical and the equations (1) and (2) reduce to

$$u^r=R_{12}f(s-2k_0a)+T_{12}R_{21}T_{21}\sum_{m=1}^{\infty}R_{21}^{2(m-1)}f(s-s_m);\quad s_m=2k_0a+m2kh$$

$$u^t=T_{12}T_{21}\sum_{m=0}^{\infty}R_{21}^{2m}f(s-s_m);\quad s_m=h[(2m+1)k-k_0]$$

Let us define the Fourier Transforms as

$$F^*(\omega)=\frac{1}{\sqrt{2\pi}}\int_{-\infty}^{\infty}f(t)e^{-i\omega t}dt$$

$$F_0^*(\omega)=\frac{1}{\sqrt{2\pi}}\int_{-\infty}^{\infty}f_0(t)e^{-i\omega t}dt$$

from these we get

$$F_o^*(\omega)=e^{i2k_oa}F^*(\omega)$$

If the incident field is $u^{inc}=f_o(\omega t-k_ox)$, the reflected field is given by $u^r=Rf_o(\omega t-k_ox-2k_oa)$ where $R=(\rho_oc_o-\rho c)/(\rho_oc_o+\rho c)$. Let the reflected signal as sensed by the transducer be $f(t)$, then $f(t)=f_o(\omega t-2k_oa)$. It can be readily shown that at $x=0$, the total reflected field is given by

$$u^r(0,t)=\frac{1}{\sqrt{2\pi}}\int_{-\infty}^{\infty}F_o^*(\omega)d\omega e^{i\omega t}\left[R_{12}e^{-i2k_oa}+\sum_{m=1}^{\infty}\beta_m e^{-i\{2k_oa+2mkh\}}\right]$$

where $\beta_m=T_{12}R_{21}T_{21}R_{21}^{2(m-1)}$

Let $u^r(0,t)=g(t)$ and $G^*(\omega)$ be the Fourier transform of $g(t)$, then

$$\sum_{m=1}^{\infty}\beta_m e^{-i2mkh}=\left[\frac{G^*}{F^*}e^{2ik_oa}-R_{12}\right] \tag{3}$$

Since $1+z+z^2+z^3+\text{-----}=1/(1-z)$ for $|z|<1$

Equation (3) can be written in the form

$$R_{21}^2e^{-i2kh}=\frac{\beta}{1+\beta}, \text{ where } \beta=\frac{R_{12}R_{21}}{T_{12}T_{21}}\left[\frac{G^*}{F^*}-1\right] \tag{4}$$

By measuring F^* (FFT of the front surface reflection and G^* (FFT of the total signal with all reflections) the complex valued $k(\omega)=k_1+ik_2$ can be obtained from eq.(4).

Similarly, from the transmitted field it can be shown that

$$\frac{e^{-ih(k-k_o)}}{1-R_{12}^2e^{-i2kh}}=\frac{G^*(\omega)}{T_{12}T_{21}F^*(\omega)} \tag{5}$$

Here F^* is the FFT of the signal at the receiver when there is no sample and G^* is the FFT of the total signal after the sample has been introduced in the path.

The preceeding analysis is useful even when the sample is thin and the pulses in the received signal are indistinguishable from each other. However, if the pulses can be seperated out then any two pulses can be used to obtain

$$\frac{G^*}{F^*}-1=T_{12}T_{21}\,e^{-i2kh} \tag{6}$$

where F^* is the FFT of the first pulse and G^* is the FFT of two pulses. Substituting $k=k_1+ik_2$ into eq.(6), where $k_1=2\pi f/c$, k_2 is attenuation, c is wavespeed and f is frequency and comparing the real and imaginary terms on the two sides we get $k_1=2\pi f/c=\phi/2h$ or $c=4\pi h/(\phi/f)$ and attenuation $k_2=\left[\ln M-\ln(T_{12}T_{21})\right]$ where ϕ is the phase of G^*/F^*-1 and $M=|G^*/F^*-1|$. Detailed derivation of these equations is given in [1].

TECHNIQUE DEVELOPMENT Keeping in view the tremendous speed and reliability which can be achieved by using computers for collection and analysis of data, the equations dev-

eloped above were interpreted in a way most suitable for computer analysis. Several potential sources of errors were studied next. These are:(1) Sampling interval,(2) Frequency resolution,(3) Transducer response and (4) Adequacy of pulse seperation. The first factor is the digitizing interval for the signal. FFT of a 10 MHz signal at 10ns(100 MHz), 20ns(50 MHz) and 40 ns(25 MHz) sampling intervals was studied. It was observed that at 10 or 20 ns the frequency content of the signal is essentially the same. However, at 40 ns sampling interval the signal loses some of its high frequency content. The second factor considered was the resolution of the signal in the frequency domain. A sampling frequency of 50 MHz or higher is being used and a resolution of 0.1 MHz or less on the frequency domain is considered adequate. The third factor considered was the useful range of the transducer frequency response. The FFT of the first pulse is shown in Fig. 2b. It was found that satisfactory measurements can be obtained over a frequency range given by 25% of the peak amplitude. Fourthly, with reference to Fig.2a, another source of error is that the operator has to decide where the first pulse ends and the second one starts. Hence as described in the theoretical analysis section, methods have been developed where the full signal is analysed as given in eqs.(4) and (5). For further details see [1]. The work presented here is for specimens where the two pulses can be seperated.

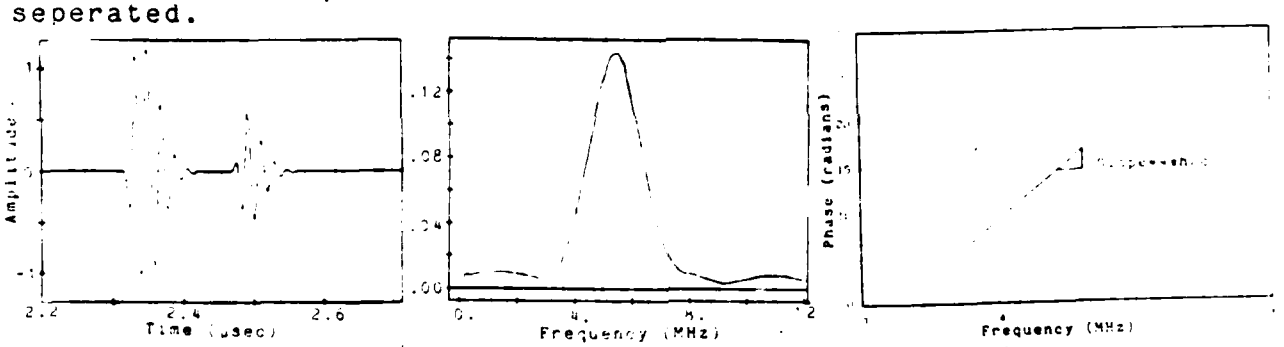

Fig.2 (a)Two gated pulses of the reflected signal (b)FFT of First pulse (c) Phase vs frequency for aluminum specimen.

EXPERIMENTAL PROCEDURE The block diagram of the experimental setup is as shown in fig. 3a. The specimens were fabricated using Magnamite AS4/3502 graphite prepreg tape made by Hercules Inc. All specimens were of 11"x1"x variable thickness. The specimens were loaded on Instron Model 1125. The tests were conducted at a crosshead speed of 0.05 in/min. Edge replication was done with the specimens under a nominal load to open up the transverse cracks.

In order to insure that each transducer was interrogating the same area, a square window was attached to the circular transducer as shown in fig.3b. These windows were made of room-temperature-curing silicone-rubber mixed with PMMA particles. To ensure that the tests were not affected by the temperature variations, the bath temperature was controlled to ±0.5°C. To eliminate the water absorption by microcracks, the edges of the cracked specimens were coated by strippable lacquer (Sherwin Williams). To avoid the spatial irregularities of the composite (ie matrix

or fiber rich regions, thickness variations, surface marks etc), to effect the measurements, tabs were provided on the specimen to replace it in the water bath to within ±0.001 in., after each mechanical loading.

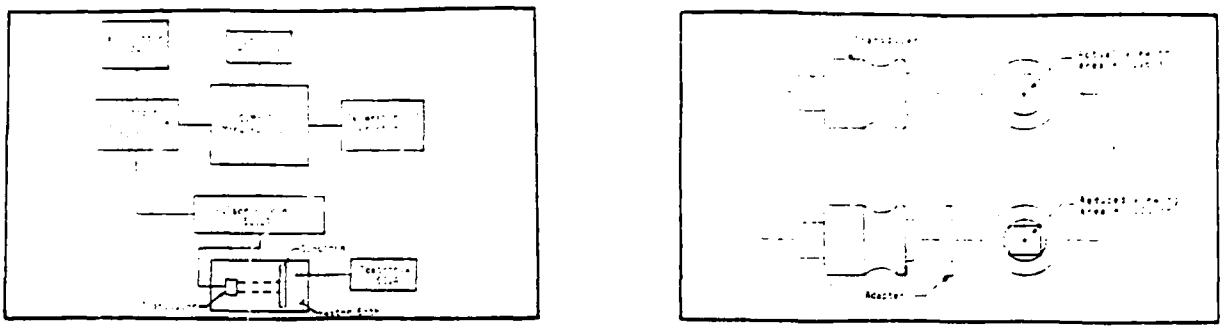

Fig.3(a) Block diagram of the experimental setup.
(b) Window attachment on the transducer.

RESULTS The technique developed here was first applied to an aluminium sample. Fig.2a shows the first and second gated pulse for the aluminium sample and the phase vs frequency plot is shown in fig. 2c. The phase as calculated by the computer is modulo 2Π. It is converted to a continuous phase by adding 2Π after each cycle completion. Slope of the phase vs frequency plot gives the group velocity. It was found that for the samples tested,the group velocity was very close to the phase velocity as the phase vs freq. plot was essentially a straight line. The wavespeed calculated from this plot was precise to ±0.02% when the specimen was not moved. If the specimen was removed between tests and replaced the precision is reduced to ±0.1%. The same tests were repeated with heavily damaged composite specimen and the precision of the tests was found to be ±0.2%.

The errors in the measurement of attenuation were larger. It was found that the attenuation could be measurement with a precision of ±1.0%. All the results are presented with attenuation in the non-dimensional form ie $k_2\lambda$. Fig.4 shows the edge replications of the damage states and the corresponding attenuation vs frequency curves. At lower frequencies the attenuation is more sensitive to the damage than at higher frequencies. It is observed that the attenuation gives a very good measure of the extent of microdamage in the off-axis plies.

Fig.5 shows the variation of the attenuation as the crack length increases. Here,the crack length is the measure of the number of cracks and is the total length of the cracks in the field of measurement.

When there are less cracks in the specimen then there is some amount of scatter in the attenuation measured, but as the total crack length increases the measurement becomes steady. For details of these results see [2].

CONCLUSIONS A new technique for the measurement of wave speed and attenuation of ultrasonic waves has been developed. To the best of our knowledge this is the first technique that gives satisfactory results even for very thin specimen.

The technique has been applied to fiber-reinforced composite material specimens. It was found that whereas the wave speed (or stiffness) is rather insensitive to transverse cracking, the through-the-thickness attenuation is a sensitive measure of the damage state and hence is a potential damage metric.

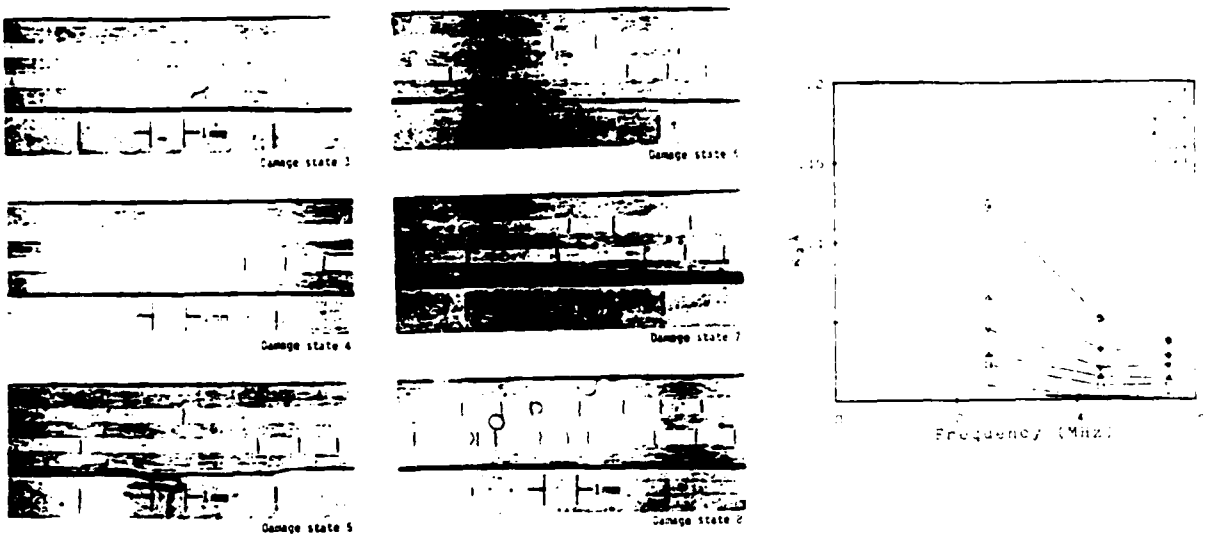

Fig.4 Edge replications of damage state and attenuation vs frequency plot.

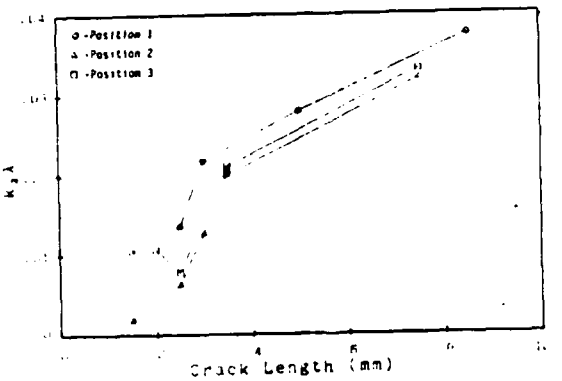

Fig.5 Attenuation vs crack length for a graphite/epoxy specimen.

REFERENCES 1. Kinra V.K.,"Ultrasonic Nondestructive Evaluation of damage in Continuous Fiber Composites".Annual Technical Report. Project AFOSR-84-0066,Apr 85.

2. Eden J.G.,"The application of Ultrasonics to assess damage in composite Materials". M.S. Thesis. Dec 85. Texas A&M University.

ACKNOWLEDGEMENTS This research is supported by the Air Force Office of Scientific Research Contract No. F49620-83-C-0067.

APPENDIX III

ULTRASONIC NONDESTRUCTIVE TESTING OF COMPOSITE MATERIALS

Dayal, Vinay and Kinra, V.K.

Graduate Student and Associate Prof., respectively,
Aerospace Engg. Dept., Texas A&M University,
College Station, TX 77840, U.S.A.

ABSTRACT

Wavespeed and attenuation, the ultrasonic parameters are affected by the internal structure or damage of the material. Accurately measured ultrasonic parameters, in a composite coupon are thus an indicator of the extent of the cumulative damage in the coupon. A through-transmission water-immersion technique has been developed for the measurement of the ultrasonic parameters. The method utilizes the Fast Fourier Transforms to convert the time-domain signal to the Frequency domain signal. Computers are used for the acquisition and analysis of data, for accuracy and speed. This technique can be used to measure the ultrasonic parameters of coupons of any thickness and material. The technique presented here has been used to measure damage in specimen made of Magnamite AS4/3502 Graphite/Epoxy. It has been observed that attenuation increase due to microcracks is a reliable measure of the damage in the composites. To the best of our knowledge, this is the first technique which can be used to interrogate specimens of any thickness.

INTRODUCTION

Fiber-Reinforced-Composites have been in use as structural members for a considerable amount of time and various methods are available for their testing. A detailed review of the methods and techniques available may be found in (1).

The complex damage state developed due to the loading (mechanical or thermal) of composite materials, changes the stiffness and the damping characteristics of the material. When an ultrasonic wave is passed through the composite, the wavespeed and attenuation measurements give the stiffness and damping of the material. Changes in wavespeed and attenuation are thus a measure of the damage in the composites. It is our endeavour to develop techniques to measure these ultrasonic parameters accurately, repeatably and quickly. We have used computers for the collection and analysis of data, with least human

intervention, so that the techniques can be automated.

The toneburst method has been the most basic method of the wavespeed measurement. Since broad bursts of the signal(about 5 cycles) are used in this method, it cannot be used when the reflections from the front and back surfaces of the specimen interfere. A computerized pulse technique was presented in (2) for the measurement of wavespeed and attenuation. This method also depends on the seperation of pulses and though thinner specimens could be tested, since a single pulse is being used, the technique failed when the pulses started interfering.

We present here a technique which can be applied to specimen of any thickness. A pitch-catch signal pulse of a 1 MHz transducer is shown in Fig 1a. When a 10 ply composite specimen is introduced in the path, the total signal received is shown in Fig 1b. The technique presented here is capable of calculating wavespeed and attenuation from the signals of Fig 1.

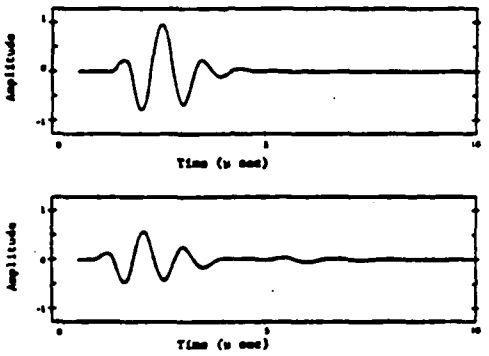

Fig. 1a. Pitch-Catch signal of a 1 MHz transducer, b. Signal when a 10 ply composite specimen introduced in the path.

The development of the technique and some results from its application to fiber reinforced composite Graphite/Epoxy AS4/3502 laminates with stacking sequences $[0,90_4]_s$ are presented.

THEORETICAL ANALYSIS

Consider a plate of a linear viscoelastic material sandwiched between two half-spaces of perfectly elastic materials. Consider also, a finite duration pulse,ray 1,incident at the viscoelastic plate as shown in Fig 2.

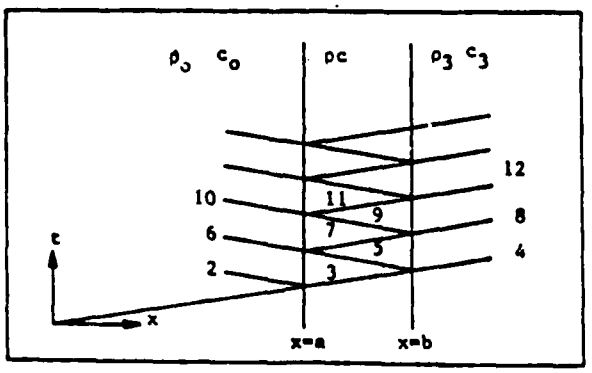

Fig.2 A series of Pulses reflected and transmitted by a plate.

Due to the mismatch in the acoustic impedence of the three materials, there will be an infinite series of reflected and transmitted pulses. These pulses contain information about the acoustic properties of the viscoelastic material.

Let the displacement field along the incident ray 1 be given by $u^{inc}=f(\omega t-k_0 x)$, where $f(s)\equiv 0$ for $s<0$ and ω and k_0 are circular frequency and wavenumber of the first half space. The total reflected field is the sum of the following rays, with ($h=b-a$ and $s=\omega t+k_0 x$).

$u^1=R_{12}f(s-s_1)$; $s_1=2k_0a$

$u^2=T_{12}R_{23}T_{21}f(s-s_2)$; $s_2=2k_0a+2kh$

$u^{10}=T_{12}R_{23}R_{21}T_{21}f(s-s_{10})$; $s_{10}=2k_0a+4kh$

where T_{ij}=Transmission coefficient from medium i to j

R_{ij}=Reflection coefficient from interface of media i&j with wave incident in medium i

The sum of these rays is

$$u^r=R_{12}f(s-2k_0a)+T_{12}R_{23}T_{21}\sum_{m=0}^{\infty}(R_{12}R_{23})^{m-1}f(s-s_m);\ s_m=2k_0a+m2kh \quad (1)$$

Similarly, the sum of the transmitted field can be written as

$$u^t=T_{12}R_{23}\sum_{m=0}^{\infty}(R_{12}R_{23})^{m}f(s-s_m);\ s_m=a(k_0-k_2)+h[(2m+1)k-k_2] \quad (2)$$

It is to be noted here that k for a viscoelastic plate is a complex wavenumber.

If we consider a plate immersed in water then in the above analysis, the two half spaces are identical and the equations (1) and (2) reduce to

$$u^r=R_{12}f(s-2k_0a)+T_{12}R_{21}T_{21}\sum_{m=1}^{\infty}R_{21}^{2(m-1)}f(s-s_m);\ s_m=2k_0a+m2ka$$

$$u^t=T_{12}T_{21}\sum_{m=0}^{\infty}R_{21}^{2m}f(s-s_m);\ s_m=h[(2m+1)k-k_0]$$

Let us define the Fourier Transforms as

$$F^*(\omega)=\frac{1}{2\pi}\int_{-\infty}^{\infty}f(t)e^{-i\omega t}dt$$

$$F_0^*(\omega)=\frac{1}{2\pi}\int_{-\infty}^{\infty}f_0^*(t)e^{-i\omega t}dt$$

from these we get

$$F_0^*(\omega)=e^{i2k_0a}F^*(\omega)$$

If the incident field is $u^{inc}=f_0(\omega t-k_0x)$, the reflected field is given by $u^r=Rf_0(\omega t-k_0x-2k_0a)$ where $R=(\rho_0c_0-\rho c)/(\rho_0c_0+\rho c)$. Let the reflected signal as sensed by the transducer be f(t), then $f(t)=f_0(\omega t-2k_0a)$. It can be readily shown that at x=0, the total reflected field is given by

$$u^r(0,t)=\frac{1}{2\pi}\int_{-\infty}^{\infty}F_0^*(\omega)d\omega e^{i\omega t}\left[R_{12}e^{-i2k_0a}+\sum_{m=1}^{\infty}\beta_m e^{-i(2k_0a+2mkh)}\right]$$

where $\beta_m=T_{12}R_{21}T_{21}R_{21}^{2(m-1)}$

Let $u^r(0,t)=g(t)$ and $G^*(\omega)$ be the Fourier transform of g(t), then

$$\sum_{m=1}^{\infty} \beta_m e^{-i2mkh} = \left[\frac{G^*}{F^*} e^{2ik_0 a} - R_{12}\right] \qquad (3)$$

Since $1+z+z^2+z^3+\cdots = 1/(1-z)$ for $|z|<1$
Equation (3) can be written in the form

$$R_{21}^2 e^{-i2kh} = \frac{\beta}{1+\beta}, \text{ where } \beta = \frac{R_{12}R_{21}}{T_{12}T_{21}}\left[\frac{G}{F^*} - 1\right] \qquad (4)$$

By measuring F^* (FFT of the front surface reflection and G^* (FFT of the total signal with all reflections) the complex valued $k(\omega)=k_1+ik_2$ can be obtained from eq.(4).

Similarly, from the transmitted field it can be shown that

$$\frac{e^{-ih(k-k_0)}}{1-R_{12}^2 e^{-i2kh}} = \frac{G^*(\omega)}{T_{12}T_{21}F^*(\omega)} \qquad (5)$$

Here F^* is the FFT of the signal at the receiver when there is no sample and G^* is the FFT of the total signal after the sample has been introduced in the path. Detailed derivation of these equations is given in (3).

Equation (5) can now be written in the following form

$$Z^2+ZY-c_0=0. \qquad (6)$$

where $Z=e^{-ihk}$
$k=k_1+ik_2$
$k_1=\omega/c$
k_2=coefficient of attenuation

$Y=(T_{12}T_{21}/R_{21})(F^*/G^*)Z_0$

$Z_0=e^{-ihk_0}$
k_0=wavenumber in the elastic mediums.
$c_0=1./R_{21}$

In (6) both Z and Y are complex.

In the water immersion case which is the one we are going to use for the tests, Z_0 can be easily calculated if the wavespeed in water is accurately known. The transmission and reflection coefficients can be calculated if the densities of the two mediums and longitudinal wavespeeds in them are known. But the wavespeed in the plate is the unknown which we want to measure. Hence to overcome this dilemma, an iteration procedure was followed where an approximate wavespeed is provided as an input to estimate the various reflection and transmission coefficients. The quadratic equation (6) is then solved to give two roots of Z. The correct root is chosen based on the fact that as the frequency increases as the phase of Z decreases. The wavespeed is calculated from the phase of Z. This wavespeed is then used to re-estimate the reflection and transmission coefficients. This iterative procedure converges rapidly to the correct wavespeed. It was estimated that even with an initial descrepancy of ±30% in wavespeed, the solution converged in fewer than 5 iterations.

EXPERIMENTAL PROCEDURE

The block diagram of the experimental setup is as shown in Fig 3.

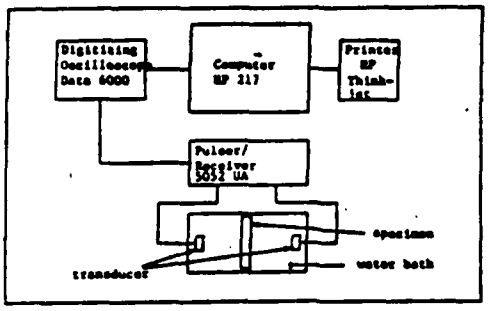

Fig.3 Block diagram of the experimental setup.

The analog signal is collected by the Pulser-Receiver (Panametrics 5052 UA) and is fed into the Digital Oscilloscope (Data- 6000). The signal is digitized in the oscilloscope. The signal processing unit of this oscilloscope then performs Fast Fourier Transform on the signal. The useful portion of the transformed signal is then acquired by the computer for the calculation of the wavespeed and the attenuation. In these steps several potential sources of errors can affect the results. These are: (1) Sampling interval, (2) Frequency Resolution and (3) Transducer Response. The first factor is the digitizing interval of the acquired signal. FFT of a 1 MHz signal at 10,20,40,100 nS sampling intervals was studied. It was observed that at 10,20 or 40 nS sampling interval the frequency content of the signal is essentially the same. However, at 100 nS sampling interval, the signal loses some of its high frequency contents. The useful digitizing intervals depend on the frequency of the transducer being used. For example for 10 MHz frequency, at 40 nS interval some of the high frequency contents are lost. The second factor considered was the resolution of the signal in the frequency domain. A sampling interval of 40 nS or less with a frequency resolution of 0.05 MHz or less is considered adequate. This factor is also transducer frequency related. The third factor considered was the useful range of the transducer frequency response. It was found that satisfactory measurements can be obtained over a frequency range given by 25% of the peak response amplitude. For further details see (4).

The specimens were fabricated using Magnamite AS4/3502 graphite prepreg tape made by Hercules Inc. All specimen were of 11"x1"x .05" size. The specimens were loaded on Instron Model 1125. The tests were conducted at a crosshead speed of 0.05 in/min. The transverse cracks were opened by a nominal load on the specimen and edge replications were taken to keep a record of the cracks. To eliminate the water absorption by the microcracks while testing by ultrasounds, the edges of the cracked specimens were coated by Strippable Lacquer (Sharvin Williams).

RESULTS

First of all, the accuracy of the measurement technique reported here was estimated. The technique was applied to a heavily damaged composite specimen. This was done to account for

measurements under the worst conditions of damage. It was estimated that the precision of the measurement was ±0.3% for wavespeed and ±1.5% for attenuation. It is to be noted here that the accuracy of the measurement will depend on the accuracy of the predetermined input parameters viz. the densities of the water and specimen and the wavespeed of ultrasound in water.

The results presented here are for Gr/Epoxy $[0/90_4]_s$ specimens tested by a broad band 5 MHz transducer. In the results presented, attenuation k_2 has been non-dimensionalized to $k_2\lambda$. Line sketches of the edge replications, where the measurements were made, are shown in fig 4. The variation of attenuation, as the applied load is increased, is shown in Fig 5. Numbers on the curves denote the location number on the specimen. The specimen were surveyed along the length for each load step to identify any preferred localization of defects. It was observed that for the layup tested, the damage was evenly distributed. As is evident from the edge replications, very few cracks are developed for stresses upto 35 ksi, and hence the increase in attenuation is also low. When the stresses were increased further, multiple cracks developed and this resulted in a large increase in the attenuation values.

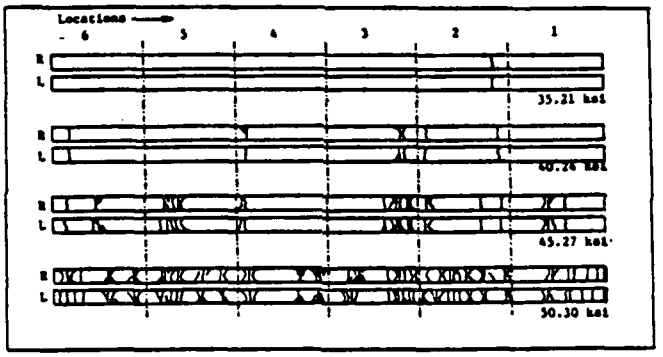

Fig 4. Line sketch of the edge replications of a $[0/90_4]_s$ Gr/Epoxy Specimen. L&R denote left & right sides of the specimen

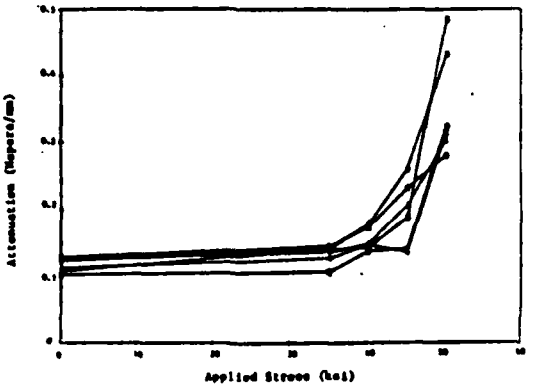

Fig 5. Variation of Attenuation as a function of Applied Stress at 6 different locations of the specimen.

It can be seen from the edge replications that the damage is evenly distributed along the specimen and no preffered sites of damage were observed. The specimen failed near the grips.

As expected, for the tests conducted, no significant variation in wavespeed was observed. The reason is that in this configuration of the testing, the wavefront is perpendicular to the plane of the crack, or the wave propagation direction is in the plane of the crack. Hence, the cracks do not change the wavespeed appreciably.

CONCLUSIONS

A new technique for the measurement of wave speed and attenuation of ultrasonic waves has been developed. This technique is fully computerized and does not need any human interference except the placing and removing the specimen from the ultrasonic path. To the best of our knowledge this is the first technique that gives satisfactory results for specimen of any thickness.

The technique has been applied to fiber-reinforced composite material specimens. It was found that whereas the wave speed (or stiffness) is rather insensitive to transverse cracking, the through-the-thickness attenuation is a sensitive measure of the damage state and hence is a potential damage metric.

ACKNOWLEDGEMENTS

This research is supported by the Air Force Office of Scientific Research Contract No. F49620-83-C-0067.

REFERENCES

1. Bar-Cohen, Y.,"NDE of Fiber-Reinforced Composite Materials - A Review",Materials Evaluation, Vol.44, No.4, Mar. 1986, pp446-454.
2. Dayal, V., Kinra, V.K., Eden, J.G.,"Ultrasonic NDT of Fiber Reinforced Materials", Proc. of the International Symposium on Composite Materials '86, Beijing, China.
3. Kinra V.K.,"Ultrasonic Nondestructive Evaluation of damage in Continuous Fiber Composites".Annual Technical Report. Project AFOSR-84-0066,Apr 85.

END

1-87

DTIC